

Characterization of active sites and catalysis in MOFs using first principle methods (Title from DEFNET)

Title in dutch

Chiara Caratelli

Supervisor: prof. dr. ir. Veronique Van Speybroeck
Dissertation submitted in fulfillment of the requirements for the degree of
Doctor (Ph.D.) in de Ingenieurswetenschappen: Chemische Technologie

Chair: prof. dr. ir. C. Leys
Faculty of Engineering and Architecture
Ghent University
Academic year 2018–2019

check if we
dutch or en



Members of the examination committee

Chair

Prof. Dr. Ir. Luc Taerwe (Ghent University)

Reading Committee

tbd

tbd

tbd

tbd

Other Members

tbd

Prof. Em. Dr. Michel Waroquier (Ghent University)

Supervisor

Prof. Dr. Ir. Veronique Van Speybroeck (Ghent University)



This research has been conducted at the **Center for Molecular Modeling**, in collaboration with:

- Instituto de Tecnología Química, Universitat Politècnica de València (Dr. F. X. Llabrés i Xamena, Dr. Francisco García Cirujano)
- Centre for Surface Chemistry and Catalysis, University of Leuven (Prof. R. Ameloot, João Marreiros)
- Van 't Hoff Institute for Molecular Sciences, Universiteit Van Amsterdam (Prof. E. J. Meijer, Prof. B. Ensing)

Contents

List of Abbreviations	iii
List of Symbols	v
Samenvatting	vii
Summary	ix
I Towards modeling catalytic processes in UiO-66 metal-organic framework at operating conditions	
1 Introduction	1
1.1 Metal Organic Frameworks	4
1.2 Outline and goal of the thesis	16
2 Modeling metal organic frameworks	19
2.1 Framework topology	19
2.2 Theoretical methods	22
2.3 Free energy	30
2.4 Exploring the free energy surface	33
3 Major research results	39
3.1 Activation processes in zirconium-MOFs	40
3.2 Role of solvent: towards operating conditions	55
4 Conclusions and perspectives	67
II Published papers	71
A Publication List	73
Publications in international peer-reviewed journals	73
Conference contributions	74
Bibliography	79

List of Abbreviations

AIMD	<i>Ab Initio</i> Molecular Dynamics
BDC	Benzene-1,4-dicarboxylate
BTC	Benzene-1,3,5-tricarboxylic acid
BO	Born–Oppenheimer
BOMD	Born–Oppenheimer Molecular Dynamics
CMM	Center for Molecular Modeling
CPMD	Car–Parrinello Molecular Dynamics
CN	Coordination Number
CV	Collective Variable
DFT	Density Functional Theory
FES	Free Energy Surface
FFA	Free Fatty Acids
FTIR	Fourier-Transform Infrared
GCMC	Grand Canonical Monte Carlo
GGA	Generalized Gradient Approximation
HF	Hartree–Fock
HKUST	Hong Kong University of Science and Technology
HPC	High-Performance Computing
IR	Infrared
IRMOF	Isoreticular MOF
LDA	Local Density Approximation
LSDA	Local Spin Density Approximation
M–L	Metal–linker coordination
MC	Monte Carlo
MD	Molecular Dynamics
MIL	Matériaux de l’Institut Lavoisier
MOF	Metal–Organic Framework
MPV	Meerwein–Ponndorf–Verley
MTD	Metadynamics
MTK	Martyna–Tobias–Klein
NEB	Nudged elastic band
NU	Northwestern University
PBC	Periodic Boundary Conditions
PCM	Polarizable Continuum Model
PCP	Porous Coordination Polymer
PHVA	Partial Hessian Vibrational Analysis
PES	Potential Energy Surface
PSE	Post–Synthetic Exchange

PSLE	Post–Synthetic Ligand Exchange
PSM	Post–Synthetic Modification
PXRD	Powder X–Ray Diffraction
QM	Quantum Mechanics
RE	Replica Exchange
RDF	Radial Distribution Function
SBU	Secondary Building Unit
SCF	Self–Consistent Field
SXRD	Single–Crystal X–Ray Diffraction
TFA	Trifluoroacetic Acid
TGA	Thermogravimetric Analysis
TPS	Transition Path Sampling
TS	Transition State
TST	Transition State Theory
UiO	Universitetet i Oslo (University of Oslo)
US	Umbrella Sampling
WHAM	Weighted Histogram Analysis Method
XRD	X–Ray Diffraction
ZPE	Zero Point Energy

List of Symbols

\ddagger	Transition state
ΔE^\ddagger	Electronic energy barrier
ΔH^\ddagger	Enthalpy barrier
ΔG^\ddagger	Free energy barrier
B_0	Bulk modulus
E	Electronic energy
E_{ZPE}	Zero-point vibrational energy
F	Helmholtz free energy
G	Gibbs free energy
\hat{H}	Hamiltonian operator
H	Enthalpy
h	Planck constant
k	Rate coefficient unimolecular reaction
k_B	Boltzmann constant
N	Number of particles
N_A	Avogadro constant
N_{dof}	Number of degrees of freedom
p	Pressure
P	Product
Q	Overall partition function
Q_{trans}	Translational partition function
$Q_{rot,ext}$	Rotational partition function
Q_{vib}	Vibrational partition function
q_X	Partition function of species X
R	Reactant
R	Universal gas constant
r_{ij}	Distance between atoms i and j
S	Entropy
T	Temperature
U	Internal energy
V	Volume
V_0	Equilibrium Volume
ε_0	Electronic energy
ν_i	Vibrational frequency
ρ	Density

Samenvatting

Summary in Dutch here

Summary

In the past decades, nanoporous materials have become an intense field of study due to their numerous potential applications. Their extremely high surface area and pore volume make them very appealing for many processes in different scientific and industrial sectors, primarily as heterogeneous catalysts or adsorbents. Examples of stable and well-known nanoporous materials are zeolites and activated carbon, widely used in petrochemistry, medicine and environmental applications.

Recently, new nanoporous materials, called Metal Organic Frameworks (MOFs), entered the stage and rapidly became one of the most deeply investigated classes of materials due to their outstanding properties. MOFs, or Porous Coordination Polymers (PCPs) are hybrid nanoporous materials, in which metal or metal–oxo clusters are connected by multtopic organic linkers via coordination bonds to form 1-, 2- or 3-D crystalline structures. Their particular building block design allows for a plethora of structures that can be generated, with different metals, metallic nodes, organic linkers, topology and pore size. Moreover, these building blocks can be further functionalized by post-synthetic modifications. The ease in their design makes them very appealing for a broad range of applications, as they can in principle be finetuned to target a specific property. In contrast to zeolites, the most well-known inorganic nanoporous materials, in which the robust Si–O bonds can be broken only at harsh conditions, MOFs are characterized by weaker metal–ligand (M–L) bonds. They have a much higher structural diversity and can be more easily tuned in terms of types of metal, topology and chemical functionality. The high (and tuneable) porosity, metal content and crystallinity, as well as the possibility to include different functionalities, are very attractive characteristics for catalytic applications. In this sense, MOFs could be engineered to maximize the outcome of a given reaction, in terms of yield and selectivity for a desired product. Moreover, as heterogeneous catalysts, they can bring numerous advantages to industry, as they are often less toxic or corrosive and can be easily separated from the products after the catalytic cycle. One of the most striking features which has drawn a lot of attention in the past years is the presence of structural defects and disorder in their structure. If at first this was seen as a drawback, currently it has become clear that they can have a beneficial effect on their performance. In applications such as catalysis they can be the source of functionality, both directly, by generation of active sites with undercoordinated metal atoms, and indirectly, by increasing the pore size. However, we are still yet to understand the nature of defects at the molecular level, due to their intrinsic randomness that puts them in a continuum between order and disorder.

The inherent complexity of MOFs in terms of extremely high number of possible structures and defectivity makes their experimental characterization a particularly challenging task. In these materials, the active sites are often generated by intentional creation of defects, and their inherent randomness entails a high complexity in their study. It is not trivial to have direct experimental insight on active sites arising from defects and to draw clear structure–property relationship when such disorder is involved. Nevertheless, the molecular understanding of their active sites, which can be done with computational models, is crucial to predict their behavior and to design specific MOFs for target applications. The past decades have seen a flourishing in computational techniques, which provided new opportunities for exploration and understanding of chemical systems. Computational methods, guided by experiments, allow the study of MOFs at the nanoscale, offering a platform to understand and rationalize experimental observations. Besides supporting experimental data, they can be used to generate novel concepts, make predictions and design new materials and experiments. Theory can this way support experiments, and experiments can ultimately be used to validate theoretical predictions.

Nowadays, a rich toolbox of molecular modeling techniques is available for the study of nanoporous materials which can be applied to MOFs. When studying such complex materials, there is always a trade-off between computational cost and complexity of the model. At given computational cost, one has to make wise choices on what to prioritize between size of the model, length of the simulation, and chemical accuracy. For certain applications, such as the study of defects for adsorption, large systems are used, but with an approximate characterization of the chemical interactions. For catalysis, however, a high chemical accuracy is needed to describe active sites and reaction mechanisms, and this is often done at the expenses of the size of the model. This way, only the region directly involved in the process is prioritized, in which the description of realistic experimental conditions is neglected. Nevertheless, confinement effects, pressure, temperature and presence of guest molecules are all factors that can play a major role in the behavior of the active sites influencing the reaction mechanism to a large extent. Luckily, computational power has grown substantially, allowing to include more complexity in the model, moving towards a description of chemical processes at operating conditions.

To understand active sites in MOFs from a computational point of view, it is important to work on well-studied materials, where experimental information is the most available. Among the plethora of known MOFs, UiO–66, composed by zirconium–oxide bricks and terephthalate linkers, is characterized by an exceptional stability that arises from the nature of its M–L bonds and its high structural connectivity. In the material, each inorganic brick is connected to twelve linkers, and the structure is therefore extremely robust and able to withstand the chemical and thermal conditions at which reactive processes may take place. For this reason, it is at present moment one of the more widely investigated MOFs. Furthermore, the highly connected material allows for the presence of crystal defects such as missing linkers, which are responsible for its catalytic activity. For all these reasons, UiO–66 and its derivatives represent prototype MOFs that have a high potential

for industrial applications.

In this work of thesis, the active sites in the UiO–66 material were studied with different advanced modeling techniques such as static period calculations and *ab initio* molecular dynamics simulations. Density functional theory (DFT) was used as the method of choice that offered the best compromise between accuracy and computational cost, while allowing to study complex events involving bonds being broken and formed. Starting from extended cluster models, to gain a first insight into the active sites, we then made use of a proper periodic description of the MOF model that included confinement of the reactants and defective sites with undercoordinated zirconium atoms, that are generated upon removal of a linker. By modeling a Lewis–catalyzed reaction in the hydrated and dehydrated material, we came to the conclusion that the active sites are more complex than originally anticipated. We observed that water has an unexpected beneficial role in the reaction and UiO–66 is a dual Lewis/Brønsted catalyst where solvent plays a role in the reaction mechanism by providing support for proton transfers.

With these observations, it is clear that for such complex phenomena, static methods are not always sufficient to study the nature of the active sites in these materials, and that a dynamic approach has to be followed. Allowed by the increase in computational power of high–performance computing (HPC) facilities, we increased the complexity of the model by including an explicit treatment of the solvent at realistic experimental conditions. We gained valuable insight into the dynamic events that can take place in the pores of the material. From these simulations, we understood that solvent can indeed modulate the properties of the active sites, by strongly interacting with the undercoordinated zirconium atoms, transferring protons, and providing a platform for stabilization of charged intermediates. Moreover, by means of enhanced sampling MD simulations, we shed light on how the strong interactions around the defective sites can help modulate the defectivity of the material, by inducing dynamic and reversible rearrangements of the structure. Linkers are more mobile than originally anticipated, and can de-coordinate, translate, rotate and coordinate again to the zirconium atoms, without disrupting the stability of the structure. By understanding how these M–L bonds can evolve, we gained insight onto the post–synthetic ligand exchange process (PSLE) in UiO–66, that represents an optimal and easy way to functionalize MOF materials. We observed similar dynamic behavior at dehydration conditions, when water is removed from the brick. Starting from the excellent physical and chemical understanding obtained on UiO–66, we could focus on the structural properties of MOF–808, another Zr–MOF that shows high potential for catalytic applications and is not yet so well explored.

In summary, in this work of thesis we made use of a rich computational toolbox with a multilevel modeling approach to understand the nature, properties and applications of active sites arising from defects in Zr–MOFs. Starting from simple models, the complexity was built towards a description of the system at operating conditions, which has been done for the first time for such materials. The results obtained highlight the importance of computational techniques in elucidating the properties of such complex systems on the molecular level. Theory, combined

with experimental insight, forms an efficient and effective way of exploring the world of such fascinating and advanced materials. This work shows that theory and experiments have to go hand in hand, by supporting each other, to better understand and predict realistic phenomena.

List of Figures

1.1	Schematic representation of the building block design in Metal-Organic Frameworks (MOFs). Left panel: some examples of inorganic bricks; middle panel: some examples of organic linkers; right panel: some MOFs with different topologies, pore size and shape	5
1.2	Schematic representation of some of the numerous MOF applications.	6
1.3	Number of publications on MOFs and catalysis in MOFs in years 1985–2018, showing the importance of catalysis in MOFs as indicated by Web of Science	7
1.4	Structure of UiO–66 (top) and MOF–808 (bottom), the two Zr-MOFs investigated in this work of thesis.	9
1.5	Representation of the UiO–66 material with missing linkers and clusters displayed in red. In this dissertation, we mainly focus on missing linkers.	11
1.6	Lewis and Brønsted sites that are created when a linker is removed from the UiO–66 zirconium brick, with different number of coordinated water molecules.	14
1.7	Schematic representation of as synthesized and upon activation MOF–808 structures	15
2.1	Left: extended cluster model cut from the periodic structure of UiO–66. The cluster contains the active site, the brick and the linkers in the closest proximity to the active site. Right: representation of the unit cells containing the defect. In blue, the conventional 4–brick unit cell, in orange, the 2–brick unit cell used for the calculations. The two different bricks are highlighted in orange. The 10–fold coordinated brick has two terephthalate linkers missing.	21
2.2	Representation of the different ways to remove up to three linkers from a 4–brick UiO–66 unit cell	22
2.3	The two lowest PES in the BO approximation for a diatomic molecule. In blue, the electronic PES for the ground state and first electronic excited state (UV–Vis transitions). In orange, the vibrational energy levels (IR transitions), in grey the rotational levels (microwave transitions).	23
2.4	Representation of some of the molecular modes taken into account in a generic force field model.	24

2.5	Schematic representation of the potential energy surface and the stationary points.	27
2.6	Representation of the atoms taken into account in the Partial Hessian Vibrational Analysis (PHVA) approach. Top: a schematic representation of a reactive process in nanoporous material, bottom: a snapshot from the static calculations where the atoms of the active site and the adsorbates are highlighted	29
2.7	1D free energy profiles for a given reaction with and without catalyst, indicating the adsorbed initial, final states and the localized transition state, schematically illustrated in below. The adsorption free energy, intrinsic and apparent barriers are obtained by static calculations and indicated by ΔG_{ads} , $\Delta G_{‡}$, and ΔG_{app} , respectively;	32
2.8	a) 1D free energy profiles for a given reaction on two different active sites in UiO-66 (insets), indicating the adsorbed initial and final states and the localized transition state for this reaction; (b) possible 2D representation of the given reaction on the two active sites as obtained using advanced dynamic techniques, indicating the three critical points on the potential energy surface.	33
2.9	Schematic representation of different MD techniques that can be used to explore the PES.	36
3.1	Schematic representation of the UiO-66 structure with possible configurations of the bricks that give rise to coordinatively unsaturated Zr atoms. The colors indicate the coordination of the Zr atoms.	40
3.2	Coordination free energies at reaction temperature of 351 K of one, two and three water molecules at coordinatively unsaturated Zr-bricks in defective UiO-66 with respect to a water coordination free site (site R). The structure of the opposite site B corresponds with configuration 2' with two water molecules and consistently used in all periodic calculations considered in the figure. Free energies (in black) are given in kJ/mol, and their decomposition into enthalpic ΔH (blue) and entropic $-T\Delta S$ (grey) contributions. Energies are resulting from periodic calculations with PBE-D3 level of theory. In each configuration Lewis acid and Brønsted sites are indicated.	41
3.3	Top: Fischer esterification reaction; bottom: three different types of UiO-66 active sites.	43
3.4	Mechanism and free energy profile for the esterification of propionic acid with methanol on a hydrated and defective UiO-66 material (blue), a hydrated defective UiO-66 material with amino functionalization of the BDC linkers (red), and on a dehydrated defective UiO-66 (black). Periodic calculations at B3LYP-D3//PBE-D3 level of theory, T=351 K. R corresponds with an empty frame with one linker defect and a pool with all reactants to guarantee mass balance. In P the defective Zr-brick is coordinated with two water molecules (configuration 2'). P' corresponds to the empty frame with the ester as final product and remaining water molecules in gas phase.	44

3.5 Transition states belonging to three cases where no suitable mechanism for Fischer esterification was found, suggesting that the reaction needs a concerted participation of Lewis and Brønsted sites	45
3.6 Energy diagrams for defective UiO–66 unit cells. Each dot represents a possible distribution of missing-linker defects (1 or 3 in total) within the unit cell; the connecting dotted line represents a weighted average. Values are normalized by the number of missing linkers in the unit cell. (a) Enthalpy difference between defect sites capped in different ways versus the non-defective material at T = 298, 313, 373, 473 K. (b) Temperature-dependence of the free energy difference of the defective structures indicated above (capped with H ₂ O/OH ⁻ , H ₂ O/MeO ⁻ and MeOH/MeO ⁻) versus the non-defective structure. A representation of the clusters with different missing linker connectivities is also provided.	47
3.7 Umbrella sampling in two windows of CV = 1.45 and 1.51, showing two distinct motions of the linkers. On the left column, a translation of the linker L1 generates a chelated structure and a subsequent shift in the carboxylic oxygen connected to Zr2 (configuration 4t). On the right column, a rotation of the linker L1 and a partial decoordination of linker L2 forming a hydrogen bond with an μ_3 -OH hydroxyl group is shown (configuration 4r). A proton transfer between the carboxylic oxygen O3 and the bridging μ_3 -O is also observed and is an indication of the occurrence of an intrinsic dynamic acidity. Colors indicate the coordination number of zirconium atoms.	49
3.8 Schematic representation of as synthesized and upon activation MOF-808 structures	50
3.9 Change of volume in time of the three investigated structures with different Zr coordination	51
3.10 Proposed PSE mechanism in non-defective and defective UiO–66. MeOH facilitates ligand exchange through the creation and stabilization of defects. Enthalpy differences are given in kJ/mol at 313 K (PSE temperature)	53
3.11 Network of hydrogen bonds between acid, methanol, hydroxyl group and amino groups. a) reactive complex 8, b) an additional water molecule present in solution.	54
3.12 Schematic representation of solvent being inserted in the UiO–66 unit cell.	55
3.13 Top: schematic representation of the empty pore, pore with the solvent, and confined solvent without the material. Bottom: vibrational density of states obtained from the velocity autocorrelation function power spectra of selected atoms of the simulation. Bottom left: solvated material compared to the empty material. Bottom right: water in the pores compared to bulk water.	56

3.14 Radial distribution functions or pair correlation functions $g(r)$ between oxygen and hydrogen of water ($O(w)$, $H(w)$), and different atoms of the material obtained from the simulation with 80 water molecules in the unit cell. Full lines indicate the $g(r)$, dashed lines indicate its integral. Left panel: RDFs between water and linker carbons and hydrogens ($C(l)$, $H(l)$); middle panel: RDFs between water and oxygen atoms of the linkers and bricks ($O(l)$, $\mu_3\text{-OH}$, $\mu_3\text{-O}$); right panel: RDFs between water and zirconium atoms of defective and pristine bricks ($Zr(\text{def})$, $Zr(\text{pris})$)	57
3.15 Dynamic Brønsted acidity in one of the structures established on the active site in defective UiO-66 and liquid methanol in the pores.	59
3.16 Top: Ring configurations observed at site A and site B originating from the interaction between the Zr-bonded hydroxo and water and the solvent molecules. Bottom: Appearance of the various structures during the simulation. The frequency of occurrence of the different structures is also reported. A threshold of 2.2 Å for the donor-acceptor distance was chosen to determine a hydrogen bond and observations were smoothed over 0.5 ps.	60
3.17 Three snapshots of the molecular dynamics simulation which starts from a deprotonated site A and a protonated methanol molecule, with corresponding schematic representation of the process (above). 1) starting structure with protonated solvent 2) a snake-like chain of hydrogen bonds is formed which leads a proton to site B 3) site B is protonated, while site A is missing a proton.	61
3.18 Coordination numbers used in the simulation a: coordination number CN_W between zirconium and all water oxygens. Also the linker that shows dynamic movement which induces changes in the zirconium coordination number is visualized. b: coordination number CNL between each zirconium atom and linker oxygen atoms. n_{OW} and n_{OL} are the number of oxygen atoms considered in the two cases, r_i is the zirconium-oxygen distance, r_0 a cutoff distance of 2.9 Å. In yellow, the zirconium atoms considered in the CN. In green, the oxygen atoms that have a weight close to one and substantially different from zero in the summation.	62
3.19 Coordination and value of the CV during (a) the exchange of solvent and (b) linker decoordination in the MTD simulations. top paths: stepwise pathway which goes through undercoordinated zirconium; bottom paths: concerted pathways which go through overcoordinated zirconium.	63
3.20 Top: evolution of the collective variable CN_W and free energy profile for the first MTD simulation along the CV representing the coordination between the zirconium atom Zr1, highlighted in yellow, and all water molecules (green curve). CN_L between Zr1 and the neighbouring defect-bridging linker oxygen (red curve) is also monitored; bottom: snapshots on the linker decoordination triggered by overcoordination	64

3.21 Top: free energy profile for the first MTD simulation along the CV representing the coordination between two zirconium atoms and a linker, middle: evolution of the collective variable, bottom: snapshots of the linker decoordination	65
--	----

Part I

Towards modeling catalytic processes in UiO-66 metal-organic framework at operating conditions

this title has
the same as the

1

Introduction

In order for the wheel to turn, for life to be lived, impurities are needed, and the impurities of impurities in the soil, too, as is known, if it is to be fertile. – Primo Levi –

Catalysis, from Ancient Greek *κατά* (katá = “down”) and *λύω* (lúō = “loosen”), is at the heart of almost every industrially relevant chemical process. A catalyst intervenes in the reaction, allowing chemical species to come in contact and react with a specific mechanism, without being consumed. Outstanding catalysts do not only increase the rate of a given reaction, enabling processes that would not happen spontaneously, but can even be selective towards specific end products. Catalysts can be divided in homogeneous and heterogeneous, according to the phase where they are located with respect to the reactants. Homogeneous catalysts share the same phase with the reactants, and can be for instance molecules dissolved in a solvent, such as with organometallic compounds. These type of catalysts are used in many industrial processes, but have the drawback of being difficult to separate from the products, and in many cases separation is the most costly step in the catalytic cycle. For instance, in the case of biodiesel production, the recovery and purification of the products accounts for 60-80% of the whole cost [1].

Heterogeneous catalysts, on the other hand, are located in a different phase with respect to the reactants, and for this reason they have the advantage of being easily separable from the reaction products. Especially green chemistry can widely

benefit from heterogeneous catalysts, lowering the production costs and providing a viable alternative to petroleum [2]. Even if the name heterogeneous does not refer to a specific phase, industrially relevant heterogeneous catalysts are often in the solid phase. In order to exert their function, these materials must possess specific active sites that are easy to reach for the reactants, where these can adsorb, react, desorb, and ultimately diffuse back in the bulk to leave space for a new cycle. For these processes to occur, the number of active sites and the area of contact between the two phases (or surface area) must be sufficiently high, and reactants and products must be able to easily diffuse in the material.

All the above mentioned properties can be found in nanoporous materials, which possess pores with a diameter of <100 nm, and are extensively used in the field of heterogeneous catalysis. According to the classification by the International Union of Pure and Applied Chemistry (IUPAC) [3], they can be differentiated on the basis of their pore size into microporous (pore size <2 nm), mesoporous (pore size between 2 and 50 nm) and macroporous (pore size >50 nm). Their pore structure provides them with an exceptionally high surface area, that for some materials can reach values larger than $7000\text{ m}^2/\text{g}$ [4,5]. This facilitates diffusion of reactants inside the material, and allows shape selectivity to give specific products. Well-known classes of nanoporous materials include zeolites and metal organic frameworks (MOFs) [6]. Zeolites were one of first heterogeneous catalysts to be industrially exploited, and are the workhorses of petrochemistry, among other applications. They are extremely robust due to their inorganic nature and can withstand harsh reaction conditions. In contrast, MOFs are novel hybrid materials that are less robust, but extremely versatile. They possess even higher porosity, diverse composition, high metal content and tunable organic functions, and for these reasons they have a high catalytic potential.

In general, the study of solid heterogeneous catalysts is not trivial, as the exact concentration and nature of the active sites is often unknown. It is not always clear, in fact, where exactly the active sites may be located in the material, and how they interact with molecules. Moreover, these materials are far from perfect, and are often the defects which are tremendously important to induce the catalytic properties. In this sense, molecular modeling offers a complementary platform, not only to understand the catalytic function, but also to determine structure–activity relationships and to design structures to target specific applications [7].

1.1 Metal Organic Frameworks

MOFs are one of the most intriguing class of materials of current science. These materials, first called 'porous coordination polymers' (PCPs) were discovered in the late 50's, but only at the end of the past century with the works of Robson [8,9], Kitagawa [10,11], Yaghi [12] and Férey [13], the scientific community started to understand their full potential. At first the main focus of MOF research was in the

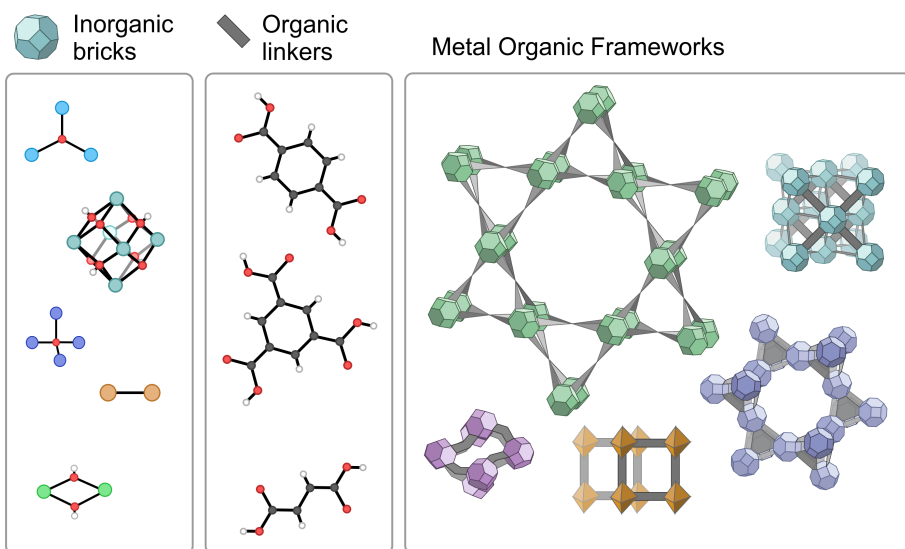


Figure 1.1: Schematic representation of the building block design in Metal-Organic Frameworks (MOFs). Left panel: some examples of inorganic bricks; middle panel: some examples of organic linkers; right panel: some MOFs with different topologies, pore size and shape

discovery of new structures. However, in the last few decades, the field has seen an incredible explosion in scientific and industrial interest, with new applications being continuously explored [14]. MOFs are hybrid nanoporous materials that are composed by metal or metal–oxo clusters connected by multtopic organic linkers, to form multidimensional pore structures. Compared to the already well-known zeolites, MOFs can be constructed without templating agents, with a far greater number of metals and with an exceptional structural diversity. In fact, their particular building block design (Fig. 1.1), that makes use of secondary building units (SBUs), allows the creation of an almost infinite number of crystalline structures with different topology and chemical composition. The coordination bonds which lie at the basis of MOF structures are weaker than the inorganic zeolites. This on the one hand makes them less robust, but on the other allows facile structural modifications which are impossible to do on zeolites. In principle, the nature of the SBUs and their association can be finetuned [15], allowing control of properties such as pore shape and size, functionalization, or surface area. The response to chemical and physical stimuli can this way be easily modulated [16, 17]. One of the most intriguing concepts is the isoreticular synthesis, by which inorganic or organic SBUs can be replaced by topologically identical (or similar) building blocks. This way, starting from a given MOF precursor, whole families of MOF materials can be synthesized spanning a range of pore size and functionality. For instance, the pore size can be significantly increased up to the mesoporous range by using longer isoreticular linkers, such as in the IRMOF series, based on the MOF-5

precursor [18].

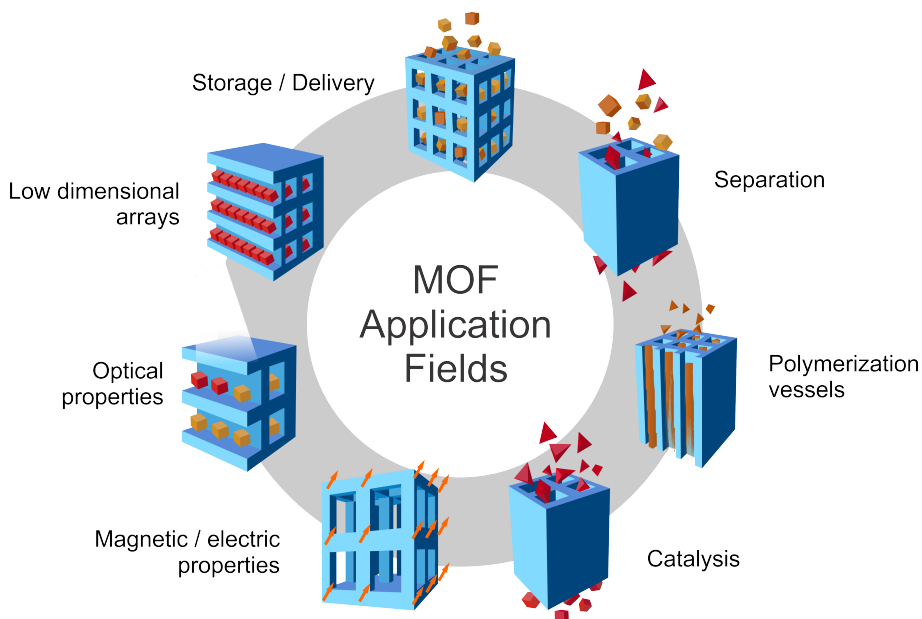


Figure 1.2: Schematic representation of some of the numerous MOF applications.

The tunability of MOF structures, along with their high crystallinity, metal content and porosity, are very appealing for application in different industrially relevant fields, such as catalysis, gas storage and separation, drug delivery or sensing, as displayed in Fig. 1.2. More specific applications are being further explored, such as warfare agents decomposition, magnetic applications, or membrane separation [14].

Defects

MOFs are crystalline materials, but they are not perfect, and possess structural disorder. Defect-containing MOFs have become an active field in MOF research, as defect sites can play a key role in the performance of the material. Following the classification proposed by Sholl *et al.* [19], these defective sites in MOFs can be either point vacancies (such as missing linkers or clusters) or extended ones. Fang *et al.* [20] further divide extended defects into dislocations, planar defects, and micro- and mesoscale volume defects.

Common experimental strategies for the characterization of defects in MOFs involve electron and fluorescence microscopy, Raman, infrared and X-ray spectroscopy, power and single-crystal X-ray diffraction.

At low defect concentration, a random distribution of isolated point defects can be found, whereas at higher concentrations clustering could occur [21], if the

presence of a vacancy is influenced by other vacancies in proximity. This complexity makes the study of defective sites and disorder a current challenge in MOF research. In particular, the control of their effect on specific properties is heavily limited if their location, type and dispersion are unknown. This randomness can be partially limited by judicious defect engineering during and post-synthesis. In order to identify and characterize defects in MOFs, it is particularly important to obtain atomic scale resolution on the defect sites and understand how they impact certain properties.

MOFs as single site catalysts

After the discovery of MOFs, with their tunability and ease in functionalization, the study of their application in catalysis followed naturally, and after adsorption was one of the earliest documented applications [22]. Their high porosity, in particular, allows chemical species to diffuse in the pores and access the active sites, and the high metal content offers the possibility to have many guest interactions sites. In this sense, provided the structures are stable at reaction conditions (i.e. no leaking is observed), MOFs can be considered true single-site heterogeneous catalysts, that contain well-defined active sites which are inherent part of the framework [23]. According to the classification proposed by Rogge *et al.*, we can distinguish between three types of single-site catalysts in nanoporous materials, in which active sites for catalysis can arise from coordinatively unsaturated metals (type I), metal atoms embedded in porphyrin-based ligands (type II) or reactive functional groups (type III). **Unsaturated metal sites of type I are the focus of this thesis. A plethora of MOFs has been synthesized possessing unsaturated metal sites within the pores which offer different Lewis acidity.**

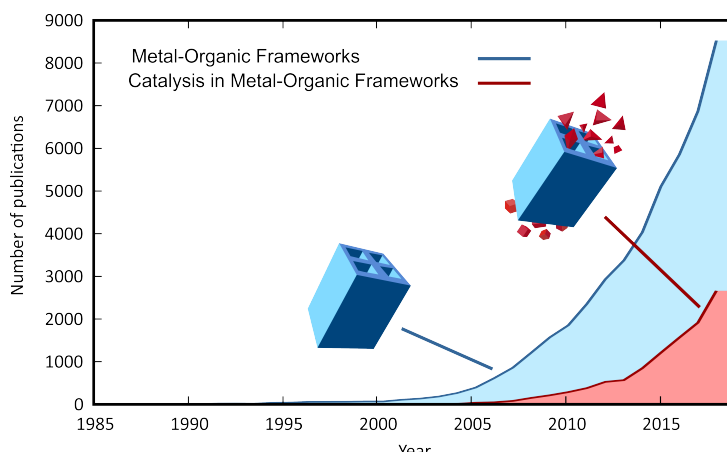


Figure 1.3: Number of publications on MOFs and catalysis in MOFs in years 1985-2018, showing the importance of catalysis in MOFs as indicated by Web of Science

Post-synthetic modification

When it is not possible to introduce functionalities with direct synthesis, post-synthetic modification (PSM) [24] has become a well established procedure that allows the preparation of MOF materials with specific chemical composition. Via this technique, it is possible to modify the crystal after the synthesis, allowing to finetune the properties of the material. Moreover, multi-functional sites can be integrated at the same time in the crystals [25]. PSMs include encapsulation of guest molecules or nanoparticles in the pores, modifications of the linkers without breaking the metal-ligand bond, or post synthetic exchange (PSE) of linkers and metals, where building blocks are dynamically exchanged. PSE can also involve terminal ligands, or modulators, that do not contribute in connecting different bricks. This way, building blocks can be exchanged, but also eliminated to create vacancies, provided the material retains its stability. For this reason, PSM has been used as an efficient strategy to introduce defective sites in MOFs.

Stability

In general, to function at operating conditions, materials need to retain their thermal, mechanical and chemical stability at those conditions. For instance, mechanical stability is needed when compressing MOF in pellets or other shapes for industrial processes [26], while chemical stability is crucial for any application, such as drug delivery, molecular separation, or catalysis [27]. Catalysis often also requires thermal stability, as the materials must be able to resist harsher conditions for certain processes such as in petrochemistry. However, the metal-ligand coordination bond that makes MOFs so tunable is also regarded as one of their main drawbacks [28–30], as it is responsible for the lower structural stability when compared to already established nanoporous catalysts such as zeolites. For example, the first synthesized MOFs such as Cu_2^+ trimesate HKUST-1, or MOF-5, composed by Zn_2^+ clusters and BDC linkers were degraded by water even at mild conditions [31–34].

Following the nomenclature proposed by Kitagawa, we can differentiate between three generations of MOFs [35]. First generation MOFs are defined as having a guest-molecules supported pore system that collapses when these are evacuated. For this reason, this first generation of MOFs found very limited use for practical applications. Those of second generation are more robust and have permanent porosity, that is retained even in absence of guest molecules. These materials show high potential for catalysis and other applications and are the main object of this dissertation. Finally, third generation MOFs are characterized by flexible pores that can reversibly change shape with the presence of guest molecules, or upon certain stimuli, such as temperature or pressure. Matsuka et al. [36] identified five types of response mechanisms in MOFs, denoted as shrinking, expanding, reshaping,

swelling and gate opening or closing. A perspective on the types of stimuli that can induce responsive in MOFs has been reported in the work of Coudert [37].

Zr-based MOFs

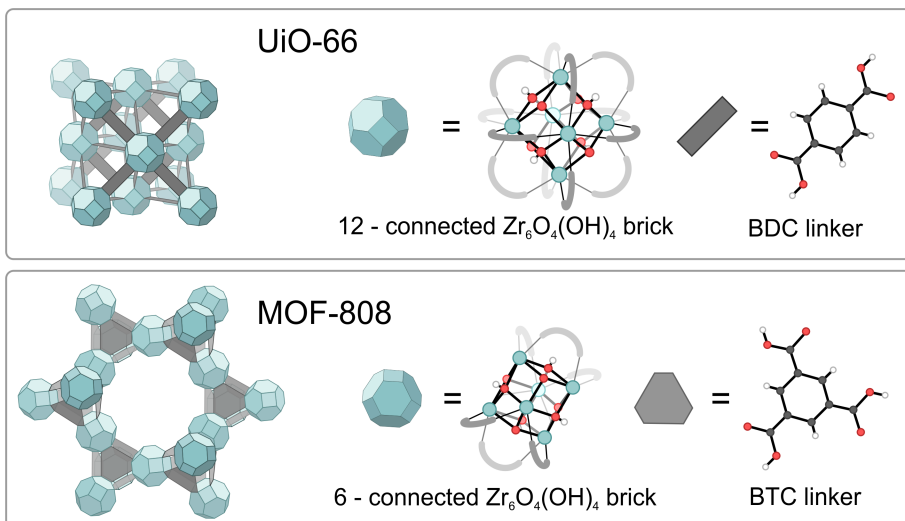


Figure 1.4: Structure of UiO-66 (top) and MOF-808 (bottom), the two Zr-MOFs investigated in this work of thesis.

Recently, a class of robust MOFs have been synthesized showing an unprecedented stability [38]. Zr-based MOFs [39] which exploit the robustness of the Zr–O bond, show an outstanding stability and are at present time one of the most studied classes of MOFs. Moreover, zirconium is an ubiquitous metal that is present in biological systems and has low toxicity, as well as limited cost. This makes these materials particularly promising for applications in catalysis, gas sorption, and drug delivery. An overview of the plethora of possible structures that can be synthesized with different inorganic SBUs can be found in a recent review by Bai *et al.* [39].

The vast majority of these materials is characterized by Zr(IV) atoms in a high coordination state (Fig. 1.4), which interact strongly with the oxygens of carboxylate linkers of various topology. These MOFs are characterized by a $\text{Zr}_6\text{O}_4(\text{OH})_4$ cluster in which each of the 6 zirconium atoms is connected to 4 oxygen atoms (two $\mu_3\text{--OH}$ and two $\mu_3\text{--O}$), each of which is in turn connected to three zirconium atoms, forming a polyhedron. Each zirconium atom can form 4 other bonds with ligands, accommodating up to 24 metal–ligand bonds per cluster. Every zirconium atom can therefore form a total of 8 coordination bonds oriented in a square–antiprismatic geometry, yielding a rich range of possible structures that can be synthesized with connectivity ranging from 12, as in UiO-66 [40], to 6

which is found in MOF-808 [38] (see Fig. 1.4). The dual Lewis acid/base nature of the Zr–carboxylate bonds, along with the high metal oxidation state, gives rise to strong interactions between the SBUs, thus allowing processes such as PSM without compromising the stability of the structures. The stability of Zr-based MOFs depends on the connectivity between the inorganic and organic SBUs, as well as the number of M–L bonds that are present in the structure [39]. However, open metal sites in these materials are present only when the connectivity of the linkers is less than 12. Zirconium atoms that remain undercoordinated in these materials are Lewis acid sites where reactants can adsorb and that can function as catalytic centers.

UiO–66

The first material belonging to this class of Zr-based MOFs is the Zr–thephthalate based UiO–66, and was first synthesized at the Universitet i Oslo (UiO) by Lillerud and coworkers [40]. This UiO–66 material is one of the most studied MOFs thus far and was an inspiration of other MOFs within this family. UiO–66 is characterized by an extremely high connectivity that gives rise to an exceptional structural stability. In this material, each Zr_6 SBU is connected to 12 thephthalate (or benzenedicarboxylate (BDC)) linkers forming a cubic close packed structure with a space group $F\bar{m}3m$, No. 225. In this structure there are two different cavities of octahedral and tetrahedral shape, with window sizes of 10 Å and 25 Å, respectively. Each octahedral cage shares triangular windows with eight tetrahedral cages. This results in an extremely robust material which is stable up to 648 K and in a broad range of protic and aprotic solvents and pH conditions. Moreover, the $Zr_6O_4(OH)_4$ bricks can be reversibly dehydrated upon thermal treatment at temperatures between 523 and 573 K. Up to two water molecules can be formed this way, yielding a Zr_6O_6 brick, where the zirconium atoms have a coordination of 7 [41].

A whole family of isoreticular MOFs can be derived from UiO–66 by using linkers of different size, spanning from fumaric acid [42] up to terphenyldicarboxylic acid [43], allowing to significantly tune pore size and surface area. Interpenetrated MOFs with UiO–66 topology have been also reported if longer linkers are used [44], with a decrease in surface area. Moreover, different functional groups can be appended to the phenyl rings, such as bromo, amino, nitro, or naphthalene. Garibay and Cohen showed that UiO–66–NH₂ can be further modified to yield new functionalized frameworks [45]. Also the inorganic SBUs can be modified, for instance introducing titanium or hafnium [46]. The exceptional thermal and chemical stability of UiO–66, along with its high connectivity, allows all these modifications of the structure, and for this reason, this material is often considered as a perfect MOF archetype, where new techniques can be tested.

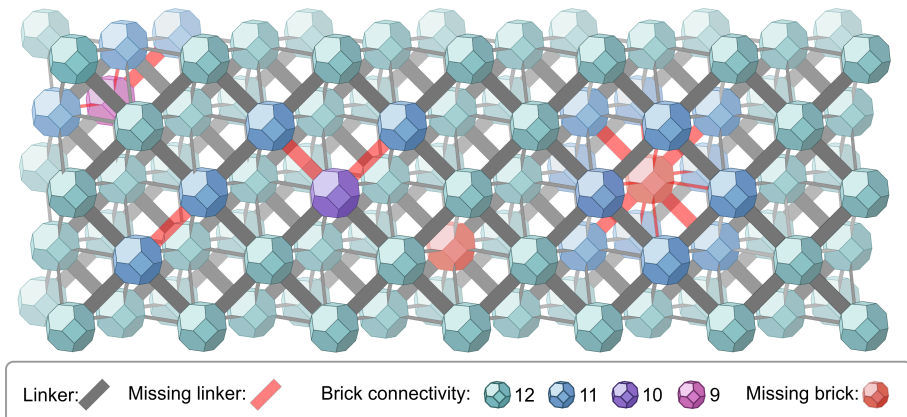


Figure 1.5: Representation of the UiO-66 material with missing linkers and clusters displayed in red. In this dissertation, we mainly focus on missing linkers.

Defects on UiO-66

revise this sentences

The perfect crystalline UiO-66 structure, where every zirconium atom is 8-fold coordinated, does not possess undercoordinated Lewis acid sites available for catalysis. However, it became clear that the synthesized UiO-66 showed a behavior that deviated from the theory and pointed towards the presence of defective sites. Different indications of the presence of defects were observed, such as symmetry-forbidden reflections in the PXRD pattern, metal-linker ratio obtained by thermogravimetric analysis (TGA), higher than expected surface area, appearance of O-H stretching bands in the FTIR spectrum etc. [41, 47]. It has been generally accepted that the material contains defects in the form of missing linkers or clusters (Fig. 1.5), and that these are not only naturally occurring during synthesis, but their number can easily be tuned by adapting the synthesis conditions, such as temperature and type of modulator [48, 49].

Defects can influence the material properties to a large extent. The beneficial role of defects in UiO-66 has been explored in many applications such as gas storage and separation [48, 50], sensing [51], drug delivery [52] and catalysis [53, 54].

The physical properties of defective UiO-66 differ according to the number of defects and their location, as has been extensively studied both theoretically and experimentally [21, 55–57]. A decrease in the connectivity in the structure will naturally lead to a decrease in stability of the material. However, the extremely high connectivity of UiO-66 allows the presence of numerous missing linkers or cluster without loss of crystallinity. In this context, Rogge et al. investigated the influence of all possible configurations of one to two linker vacancies on the stability of UiO-66. The equilibrium volume is not affected by such vacancies,

however properties such as bulk modulus and loss-of-crystallinity pressure, which in turn influence the stability, are affected by the number and configuration of missing linkers [55]. De Vos et al. [56] investigated the electronic properties for all possible configuration of defective UiO–66 with up to three missing linkers, showing that some configurations are energetically more stable than others, and that the number and position of missing linkers affect the band gap of the material. From these studies performed on small unit cells, it is already clear that the number of possible defective configurations can be extremely high, and it is still unclear to what extent such point defects are disordered in the material. A regular distribution of point defects that involve missing clusters can lead to different phases in the material, from fcu (non-defective), to bcu (missing linkers with open channels), reo (missing clusters) to scu (missing linkers and missing clusters). Missing clusters could in principle increase the catalytic activity of the material more than missing linkers due to the larger pore size. Recently, Cliffe et al. [21] showed in a combined theoretical-experimental work that missing clusters on UiO-66(Hf) were correlated and formed nanodomains in the material, characterized by a reo phase. This work shed light into the complexity of modeling disorder in nanoporous materials.

Active sites for catalysis in UiO–66

One of the breakthroughs of MOF research was the discovery that UiO–66 could contain a high number of open metal sites. As reported earlier, active sites for catalysis in UiO–66 and other Zr–MOFs are present when the zirconium connectivity is decreased from its equilibrium value of 8.

A first way to obtain coordinatively unsaturated zirconium sites is by creation of defects, in the form of missing linkers or clusters. The inherent vacancies in UiO–66 bring unsaturated zirconium Lewis acid sites [47, 48, 53, 58, 59] and at the same time enhance the accessibility of the reactants to the active sites as the pore volume increases. The synthesis of defective UiO–66 can be tuned via modulators such as formic acid or trifluoroacetic acid (TFA), that are competing with BDC linkers in binding to the inorganic SBU. Vermoortele et al. first showed in a dual computational–experimental study that the Lewis catalyzed cyclization of citronellal requires missing linkers [60]. For Meerwein reduction, another Lewis catalyzed reaction, the catalytic activity of UiO–66 could be significantly increased by making use of TFA, that introduced a large number of linker vacancies. Additionally, the non-modulated material that contained only a small number of defects showed nearly no catalytic activity [53]. Such relationship between catalytic activity and amount of defects has been reported for different Lewis catalyzed reactions giving clear evidence that the catalytic centers are located on the defective sites [53, 60].

The molecular characterization of the defective sites on UiO–66 has been an ongoing research interest in MOF literature. Lillerud and coworkers [61] reported that when linker vacancies were present, XRD characterization of the material

showed two type of Zr–bonded oxygen atoms. The first type was BDC oxygen, and the other was associated to water species coordinated to the zirconium on the defect site. Later from SXRD measurements, the group of Yaghi [62] proposed that the two Zr–bonded oxygens belonged to physisorbed water molecules and that the charge compensating species was a hydroxyl group. However, further work did not confirm such configuration. Molecular simulations were essential to shed light into the detailed molecular structure of the defective brick. Ling and Slater [63] performed MD simulations starting from the configuration proposed by Yaghi and showed a progressive stabilization towards another structure where the two adjacent zirconium atoms were coordinated to a physisorbed water molecule and a hydroxyl group, as shown in Fig. 1.6. These sites have been confirmed by a comprehensive computational study of different adsorption possibilities of up to three water molecules on defective UiO–66 performed by Vandichel et al. [64] and by simulations performed in this work of thesis. Such water and hydroxy species are strongly interacting with the zirconium atoms and are sources of Brønsted sites, as indicated in Fig. 1.6. It was remarkable to discover that some catalytic processes are not catalyzed by undercoordinated Lewis acid sites, but need also Brønsted sites arising from defect–coordinating species, as will be shown in **PAPER I**. Serre and coworkers reported that a hydrogen bonded network that spans the octahedral and tetrahedral cages is responsible for the high proton conductivity showed by UiO–66 at high temperatures [57]. Kitagawa et al. showed the positive role of defects in proton conductivity in the UiO–66 material, as defective sites provide both larger pores and zirconium undercoordinated sites where water species are adsorbed and can function as proton donors [65]. Farha and coworkers identified three types of acidic protons in the material by means of potentiometric titration: $\mu_3\text{--OH}$ belonging to the inorganic SBU, and two arising from subsequent deprotonation of the physisorbed water and hydroxyl group on the defective site. They made use of the acidic protons belonging to physisorbed water for a quantification of defects in the material [66]. The mechanism associated to the change in topology of the hydroxyl groups on the inorganic SBU has been investigated by Yang et al. [67]. The interaction between defect–coordinating water molecules and zirconium atoms is strong, and UiO–66 can be partially hydrolized [68] while retaining its stability, as will be further discussed in this dissertation.

The defect–coordinating species can be removed by thermal activation at $T > 423$ K (more information on this process is given in **PAPER I**). The more loosely bonded physisorbed water is the first to leave the defective site, followed by the chemisorbed water. The dehydrated active site obtained this way is missing a $\mu_3\text{--OH}$ proton and has two 7-fold coordinated zirconium open metal sites as shown in Fig. 1.6.

The second activation process by which open metal sites can be created on UiO–66 is the reversible dehydration of the $\text{Zr}_6\text{O}_4(\text{OH})_4$ cornerstone to obtain Zr_6O_6 by removal of up to two water molecules performed at a temperature range between

523 and 573 K [41]. In this case also 7-fold coordinated zirconium atoms are created and may take the role as Lewis active sites, however the increase in pore size due to linker vacancies does not occur, and the active sites are less accessible than in the defective material.

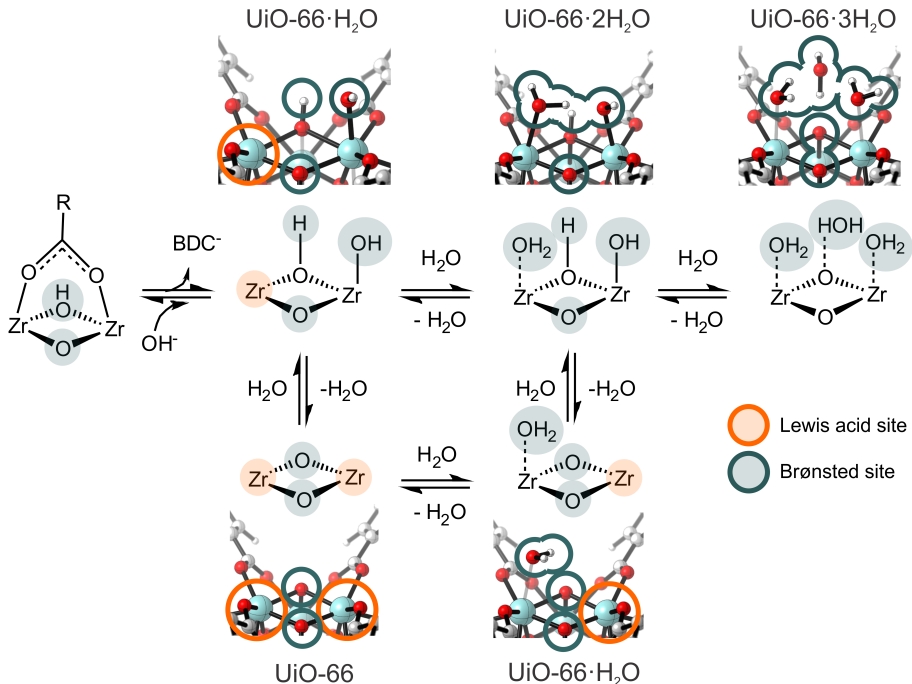


Figure 1.6: Lewis and Brønsted sites that are created when a linker is removed from the UiO-66 zirconium brick, with different number of coordinated water molecules.

Functionalization

As anticipated earlier, the nature of the active sites can also be influenced by linker functionalization [69–71]. The presence of electron-donating substituents showed an increase in catalytic activity for jasminaldehyde condensation [72]. A positive effect of electron-withdrawing group was found by the same authors for Lewis catalyzed citronellal cyclization [60]. The beneficial role of amino groups was reported as well by Timofeeva et al. [73] for acetylation of benzaldehyde, as well as by Cirujano et al [74,75] for esterification. The electron donating effect of amino groups would in principle lead to a decrease in the Lewis acidity of the defective zirconium atoms, lowering the reaction rate. Therefore, a change in mechanism in the presence of BDC-NH₂ was hypothesized. However, Hajek et al. further studied aldol condensation in a computational work [76], and reported a beneficial, but

passive role of amino groups, which is further confirmed in **PAPER I** for Fischer esterification.

Active sites on MOF-808

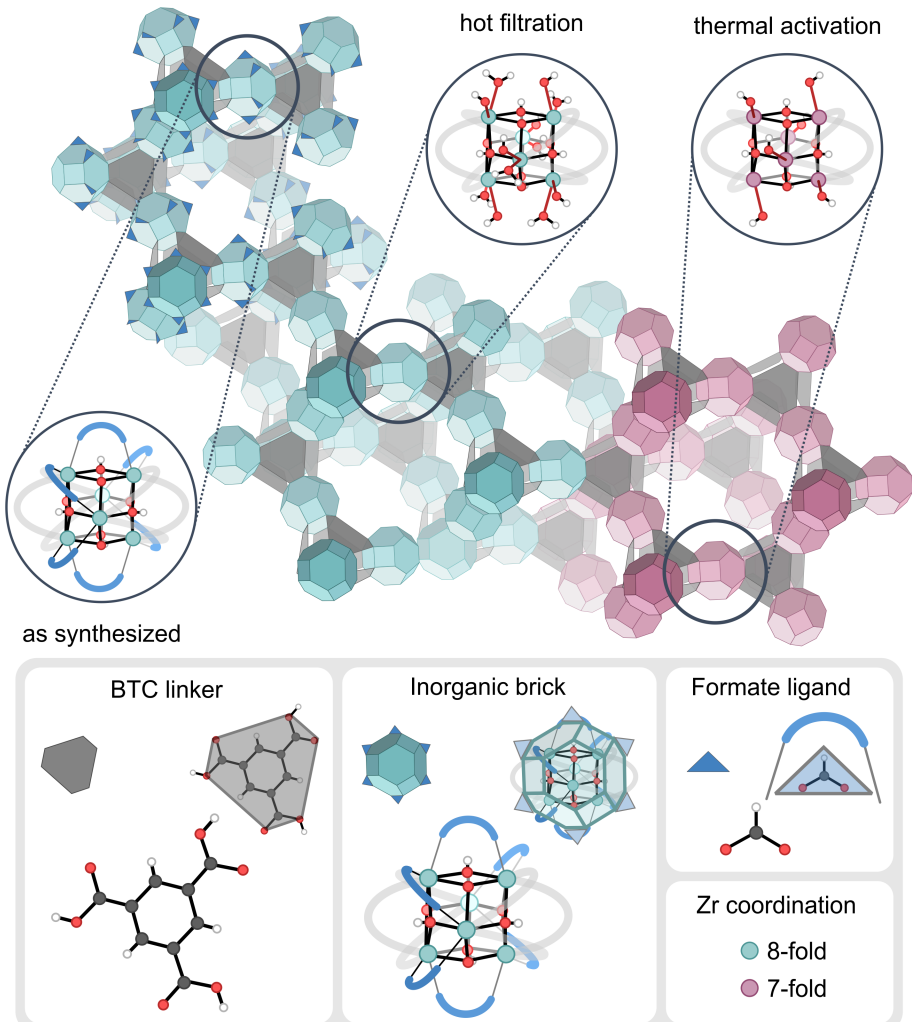


Figure 1.7: Schematic representation of as synthesized and upon activation MOF-808 structures

MOF-808, formed by the inorganic $\text{Zr}_6\text{O}_4(\text{OH})_4$ cornestone and trimesate (BTC) linkers, represent the least connected MOF in the Zr-MOF family [38], and its brick can be regarded as an extreme case of the defective UiO-66. The rigid BTC tritopic linkers stabilize the structure and yield exceptionally wide channels which are required for the diffusion of substrates. The octahedral crystals contain

6 BTC linkers per inorganic node and are characterized by a *spn* topology. In the material, each zirconium atom is bonded to four oxygens from the inorganic brick and two oxygens from the BTC linkers. The other two bonds that are needed to reach the total coordination of 8 are provided by species present in solution that do not contribute to the framework connectivity.

In the as-synthesized material, the zirconium atoms are capped with the relative mobile formate modulator. The material at this stage does not contain catalytically active sites and must be activated by post-synthetic treatment. By hot filtration, the formate groups can be eliminated and replaced by water and hydroxyl groups. In the catalytically active material, each brick is connected to six BTC linkers, six water molecules and six hydroxyl groups, and possesses a high number of potential Brønsted sites. Klet et al. report the presence of four different types of protons in the material [66]. Lewis acid sites can be created by thermal activation, similarly as in UiO-66. In this case, hydroxyl groups remain connected to the zirconium atoms and the material possesses both Lewis and Brønsted sites. The hydroxyl groups could also be used as anchors to incorporate new features, for instance by molecular docking of a single-site catalyst to immobilize it on a MOF-scaffold. MOF-808 is a promising catalyst that is still less studied than UiO-66, but has a lot of potential for possible applications. For instance, it shows a higher catalytic activity for certain Lewis catalyzed reactions, such as Meerwein-Ponndorf-Verley (MPV) reduction [77, 78]. Moreover, MOF-808 represents the first evidence of a superacid in MOFs, showing superacidity after post-synthetic treatment with sulfuric acid [79].

1.2 Outline and goal of the thesis

In this chapter, the main characteristics of MOFs making them appealing for catalysis have been introduced, as well as the current challenges that MOF research is facing. The properties of catalytically active sites on defective UiO-66 and MOF-808 were studied by means of molecular modeling techniques. Molecular modeling can give fundamental insight into the properties of MOFs, and at present time a plethora of different techniques are available for this purpose. To model processes in MOFs, knowledge of both power and limitations of these methods and experimental insight into the scientific question are required to find the appropriate combination of techniques.

This PhD thesis is organized as follows:

- In Chapter 2, a condensed theoretical overview of current molecular modeling techniques within MOF research is given. Particular attention is drawn on how these techniques can be applied to obtain insight into structural and catalytic properties at operating conditions.

- In Chapter 3, the main results of this PhD thesis are summarized. The links between theory and experiment are highlighted throughout the chapter. All results are the result of fruitful experimental and theoretical collaborations and have been published in international peer-reviewed journals.
- In Chapter 4, the main conclusions of this thesis work, as well as perspectives on future research are given.

2

Modeling metal organic frameworks

We are reaching the stage where the problems we must solve are going to become insoluble without computers. I do not fear computers. I fear the lack of them. – Isaac Asimov –

The understanding of catalytic processes in MOFs is a very challenging task. MOFs are materials of complex nature, and reactive processes in these materials are elusive and difficult to track on a purely experimental basis. Molecular simulations offer an alternative approach that starts from the construction of models that can explain, complement, and predict experiments. With growing computational power, computational models can aim at giving a more and more accurate description of materials at operating conditions, narrowing the gap between theory and experiment. Often, the structural properties and chemical transformations that take place on the active sites need to be investigated using a combination of multiple computational techniques, and the problems need to be tackled from different angles. In this chapter, an overview of the different computational methods that can be used to study reactive processes in MOFs will be given.

2.1 Framework topology

A crucial decision when performing simulations lies in the choice of the model system, and what should be included in it. When choosing a model to represent

the system under study, there is always a fine balance between accuracy and computational cost. On the one hand, it is crucial to use a computational model that captures all the relevant properties of the material and mimics the experimental structure as closely as possible. On the other, it is often convenient to approximate and neglect certain properties in favor of a larger scale description of the processes. The focus in this work are the active sites that can be used for catalysis, therefore an accurate electronic description of this region of the material is imperative. Nevertheless, the activity of these sites for chemical reactions can also be influenced by other factors, such as the pore size or functionalization. Therefore, to describe active sites in MOFs and other nanoporous materials, which can have rather large unit cells and non-periodic structural defects, the first question that needs to be asked is how to account for periodicity. Two conceptually different approaches can be used as shown below.

Extended cluster model

A very computationally efficient approach consists in neglecting periodicity and extracting a finite cluster of atoms from the periodic structure. This cluster model, displayed in Fig. 2.1, contains the active sites and their surroundings but consists in a limited number of atoms, allowing to substantially decrease the computational cost. This allows both a more accurate treatment of the electronic structure, and a screening of different possible geometrical configurations of adsorbates, which is useful in the search for transition states (TS). Moreover, very efficient TS searching algorithms have been developed for such systems in Gaussian, the most widely used code for cluster calculations. When extracting a cluster, particular attention has to be drawn to the termination of bonds and the charge compensation, that have to be done in the most realistic way. The rest of the crystal structure does not surround the external cluster atoms. Some of these atoms need to be fixed in order to mimic the periodic environment and prevent nonphysical deformations that would affect an estimation of the entropy [80].

Cluster calculations are an excellent way to benchmark and perform a first qualitative screening of reactions and possible configurations and have been for long the standard computational tool when studying reaction in nanoporous materials. However, they are not adequate to correctly describe complex reactive processes, where confinement effect of the pores and structural rearrangements can play an important role. The role of solvent in the pores can also be crucial for the outcome of a reaction and cannot be explicitly studied by cluster models. Periodic calculations resolve this shortcoming, and as computational power grows, the heterogeneous catalysis community is shifting towards these more expensive, however more accurate models.

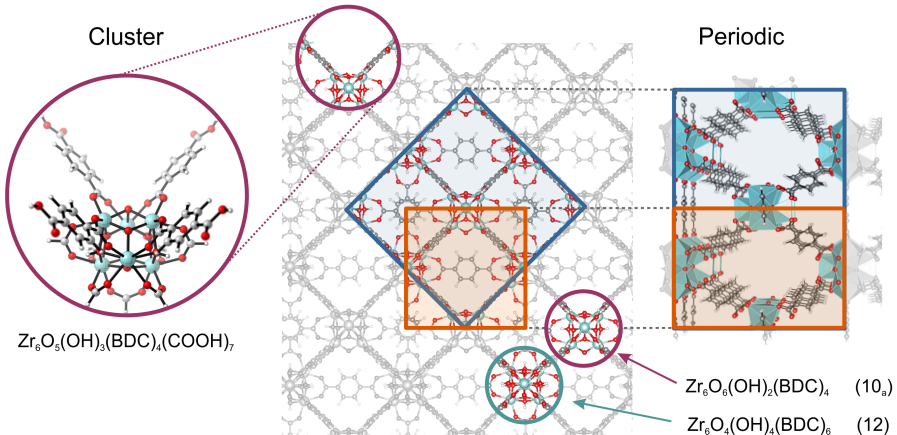


Figure 2.1: Left: extended cluster model cut from the periodic structure of UiO-66. The cluster contains the active site, the brick and the linkers in the closest proximity to the active site. Right: representation of the unit cells containing the defect. In blue, the conventional 4-brick unit cell, in orange, the 2-brick unit cell used for the calculations. The two different bricks are highlighted in orange. The 10-fold coordinated brick has two terephthalate linkers missing.

Periodic model

Periodic models, that fully take into account the periodicity of the crystal, enable to describe the whole topology of the framework. These calculations make use of periodic boundary conditions (PBC), which allow to simulate bulk phases with a limited number of atoms. In this model, the unit cell is replicated infinite times in each direction. When one atom disappears from one side of the unit cell it will reappear on the opposite side and each atom interacts with its neighbors in the same unit cell but also in the adjacent ones. Spurious interactions between the atoms can be avoided by applying a *minimum image convention*, for which each atom interacts with its nearest neighbor or periodic image. In the case of long range interactions, such as the electrostatic ones, other techniques need to be used, such as Ewald summation [81], where the potential is divided into a short range contribution, calculated in real space, and a long range contribution, calculated in reciprocal space using a Fourier transform.

In the case of UiO-66, the conventional unit cell [40] contains 4 zirconium bricks (Fig. 2.2, blue). In the calculations of this thesis, BDC linkers have been removed from the unit cell to introduce defects which are active sites in catalysis. Different amounts of missing linkers with different topologies have been considered 2.2. An interesting topology is the one denoted as type 6 in the work of Rogge et al. [54] that is characterized by a channel which offers good perspectives for the diffusion of guest molecules. This unit cell (displayed in blue in Fig. 2.2) can be

reduced by symmetry to a 2-brick unit cell (in orange, Figure 2.1) which offers the best compromise between accuracy and computational cost. This reduced unit cell is used in most of the calculations performed in this thesis. In **PAPER I** we show that for catalytic purposes, the free energy differences calculated for the same chemical processes on the two unit cells is negligible, therefore the 2-brick unit cell represents a good model system. When modeling disorder, however, periodicity decreases and bigger unit cells have to be taken into account. For this reason, in **PAPER IV**, we studied defective 4-bricks unit cell with missing linkers ranging from zero to three.

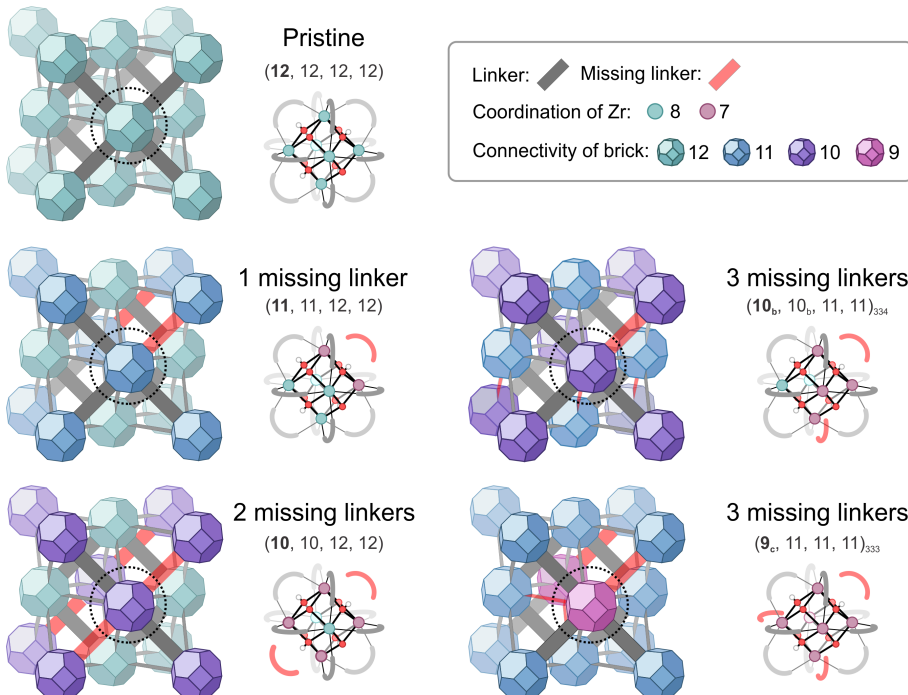


Figure 2.2: Representation of the different ways to remove up to three linkers from a 4-brick UiO-66 unit cell

2.2 Theoretical methods

Electronic energy methods

A basic quantity to study any chemical or physical transformation is the potential energy surface (PES), which is a function of the coordinates of all the atoms of the system. The PES is always the reference quantity in our simulations and every atomic configuration can be represented as a point in this hypersurface, with a given value of potential energy (Figure 2.3).

Ideally, by calculating the value of the PES for each atomic configuration we can obtain all information on the system and on the transformations that can occur. However, the complexity of this surface escalates quickly with the number of atoms, and the sampling of its relevant regions represents the main challenge of molecular simulations. The information gained by exploring the PES is tightly connected to the experimental observables. Statistical physics acts like a bridge between the microscopic insight that is gained through molecular simulations and the macroscopic properties which are measured experimentally. In principle, all macroscopic properties of a system can be derived from its wavefunction. To calculate it, the stationary Schrödinger equation is solved:

$$\hat{H} |\psi\rangle = E |\psi\rangle$$

where ψ is the wavefunction, \hat{H} is the Hamiltonian of the system, and E is the total energy. The resolution of this equation is at the heart of computational chemistry and will in principle provide the exact description of matter, but it is nevertheless extremely difficult to solve for most of the electron systems. The presence of electron–electron interactions makes it a highly coordinated problem, and for this reason, different approximations need to be applied, to remove the interactions that have a minimal contribution to the energy.

Born–Oppenheimer approximation

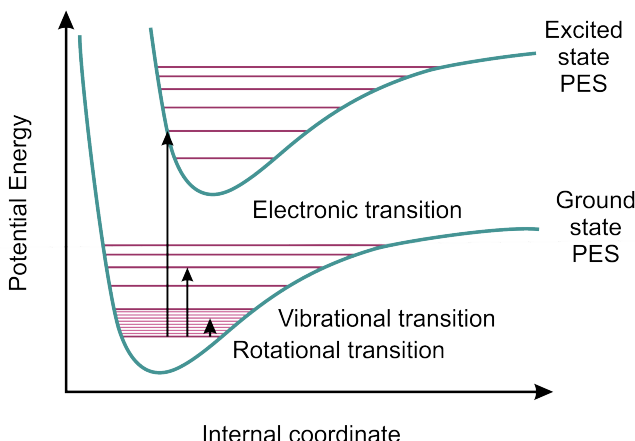


Figure 2.3: The two lowest PES in the BO approximation for a diatomic molecule. In blue, the electronic PES for the ground state and first electronic excited state (UV–Vis transitions). In orange, the vibrational energy levels (IR transitions), in grey the rotational levels (microwave transitions).

For all calculations performed in this work, we rely on the so-called Born–Oppenheimer (BO) approximation [82]. In this treatment, nuclei are considered

as classical points which move in the potential energy surface generated by the electrons (Figure 2.3). This way, to each nuclear configuration a corresponding electronic energy can be assigned, and nuclear coordinates enter in the Schrödinger equation only as parameters, allowing to construct a BO surface, or PES. This approximation holds since nuclei are much slower than electrons, therefore the motion of electrons is instantaneous from the nuclei point of view. This approximation does not always hold, especially when dealing with light nuclei such as hydrogen. In these cases, nuclear quantum effects can have an impact on the measured properties [83]. In most cases, the electronic ground state is also not interacting with the higher electronic states because of the high energy difference. In the BO approximation, the electronic energy levels are also considered fully separated and do not interact with each other. For this reason, the approximation is also called adiabatic approximation. Additional interactions have to be considered when two surfaces lie close to each other, for instance in the neighborhood of conical intersections.

Force Fields

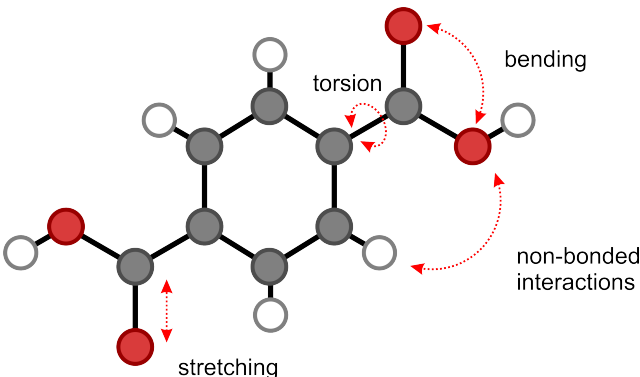


Figure 2.4: Representation of some of the molecular modes taken into account in a generic force field model.

The simplest way to describe interactions between atoms which determine the PES is the so-called “balls and springs” model. In this treatment, all interactions are represented by interatomic classical potentials which are parametrized to reproduce the results of more accurate quantum mechanical calculations. In this work, generic force field calculations have been used in some cases to give preliminary input structures for more costly *ab initio* calculations, through which the description of chemical transformations is possible. Force fields are often constituted by harmonic potentials which do not allow bonds being broken and formed (Figure 2.4). Reactive force fields, such as ReaxFF [84] are currently being developed, but their application in complex heterogeneous reactions is still an ongoing chemical challenge and is out of the scope of this work. For this reason, the description of

reactive processes needs a more advanced treatment, where electronic distributions are explicitly taken into account.

Density Functional Theory

Density functional theory (DFT) has become the method of choice for the study of chemical systems, due to its good trade-off between computational cost and accuracy of the obtained results. DFT began in the 1920's with the work of Thomas and Fermi [85, 86], but it was only in the '60s that it became a complete and accurate theory, shown in the work of Kohn, Hohenberg and Sham [87]. The fundamental property that DFT describes is electron density as opposed to many body electron wavefunctions, which allows to reduce enormously the number of variables in the case of complex systems. Two fundamental theorems by Hohenberg and Kohn state that there is a unique relation between electronic density and total wavefunction, therefore the ground state density allows us to determine all properties of the system. Moreover, the ground state density can be obtained from a minimization of the total energy functional with a variational method by solving the so-called Kohn–Sham equations. The global minimum value of the functional determines the exact ground state of the system. This way it is possible to obtain the total energy of the system and the forces which act on the atoms, two quantities which are needed in all the simulations performed in this work.

In principle, DFT is an exact method, but the minimization of energy is far from trivial. Kohn and Sham [88] introduced a method which replaces the many-body problem with an auxiliary system of non-interacting particles, allowing a fast solution of the eigenvalue problem. What needs to be added in this treatment is an additional functional which describes exchange and correlation. Nowadays one of the greatest challenges in DFT consists in the search for an accurate expression for the exchange–correlation functional. The simplest method is known as Local Density Approximation (LDA) initially proposed by Kohn and Sham [88] and can also be adapted to include spin in the Local Spin Density Approximation (LSDA) [89]. A more refined method is the Generalized Gradient Approximation (GGA) which involves the calculation of the gradient of electron density and includes functionals such as B88 [90], LYP [91] and PBE [92, 93], used in this thesis. More recent functionals are the so-called hybrid functionals, which include the Hartree–Fock (HF) exchange, such as B3LYP [90, 91, 94], which is a combination of B88, LYP and LDA with HF, and PBE0 [95], which mixes PBE with HF. These functionals can give a more accurate electronic description of the system but are computationally very expensive. As compromise between accuracy and computational cost is a geometry optimization with PBE, and a single point calculation to refine the energies with B3LYP, as performed in **PAPER I**.

Dispersion interactions

In this thesis we often encounter noncovalent interactions which need to be treated with high accuracy, such as the adsorption of guest molecules on the zirconium Lewis acid sites or interaction between solvent molecules. One of the challenges of DFT methods is the description of long range dispersive interactions such as London forces, which are commonly referred to as van der Waals interactions. These interactions are due to many particle electron correlation effects which are present also in absence of charges and can have a significant impact on the noncovalent interaction energy. To tackle this problem, various dispersion schemes have been proposed. One of the most used is currently the Grimme–D3 method [96], where a damped $-C_6 R^{-6}$ function is added to the DFT functional. Recently, more advanced dispersion schemes have been developed, such as the many body dispersion scheme [97], or the one of Tkatchenko and collaborators [98], although for the systems we are studying not many benchmarks of these new methods have been performed so far [99].

Geometry optimization

In order to obtain molecular structures that have physical significance and their relative energies, the arrangement of the atoms needs to be optimized. There are generally two types of molecular structures that we need to find in our simulations, the equilibrium geometries, which correspond to *minima* of the PES, and the transition state geometries, which correspond to first order saddle points, as displayed in Figure 2.5. These points are characterized by null first derivatives of the energy (the total forces acting on each atom are sufficiently close to zero), all positive second derivatives for local *minima* and one negative second derivative for first order saddle points, which correspond to transition states.

The geometrical optimization of reactants and products consists in a minimization of the energy along the nuclear coordinates. Often the starting point is the experimental structure which can be obtained from diffraction data. In the most used codes several minimization methods are implemented, each characterized by a different computational cost and robustness, such as steepest descent, conjugated gradient or simulated annealing. The algorithms will find local *minima*, and do not guarantee that the system will be in a global *minimum*, therefore the minimizations must start from a sufficiently good guess.

The search for transition states is far from trivial and often requires an iterative procedure involving different methods and requiring a good knowledge about the system and chemical process under study. In the calculations performed in this thesis, we often start from an equilibrium structure and as a first guess, we adapt the bond lengths and angles to be close to the transition state with a molecular editor such as Zeobuilder [100]. These bond lengths are then fixed, and the rest of the structure is reoptimized. The Hessian of this partly optimized structure

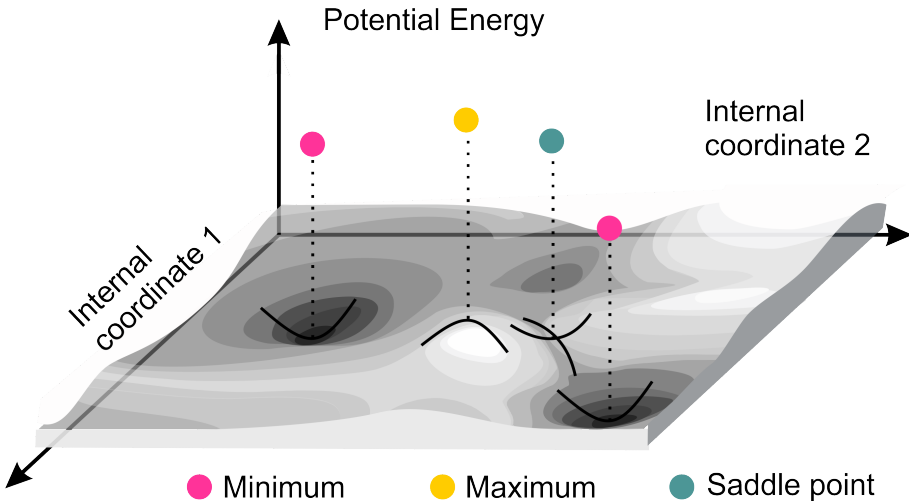


Figure 2.5: Schematic representation of the potential energy surface and the stationary points.

needs to be then computed, and the vibrational modes analyzed, to check which (if any) negative frequency corresponds to the transition state. The system can be optimized again without the constraint using an improved dimer method along a selected eigenvector [101] which is followed by the optimization with a quasi-Newton method [102]. In some difficult cases, the TS search can be initiated on simpler cluster models and optimized in a code in which methods are usually implemented to directly find the TS structure. This way, a first guess of the TS geometry might be obtained and further transferred to the periodic model. In both transition states and *minima*, if there are superfluous negative frequencies, these need to be removed. Often, it is sufficient to minimize the energy along that vibrational mode. Single point energy calculations can be performed for different values of the displacement along that mode, and the lowest point in energy can be used as starting point for a subsequent minimization of all the coordinates.

Cell optimization

In the case of periodic systems, not only the structure, but also the unit cell needs to be optimized. This is not trivial, as when using a finite plane wave basis set the number of plane waves depends on the volume of the unit cell. If the volume changes during the optimization, artificial forces which go under the name of Pulay stress can arise. This would require many iterations to optimize the volume. In this thesis, another approach was used [103] which relies on an equation of state fit. For a given volume, for instance taken from experimental data, the unit cell is optimized. Then a set of equally spaced different volumes is defined and for each of these points the geometry and unit cell parameters are optimized. This way it

is possible to construct an energy–volume curve, which for a rigid system can be fitted with a Birch–Murnaghan equation of state [104, 105], allowing to extract the volume V_0 which corresponds to the *minimum* electronic energy E_0 .

$$E(V) = E_0 + \frac{9V_0B_0}{16} \left\{ \left[\left(\frac{V_0}{V} \right)^{\frac{2}{3}} - 1 \right]^3 B'_0 + \left[\left(\frac{V_0}{V} \right)^{\frac{2}{3}} - 1 \right]^2 \left[6 - 4 \left(\frac{V_0}{V} \right)^{\frac{2}{3}} \right] \right\}$$

Where B_0 and B'_0 are the bulk modulus and its derivative. A new structure is then generated at this given volume and coordinates and unit cell parameters are optimized again.

Molecular vibrations

As seen in the previous paragraph, for many purposes in this thesis we need to calculate the second order derivatives (Hessian matrix) of the PES, which are associated to molecular vibrations. First of all, the Hessian gives us information about the curvature of the surface and the nature of the stationary points encountered during the minimization. The second order derivatives are obtained by displacing the atoms in the three directions and calculating the energies, then the Hessian is diagonalized to determine the eigenvectors that correspond to the vibrational motions. From the Hessian we can calculate the vibrational frequencies, which open the door to a lot more information on the system than a single point calculation. As a matter of fact, single point calculations are performed at 0 K, but even at this temperature nuclei vibrate around their equilibrium positions, and this movements are responsible for vibrational entropy. We can approximate these motions with those of harmonic oscillators, by using the vibrational frequencies constructed from the Hessian.

These frequencies can then be used to estimate the value of the vibrational entropy at finite temperatures, as will be explained later. In the calculations performed in this thesis, due to computational limits, a partial Hessian approach (PHVA) was used when dealing with reactions, as implemented in the TAMkin toolkit [106]. The quantity that needs to be derived from these calculations is the change in free energy, which mainly depends on the parts of the system that change during the reaction, in the case of a heterogeneous catalyst the active site and the adsorbed reactants. Therefore, restricting the entropy calculations only to this part of the system is a good approximation that allows to decrease enormously the computational cost [107]. This approach has been used in the calculation of the free energy barriers for the Fischer esterification on UiO–66 (**PAPER I**), where the atoms taken into account were the adsorbed reactants and four atoms of the active sites in their immediate proximity, as displayed in Figure 2.6.

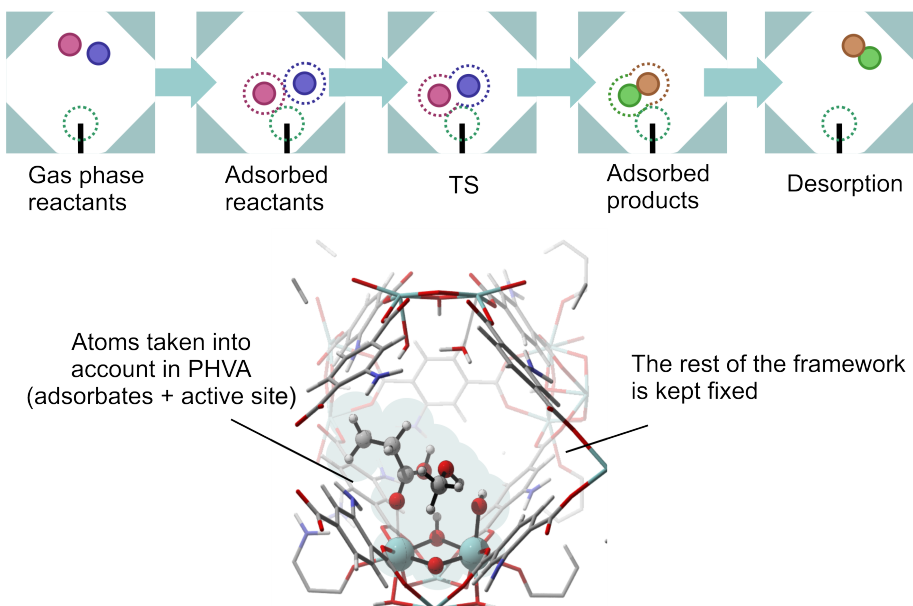


Figure 2.6: Representation of the atoms taken into account in the Partial Hessian Vibrational Analysis (PHVA) approach. Top: a schematic representation of a reactive process in nanoporous material, bottom: a snapshot from the static calculations where the atoms of the active site and the adsorbates are highlighted

2.3 Free energy

The central thermodynamic quantity that determines the outcome of a reaction is the free energy change associated to the process. In general, a chemical system will undergo changes in a direction that minimizes its free energy, until an equilibrium is reached. Knowing the difference in free energy between reactants and products allows us to know the equilibrium constant for a given reaction. The Gibbs Free energy can be decomposed in an enthalpic and an entropic contribution, that can be evaluated from the simulations knowing the molecular partition functions. Initially, the total internal energy U has to be obtained from the electronic energy ε_0 , the zero-point vibrational energy E_{ZPE} and the molecular partition function Q at constant number of particles n and volume V :

$$U = U_0 + RT^2 \left(\frac{\partial \ln Q}{\partial T} \right)_{n,V}$$

$$U_0 = \varepsilon_0 + E_{ZPE}$$

Where R is the gas constant, equal to the product $N_A \cdot k_B$ between Avogadro's number and Boltzmann constant. The molecular partition function Q can be split in its translational, rotational, and vibrational components:

$$Q = Q_{trans} Q_{rot,ext} Q_{vib}$$

The enthalpy H corresponds to the total energy plus the work associated to the change in volume.

$$H = U + p_0 V$$

The entropy S can be directly obtained from the partition function:

$$S = R \ln Q + RT \left(\frac{\partial \ln Q}{\partial T} \right)_{n,V}$$

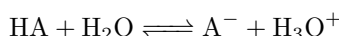
Finally, the Gibbs free energy G will be:

$$G = H - TS = U_0 + p_0 V - RT \ln Q$$

Where in the case of non-interacting particles $p_0 V = RT$ following the ideal gas law. We can therefore define a free energy surface (FES) that is function of coordinates of the system, and can be derived from the PES.

Equilibrium

As explained above, there is a tight connection between free energy and equilibrium concentrations in chemical reactions. As an example, an equilibrium which is of utmost importance in chemistry is the acidic dissociation of species in aqueous solution:



The acidic dissociation constant (K_a) is an important equilibrium constant in chemistry and is equal to the ratio between the concentration of products and reactants when the reaction reaches the equilibrium. It is often reported with its negative decimal logarithm as pK_a .

$$K_a = \frac{[\text{A}^-][\text{H}^+]}{[\text{HA}]}$$

The equilibrium constant is equal to the Gibbs free energy change from reactants to products.

$$\Delta G = RT \ln K_a$$

$$pK_a = \frac{\ln 10}{RT} \Delta G$$

Therefore, knowing the Gibbs free energy difference between reactants and products, we can have important information about the equilibrium composition of a chemical system. However, kinetic factors can sometimes play a major role, and equilibrium cannot always be easily reached.

Transition state theory

A chemical reaction is a process that through rearrangement of the atoms transforms one stable state into another. Every elementary reaction can be represented as a minimum energy path connecting two *minima* along the FES. Furthermore, along this reaction path the existence of a saddle can be postulated, which is the highest point in energy that needs to be crossed to go to the product state. The saddle point is typically called transition state or activated complex and it is the basis for the transition state theory (TST) developed by Eyring in the 1930's, one of the most successful chemical theories which allows to explain reaction rates of elementary chemical reactions. The assumption of the theory is that there is a *quasi-equilibrium* between reactants and activated complex, and the rate constant can be obtained by the size of the energy barrier and by the frequency at which the system can cross the barrier. This is possible because the barrier acts as a bottleneck in the reaction, its crossing is a rare event and all the kinetics depends only on it. For a unimolecular reaction, the rate constant can be derived from the partition functions of reactant, TS and their energy difference:

$$k(T) = \frac{k_B T}{h} \frac{q_{TS,\ddagger}}{q_R} e^{-\frac{\Delta E^\ddagger}{k_B T}}$$

Where k_B is the Boltzmann constant, h is the Planck constant, q_R and $q_{TS,\ddagger}$ are the molecular partition functions of reactants and activated complex for all coordinates except the reaction coordinate, evaluated from the zero-point vibrational level.

$$q_{vib,i} = \prod_{i=1}^{N_{dof}} \frac{1}{1 - e^{-\frac{\hbar \nu_i}{k_B T}}}$$

Where N_{dof} is the number of vibrational degrees of freedom of the system. The energy difference ΔE^\ddagger includes electronic energy and zero-point vibrational energy difference at 0 K:

$$\Delta E^\ddagger = E_0^{TS} - E_0^R + \Delta E_{0,vib}$$

$$\Delta E_{0,vib} = \sum_{i=0}^{N_{dof}-1} \frac{h\nu_i^{TS,\ddagger}}{2} - \sum_{i=0}^{N_{dof}} \frac{h\nu_i^R}{2}$$

This theory has some limitations, and may fail in the case of labile intermediates, when nuclei deviate from a classical behavior, or at high temperatures. For a given reaction, in fact, there will be many paths characterized by different barriers, and at low temperature only the lowest one will be likely to be crossed. When the kinetic energy is high enough, many other paths will be activated. The transition state will occupy a larger region of the PES, and it will not be possible to derive entropy from the vibrational partition functions.

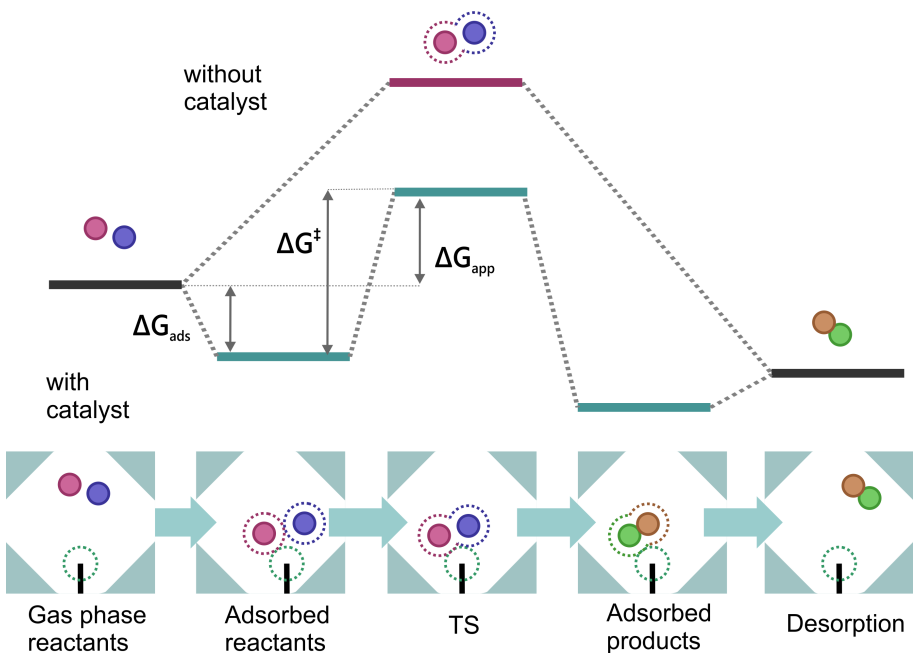


Figure 2.7: 1D free energy profiles for a given reaction with and without catalyst, indicating the adsorbed initial, final states and the localized transition state, schematically illustrated in below. The adsorption free energy, intrinsic and apparent barriers are obtained by static calculations and indicated by ΔG_{ads} , ΔG^\ddagger , and ΔG_{app} , respectively;

2.4 Exploring the free energy surface

Static calculations, where molecular vibrations are approximated using harmonic oscillators, can fail to give an accurate representation of the entropy when there is a high configurational freedom. When the FES is flat with respect to $k_B T$, the system at equilibrium can evolve in a larger region of the PES and move along more than one *minimum*. In this case, vibrational frequencies are anharmonic and it is not possible to represent the system by approximating around one single *minimum* (Fig. 2.8). Therefore, static calculations are not always sufficient in describing the system at operating conditions. In this view, molecular dynamics (MD) techniques, which follow the time evolution of the system, can resolve this shortcoming.

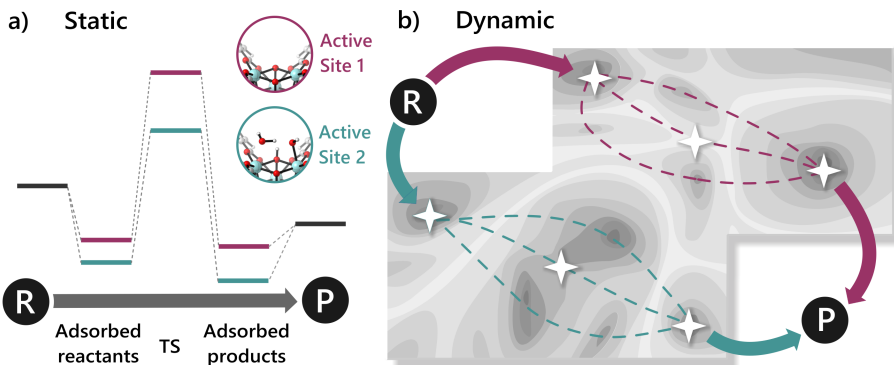


Figure 2.8: a) 1D free energy profiles for a given reaction on two different active sites in UiO–66 (insets), indicating the adsorbed initial and final states and the localized transition state for this reaction; (b) possible 2D representation of the given reaction on the two active sites as obtained using advanced dynamic techniques, indicating the three critical points on the potential energy surface.

Ab initio Molecular Dynamics

From MD simulations, thermodynamic properties such as free energy can be obtained taking into account a whole region of the PES instead of a single point. This is based on the ergodic theorem, that in one of its formulations states that the time average of equilibrium properties is equal to the ensemble average, in the limit of a sufficient long simulation.

MD simulations are based on solving Newton's equations of motion:

$$M_i \ddot{\mathbf{R}}_i = \mathbf{F}_i = -\nabla_i V$$

where M_i and \mathbf{R}_i are the mass of a given nucleus and its coordinates, \mathbf{F}_i the forces that act on it, which correspond to the gradient $\nabla_i V$ of the PES. There are

many ways to calculate these quantities and to integrate the equations of motion, and at present time, chemists and physicists can choose between a plethora of MD techniques which span a whole range of complexity, accuracy and computational cost. In the calculations performed in this thesis, potential energy and forces on the PES are calculated from first principles by means of DFT to account for the full dynamic behavior of the material by ab initio molecular dynamics (AIMD). The calculation of electronic properties which define the PES is decoupled from the propagation of nuclear motions, in a method called Born–Oppenheimer Molecular Dynamics (BOMD). Other famous AIMD methods, which differ by how the calculations of electronic potential and the equation of motion are combined, are the Car–Parrinello MD (CPMD) [108], where a fictitious electronic kinetic energy is added to the lagrangian, or the Ehrenfest MD, based on the namesake theorem [109, 110].

The first MD calculations were performed in the microcanonical (NVE) ensemble, where total energy, number of particles and volume are fixed. However, in experiments it is often the temperature that is fixed, not the energy. In general, the choice of the ensemble depends on the thermodynamic quantities that need to be determined. Nowadays there are many thermodynamic ensembles in which the simulation can be performed. The most convenient for a comparison with experiments are the canonical (NVT), with fixed number of molecules, volume and temperature, or the isothermal–isobaric (NpT), with fixed number of molecules and temperature, but where the volume can fluctuate. In order to have a fixed average temperature, some control of the kinetic energy of the atoms is needed. Various thermostats, which differ in terms of speed and robustness, are implemented in every MD code. In this thesis, Nose’–Hoover thermostat was used, where the system is connected to a heat bath. The pressure is also controlled in simulations by means of a barostat. The most commonly used is the one developed by Martyna, Tobias, and Klein (MTK) [111].

Radial distribution functions

From MD trajectories, different macroscopic properties can be derived. An important structural property is the radial distribution function (RDF) or pair correlation function $g(r)$, that describes the probability density between specific atoms as a function of the distance, normalized with respect to a probability distribution of a homogeneous gas with the same density. The RDF can be calculated from the following expression:

$$g_{ij}(r) = \frac{dn_{ij}(r)}{4\pi r^2 dr \rho_i}$$

where dn_{ij}/dr represent the number of atoms of type j within a certain distance of the atoms of type i , and $\rho_i = V/N_i$ represent the density of the homogeneous distribution. The integral of the RDF can also give valuable insight into the number

of atom pairs at a given distance, such as what is the average coordination of a certain chemical species.

Vibrational density of states

Information on the time evolution of certain quantities in the system can be obtained by calculating time autocorrelation functions. The correlation of a certain variable with itself is equal to:

$$\langle X(0) : X(t) \rangle = \lim_{N \rightarrow \infty} \frac{1}{T} \int_0^T X(t) X(t + \tau) d\tau$$

Autocorrelation functions offer a measure of the response of the system to a given stimulus, which is function of the density of states. The response of a system to a perturbation is equal to the power spectrum of the autocorrelation function of the fluctuations of the involved observable [112]. For instance, by calculating the power spectrum of the atomic velocities autocorrelation function, we can obtain the vibrational density of states, as done in **PAPER IV**. These spectra contain all the dynamic and anharmonic information that is neglected in the static frequency calculations.

Towards modeling at operating conditions

With the growth in computational time, the new challenge is constituted by modeling the system at operating conditions. Many chemical reactions, especially when performed at mild conditions, involve the presence of a solvent. In order to move closer to modeling the system at operating conditions, the solvent in the pores can also be taken into account. This adds a lot of degrees of freedom to the system, and for this reason often an implicit description of the solvent is done, such as in the Polarizable Continuum Model (PCM) [113]. In the case of the work in this thesis, however, it is necessary to fully model the solvent molecules, as they are actively involved in proton transfers. To do so, the number of solvent molecules that can fit in the unit cell needs to be estimated. Monte Carlo method (MC) is an alternative approach to MD to explore the PES for complex systems. It was initially developed for the calculation of multidimensional integrals and is nowadays largely used in chemistry, especially when dealing with adsorption. In the framework of this thesis, it has been applied in the Grand Canonical ensemble (μVT , fixed chemical potential, volume and temperature) to determine the number of solvent molecules that could fill the pores of the material at standard conditions.

Enhanced sampling MD methods

MD simulations can offer valuable insights into the behavior of a chemical system at equilibrium conditions. From these simulations, many properties can be extracted, such as equilibrium geometries, vibrational spectra, diffusion coefficients, structural

parameters etc. Configurations associated to higher (or lower) values of potential energy will be sampled for shorter (or longer) times, and in principle, if a certain process is sufficiently sampled, based on the ergodic theorem we can know its equilibrium constant, and in turn the free energy barrier associated to it. However, chemical reactions, where bonds are broken and formed, are generally rare events that will not be sampled with a regular exploration of the PES. If the free energy barrier is high compared to $k_B T$, the probability that such event would spontaneously occur during the simulation time is practically none. This is especially true for complex molecular systems, in which processes occur in different time scales and that can only be simulated for a limited amount of time. For this reason, different enhanced sampling techniques have been developed to enhance the sampling of low probability regions of the free energy landscape [114–121]. Recently, enhanced sampling techniques have been successfully applied in heterogeneous catalysis to study processes at operating conditions [122–128].

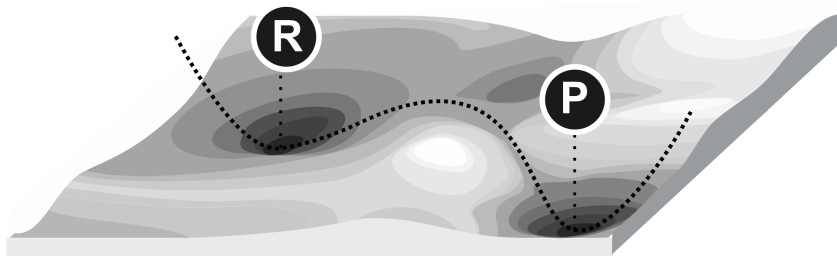
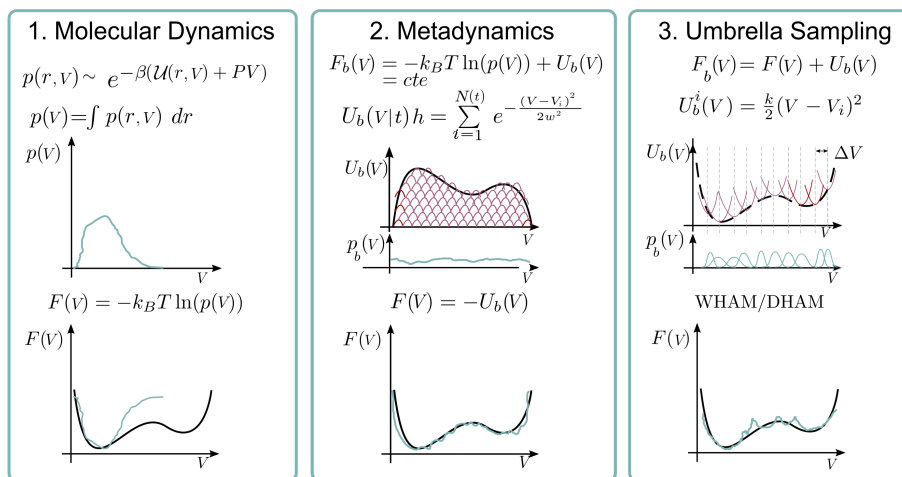


Figure 2.9: Schematic representation of different MD techniques that can be used to explore the PES.

There are two main classes of methods that can be used to explore rare events on the free energy surface. The first class is characterized by methods that encompass all degrees of freedom and do not need any prior information on

the free energy landscape between two points. Examples of these methods are Transition Path Sampling (TPS) [129] and Replica exchange (RE) [130]. The other class of techniques encompasses methods in which the sampling is enhanced along certain coordinates of the system, such as Umbrella Sampling (US) [131,132] and Metadynamics (MTD) [115], shown in Fig. 2.9.

Choice of collective variable

The PES is a highly dimensional surface, defined by the positions of all atoms in the system. However, often a reactive process can be described by few important coordinates called “collective variables” (CVs), which are projections of the high dimensional space. In fact, what can be considered a chemical configuration is an ensemble of microstates that are different in terms of absolute coordinates of each atom, but all contribute to the same macrostate. In some cases, a simple CV can represent the reaction coordinate for the process, but often the choice is not trivial [133]. In general, choosing the right collective variable is crucial to describe the correct process. Often geometric parameters are used, such as distances, angles, dihedrals, or combinations of the latter. When studying certain processes, a switch function such as a coordination number (CN) derived from distance information is often the preferred choice. CNs represent a smart choice compared to distances, because for each pair of atoms, the coordination is zero for distances higher than a certain threshold.

$$\text{CN} = \sum_{i,j} \frac{1 - (r_{ij}/r_0)^{nn}}{1 - (r_{ij}/r_0)^{nd}}$$

Where CN is defined between two sets of atoms i and j , r_{ij} corresponds to the distance between atoms i and j , and r_0 is a threshold distance. The exponential parameters nn and nd define how sharply the function behaves around the value r_0 . In processes such as in the ones of **PAPER V**, we considered the coordination between a zirconium atom and the oxygen atoms of the solvent water. Such collective variable allows to consider the possibility that different water molecules could decoordinate and recoordinate, defining the same macrostate for a given value of the CN. We show that such processes cannot be studied by employing distances as CVs.

Metadynamics

Metadynamics (MTD) is a popular enhanced sampling method, used to overcome barriers in the free energy landscape, which was first proposed by Laio and Parrinello [115,134]. During MTD, a history dependent bias potential is added in the form of gaussian hills to the PES along a certain CV. This way, potential energy is added to already visited states, allowing to escape local *minima* and explore different regions of the PES. When all states are sampled with equal probability, the free energy profile along the biased CV can be obtained from the added bias potential. As the bias is added, the system is able to evolve along all the other degrees of freedom.

For this reason, this method can also provide insight into the mechanisms that occur during the exploration of the different regions of the CV, as has been done in **PAPER V**.

Umbrella sampling

In the umbrella sampling method, a series of biased MD simulations are performed along the chosen CV. In each simulation, a bias potential is added to constrain the system to adopt a specific value of the CV, while it can evolve along all the other degrees of freedom. This way, the whole range of the CV can be explored. As each simulation is independent, this method is highly parallelizable. The free energy profile can then be estimated by using different methods to combine the information obtained from the set of simulations, such as the weighted histogram analysis (WHAM) or the multistate Bennett acceptance ratio [131, 135]. Even if the CV is constrained in each simulation, this method can also offer valuable insight into the evolution of the system at different values of the CV, as has been done in **PAPER III**.

In summary, this chapter gives an overview of the many methods that have been employed to understand the properties of MOFs. Reactive processes can be studied by using a plethora of different computational techniques that differ in cost and accuracy. Cluster calculations were used for a first estimate of the energies, whereas periodic models were used for all the remaining part of this thesis. The increase in computational time allowed to include more complexity in the model, and to explicitly take into account the role of solvent and structural modifications in the material. During the time frame of this thesis, we moved from a static description of the chemical events towards modeling at operating conditions that allows to better describe and predict real processes.

3

Major research results

This Chapter illustrates the main research results obtained in the framework of this thesis. The main goal of this work was the study of the nature of active sites on UiO–66 and MOF–808 upon activation processes, and how the solvent and the functionalization influenced their behavior. The role of active sites on defective UiO–66 was studied for Fischer esterification of free fatty acids (FFA), and it became clear that solvent played an unexpected active and beneficial role in the reaction mechanism. Different molecular modeling techniques based on static and dynamic methods have been applied to gain insight into the interaction between active sites and reactants in the material, as has been introduced in Chapter 2. Contrary to reactions in zeolites, processes in MOFs are often performed ad mild conditions in the presence of a solvent, which adds complexity to the model. So far, solvent in MOFs had been studied only with classic approaches, but with the increase in computational power it was possible to include a full *ab initio* treatment of water and methanol solvent in the UiO–66 pores and to go towards an *operando* description of activation processes in MOFs. The most important scientific results will be highlighted in this Chapter. More details are to be found in the original articles, enclosed in Part II.

3.1 Activation processes in zirconium–MOFs

One of the main challenges in MOF research is the understanding of how active sites are created and how they impact the properties of the material. For this purpose, molecular modeling offers a platform that allows to study such activation processes and nature of active sites at the molecular level. In this sense, UiO–66, characterized by an exceptional stability, represents a perfect case study where different activation and PSM processes can take place without disrupting the stability of the structure.

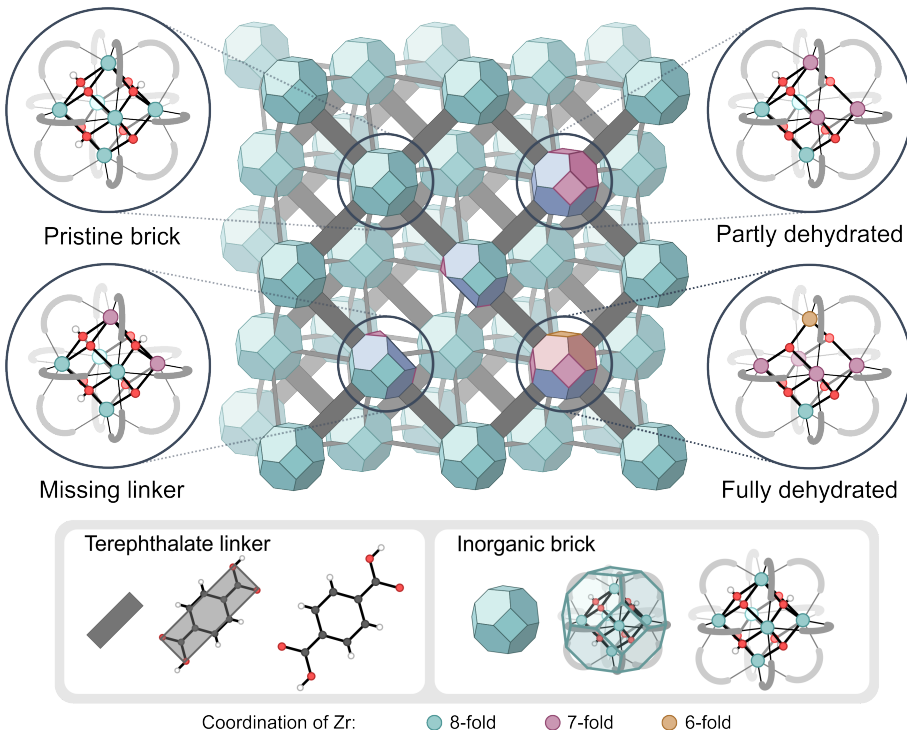


Figure 3.1: Schematic representation of the UiO-66 structure with possible configurations of the bricks that give rise to coordinatively unsaturated Zr atoms. The colors indicate the coordination of the Zr atoms.

Missing linker defects

In **PAPER I** we investigated the local defect topology upon removal of a linker on UiO-66 as starting point to investigate the catalytic role of defect coordinating species in the mechanism of Fischer esterification. This research was done in collaboration with the group of Dr. Francesc X. Llabrés i Xamena as experimental partners. When studying the catalytic behaviour of UiO-66, an essential

ingredient to understand the reactivity of the inorganic SBU is the knowledge of the molecular structure of the active sites upon removal of a linker. On these sites, defect coordinating species can be adsorbed and have an impact on the catalytic properties of the MOF by introducing additional sites that can play an active role in reactions. Upon removal of one of the twelve negatively charged

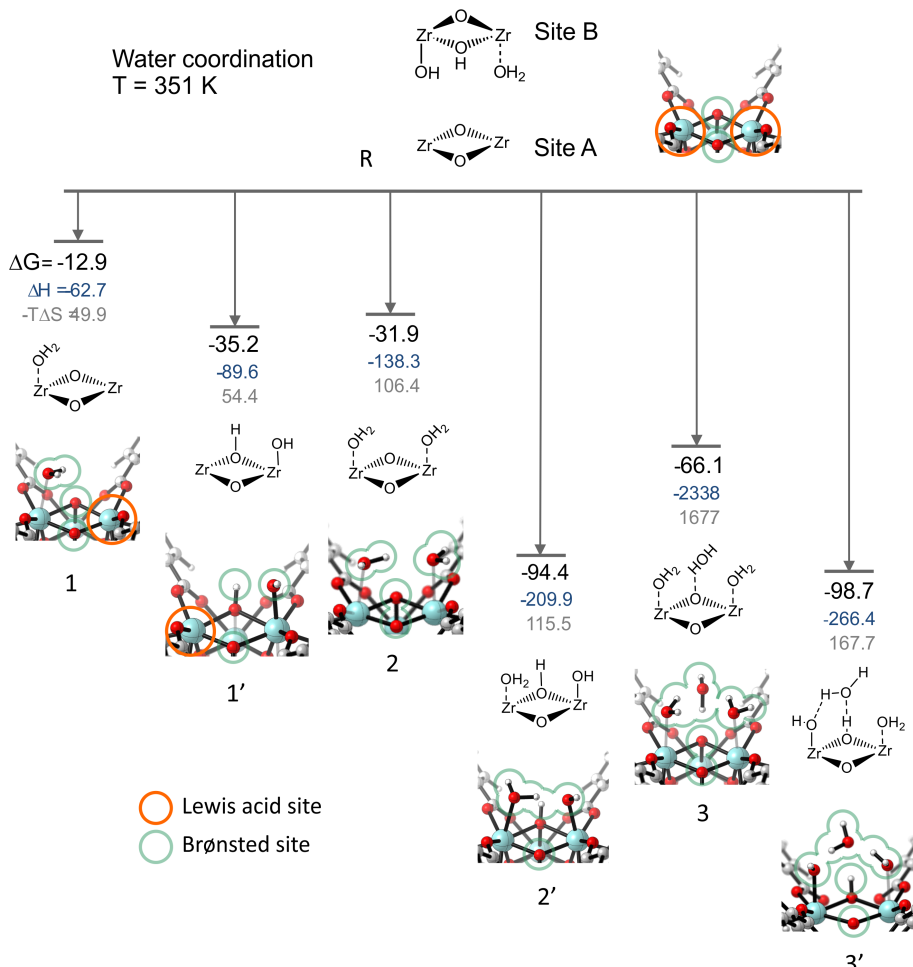


Figure 3.2: Coordination free energies at reaction temperature of 351 K of one, two and three water molecules at coordinatively unsaturated Zr-bricks in defective UiO-66 with respect to a water coordination free site (site R). The structure of the opposite site B corresponds with configuration 2' with two water molecules and consistently used in all periodic calculations considered in the figure. Free energies (in black) are given in kJ/mol, and their decomposition into enthalpic ΔH (blue) and entropic $-T\Delta S$ (grey) contributions. Energies are resulting from periodic calculations with PBE-D3 level of theory. In each configuration Lewis acid and Brønsted sites are indicated.

BDC linkers from the inorganic $\text{Zr}_6\text{O}_4(\text{OH})_4$ SBU, the positive charge left on the brick has to be compensated. Charge neutralization can be accomplished by either coordinating a negative ion such as hydroxyl group to one of the zirconium atoms, or by removing a proton from the brick. This latter case is characterized by two zirconium open metal sites, and is the type of active site that is obtained upon thermal treatment of the brick at $T > 423$ K. It was previously accepted that these Lewis sites were responsible for the catalytic activity of UiO–66, but recent studies point towards the active role of Brønsted sites in the neighborhood of defective zirconium atoms [29, 59, 61, 63, 64, 66, 136, 137]. The presence of multiple sites makes it difficult to establish a simple structure–activity relation. In particular, it is important to understand from a mechanistic point of view how the presence of defect coordinating species may affect the catalytic activity on Zr–MOFs.

The coordination of water species near the active sites can occur with different configuration schematically displayed in Fig. 3.2. In all structures the presence of possible Lewis and Brønsted sites which may play a role in reactions is highlighted. The simplest case taken as reference configuration is the unsaturated site obtained upon thermal activation, containing two μ_3 -oxygens bridging the zirconium atoms which may act as Brønsted sites. From this structure, the coordination of one physisorbed water molecule to one of the zirconium atoms is energetically favorable. A decrease in energy is observed when the molecule is deprotonated to the oxo atom as in configuration 1'. The chemisorption of this water molecule shields the Lewis character of the zirconium atom, but introduces an additional Brønsted site in proximity to the open metal site.

The most stable configurations are observed in presence of 2 or 3 adsorbed water molecules on the adjacent zirconium atoms. Two physisorbed water molecules of configuration 2' can be adsorbed to the two zirconium atoms, followed by an immediate dissociation of one of the two molecules into a hydroxyl group and a proton on the adjacent μ_3 -oxygen. This configuration is characterized by a free energy difference of -94.4 kJ/mol at reaction temperature of 351 K compared to the dehydrated defective site. The presence of two zirconium coordinating species has been reported by Lillerud [61] by means of Single-crystal X-Ray diffraction (SXRD), showing that the material is most stable when all zirconium atoms are fully coordinated. When starting from the thermally activated material that contains open Lewis sites, at standard condition, water present in the atmosphere will immediately coordinate to restore the 8-fold coordination of the zirconium atoms to give structure 2. This structure is consistent with the one proposed by the group of Farha [66] who identified three types of protons from potentiometric titration: $\mu_3\text{-OH}$, Zr-OH and Zr-OH_2 .

A third bridging hydroxyl species as charge neutralizing species was proposed by Yaghi [62] from XRD data. They propose two physisorbed water molecules bridged by an OH^- counterion that is stabilized by a hydrogen-bond interaction with the

neighboring μ_3 -OH of the brick. However, a recent study Ling and Slater [63] did not succeed in finding a corresponding minimum on the PES. In this work, we observe that the μ_3 -OH atom immediately deprotonates in proximity of such OH⁻ anion (configuration 3). Similarly as in the previous case, this structure can further stabilized by a deprotonation of one of the two physisorbed water molecules, to yield configuration 3' of Fig. 3.2, in agreement with a previous report by Vandichel et al. [64]. Adsorption of reactants involved on the Fischer esterification reaction was also taken into account. Similar considerations on the deprotonation processes can be drawn when considering methanol instead of water as reported more in detail in **PAPER I** and **PAPER II**. The energies obtained clearly demonstrate that water molecules preferentially adsorb on the zirconium atoms and the only limit to the adsorption of more water molecules lies mainly in the entropic penalty.

Nature of active sites for Fischer esterification

Among the reactions that can be catalyzed by UiO-66, Fischer esterification, shown in Fig. 3.3 is an important process in the production of biodiesel, a biofuel that is obtained from renewable sources, such as oils and animal fats. UiO-66 has been shown to be a stable and reusable Lewis catalyst with high conversion rate for the reaction [74, 75]. Experimental findings performed on both hydrated and dehydrated UiO-66 show that water has a beneficial role in the process, but a theoretical rationalization of the underlying causes was missing. Moreover, amino functionalization was shown to increase the reaction rate. To address these questions, the role of active sites on UiO-66 during the Fischer esterification reaction was studied in **PAPER I**. Two possible lowest activated reaction pathways were identified for the hydrated and dehydrated active site.

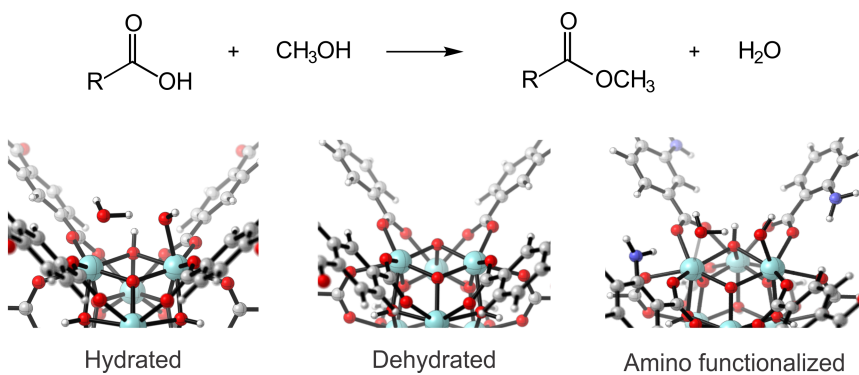
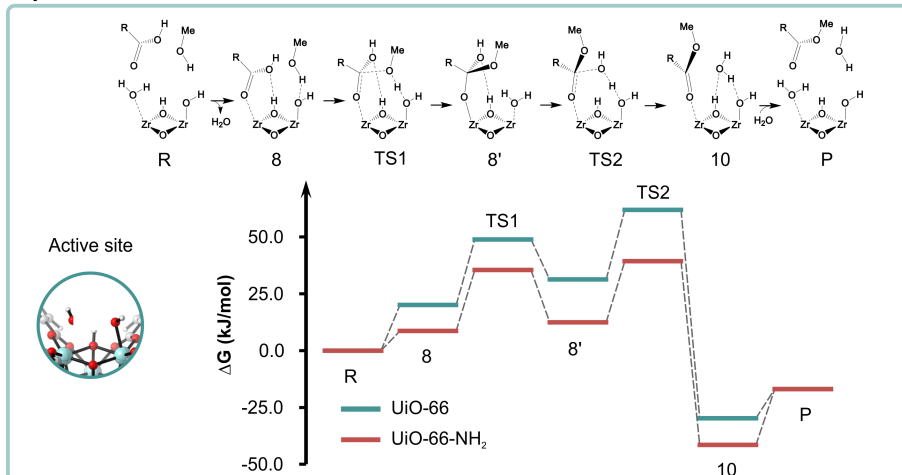


Figure 3.3: Top: Fischer esterification reaction; bottom: three different types of UiO-66 active sites.

The proposed reaction mechanism is shown in Fig. 3.4. From the reactant configuration, the physisorbed water molecule is displaced by the carboxylic acid

Hydrated material



Dehydrated material

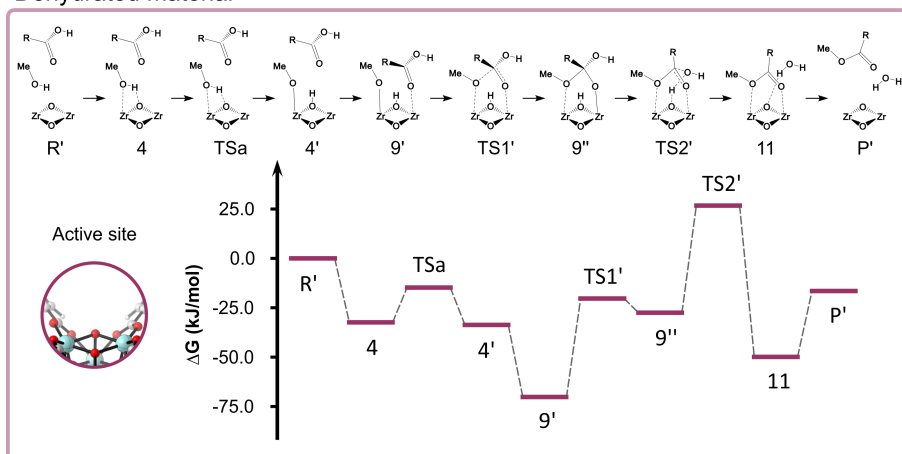


Figure 3.4: Mechanism and free energy profile for the esterification of propionic acid with methanol on a hydrated and defective UiO-66 material (blue), a hydrated defective UiO-66 material with amino functionalization of the BDC linkers (red), and on a dehydrated defective UiO-66 (black). Periodic calculations at B3LYP-D3//PBE-D3 level of theory, $T=351$ K. R corresponds with an empty frame with one linker defect and a pool with all reactants to guarantee mass balance. In P the defective Zr-brick is coordinated with two water molecules (configuration 2'). P' corresponds to the empty frame with the ester as final product and remaining water molecules in gas phase.

that coordinates on the zirconium atom. The resulting configuration was identified after a series of static calculations probing possible geometries. In this configuration, the acid carbonyl group is bonded to the zirconium, and at the same time methanol is hydrogen bonded to the hydroxyl group coordinated to zirconium. The adsorption of the acid on the Lewis acid site gives to the carboxylic carbon a more electrophilic character, making it more prone to interact with the alcohol. The oxygen of methanol is at the same time made more nucleophilic due to the hydrogen–bonding interaction with the Brønsted basic site situated in close proximity. This favors the condensation between activated carboxylic carbon of the acid and methanol. Two TS are involved in the process, in which first a tetrahedric intermediate is formed, and then water is removed. In both, the hydroxyl group plays a role, first as proton acceptor, then as proton donor, while the acid maintains the bond with the carbonyl oxygen. The low energy barriers associated to the two TS are 28.9 and 30.6 kJ/mol at 351 K. The reaction can proceed both ways, until an equilibrium is reached. This mechanism is characterized by a dual participation of Brønsted and Lewis sites, and overlays with the experimental findings.

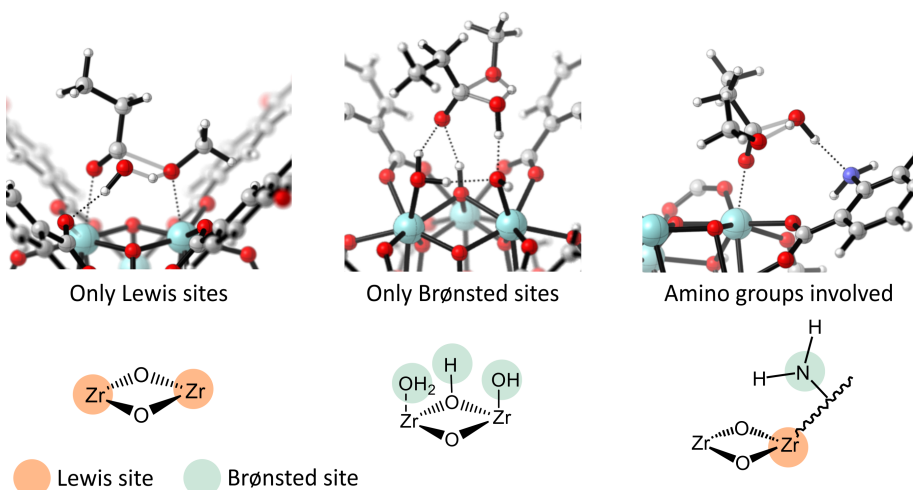


Figure 3.5: Transition states belonging to three cases where no suitable mechanism for Fischer esterification was found, suggesting that the reaction needs a concerted participation of Lewis and Brønsted sites

Upon thermal treatment at 423 K, UiO–66 loses the adsorbed solvent molecules without compromising the structure of the inorganic SBU, contrary to the dehydroxylation with release of two water molecule that takes part at $T > 523$ K [138]. In principle, these open metal sites should be more catalytically active, but a decrease in catalytic activity is experimentally observed. In the proposed mechanism, two Lewis acid sites, the zirconium atoms, and one Brønsted basic site, the μ_3 -oxygen, play an active role in the reaction. This mechanism is characterized by three TS,

in which: 1) methanol is deprotonated to the oxo atom, 2) an adduct is formed between the electrophilic carbon and the oxygen of methanol 3) the $\mu_3\text{--OH}$ group deprotonates to form water. This reaction is characterized by higher activation barriers (a total barrier of 90 kJ/mol at 351 K), which explain the lower catalytic activity of the dehydrated material.

Other mechanisms that do not make use of either Lewis or Brønsted sites were investigated without success (Fig. 3.5), as the energy barriers were too high to be likely to occur. Both proposed mechanisms are characterized by a dual participation of Lewis and Brønsted sites that work complementary to each other. The presence of acid and basic centers within molecular distances has been shown to be essential in the performance of the catalytic reaction as they cooperate in a concerted way during the chemical transformation. Most of the previous mechanistic studies on the UiO–66 material merely focused on the Lewis acidity of the undercoordinated sites, but it has become more and more clear that the bifunctional nature of the UiO–66 catalyst will play an important role in its future applications.

Role of defect topology

The adsorption of species present in the reaction environment of PSLE process was studied in the framework of **PAPER IV**. In this process, we wanted to see how defect-free and defective UiO–66 material would interact with water and methanol species. To obtain this information, we made use of a larger unit cell, to be able to represent different amount of missing linker defects. This increase in complexity reflects in the higher computational cost of modeling such structure. The defective structures taken into account in the modeling are obtained by removal of linkers from the conventional unit cell containing four inorganic $\text{Zr}_6(\text{O})_4(\text{OH})_4$ bricks [40]. Different numbers of missing linkers were modeled, to represent the different amount of defects in the experimental samples. A case with a low amount of defects is modeled by a unit cell with one missing linker. In this structure, two bricks are 12-fold coordinated, and two bricks are 11-fold coordinated, with an average of 11.5 linkers per brick. A second type of unit cell was taken with three missing linkers, corresponding to a higher amount of defects, with an average of 10.5 linkers per brick. De Vos et al. and Rogge et al. [55, 56] shown in their comprehensive studies that there are multiple topologically diverse possibilities to remove linkers from a 4-brick unit cell. In this work, we chose two possible, discrete cases to represent different coordination of the inorganic brick with this amount of defects. In a first unit cell with three missing linkers, two bricks are 10-fold coordinated and two are 11-fold coordinated. The other represents a more extreme case, with one 9-fold coordinated brick and three 11-fold coordinated bricks. The structures taken into account are denoted as $(10_b, 10_b, 11, 11)_{334}$ and $(9_c, 11, 11, 11)_{333}$ in the work of De Vos et al [56].

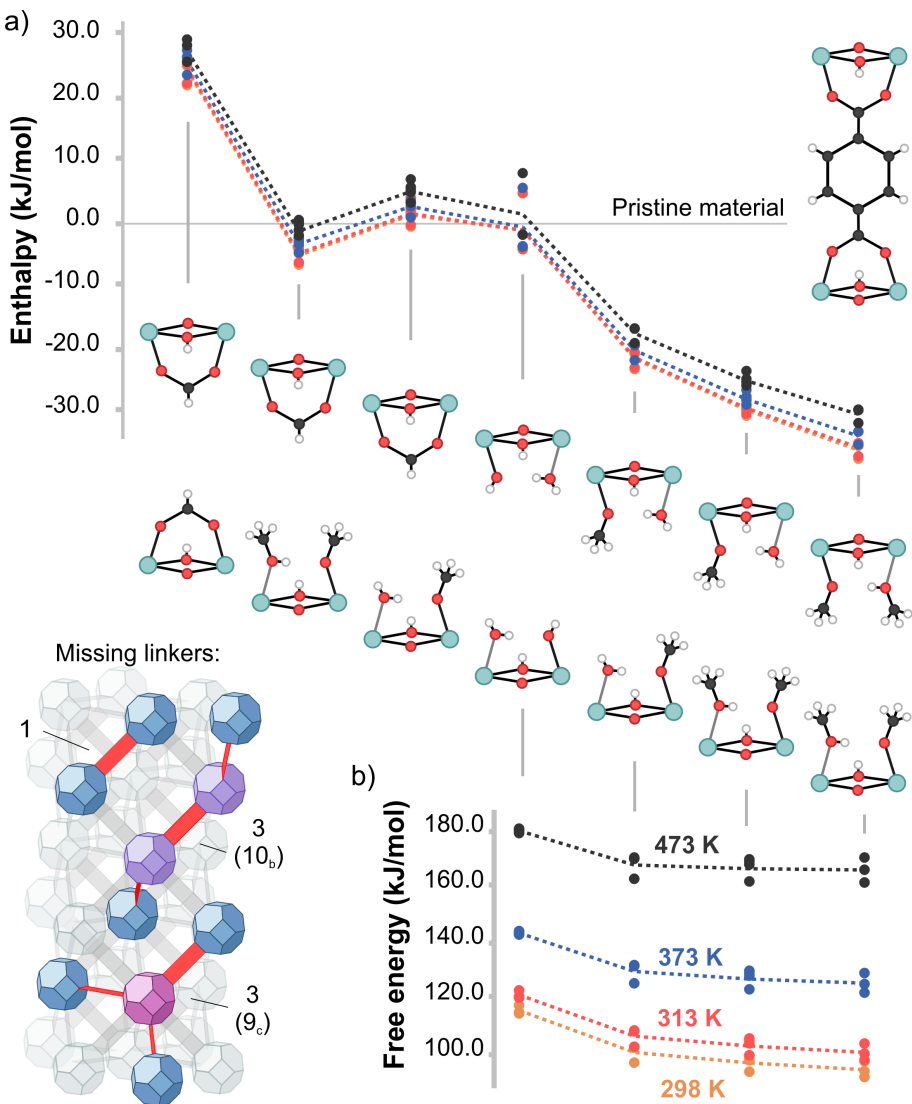


Figure 3.6: Energy diagrams for defective UiO-66 unit cells. Each dot represents a possible distribution of missing-linker defects (1 or 3 in total) within the unit cell; the connecting dotted line represents a weighted average. Values are normalized by the number of missing linkers in the unit cell. (a) Enthalpy difference between defect sites capped in different ways versus the non-defective material at T = 298, 313, 373, 473 K. (b) Temperature-dependence of the free energy difference of the defective structures indicated above (capped with H₂O/OH⁻, H₂O/MeO⁻ and MeOH/MeO⁻) versus the non-defective structure. A representation of the clusters with different missing linker connectivities is also provided.

The zirconium atoms on the defect sites have been capped by all species which can be present in the framework during the activation process, studying different combinations by means of water, hydroxo species, methanol, methoxide and formate. In our models, all zirconium atoms have been capped and are fully (8-fold) coordinated, being the most stable state at experimental conditions. On each defect site there is always a negatively charged species, to compensate for the removal of a carboxylate. Given the symmetry of the unit cell, when possible, multiple choices for the positioning of these species were taken into account and modeled. The removal of a negative charge can be also compensated by removal of a proton, as obtained in the dehydrated material, with subsequent physisorption of two neutral species, but these configurations are higher in energy, as seen in **PAPER I**. These results show a clear enthalpic preference for the methanol/methoxide pair in detriment of formate and water. The defective material synthesized with formate modulator is promptly attacked by methanol species present in solution. The obtained results are in line with a previous report [67] and highlight the preference of zirconium active sites for MeOH/MeO^- substitution as opposed to $\text{H}_2\text{O}/\text{OH}^-$, alternatively assumed as preferential charge balancing element for missing linker defects [62, 63]. No substantial difference in enthalpy is observed between the unit cells with different amount of defects (energy in each defective structure represented by a dot in Fig. 3.6). This is an indication that the thermodynamics that governs the process does not depend on the starting number of missing linkers, in agreement with the experimental observations of **PAPER IV**. The effect of temperature on the free energy was also investigated on the relative stability of defective configurations with respect to the pristine unit cell, where the linker is not missing. The first observation is that configurations involving water and methanol are more stable at lower temperature, thus the formation of missing linker defect through ligand exchange is enthalpically driven and favored by lower temperatures. Secondly, at 473 K the energy of the non-defective framework is much lower than the defective cases, which explains why the synthesis of the non-defective UiO-66 is favorable at such high temperature [47].

Activation by dehydration

The other process that can lead to activation of the UiO-66 material is the reversible dehydration of the brick performed at $T > 523$ K. The dehydration mechanism may have a decisive effect on certain catalytic reactions, where next to the Lewis acid site also the neighboring Brønsted base or acid site may take a cooperative role in the reaction mechanism. At elevated temperatures and low pressures, the zirconium core gets dehydrated and rearranged, and two water molecules are subsequently removed from the brick, as displayed in Fig. 3.1. The fully dehydrated Zr_6O_6 brick contains undercoordinated sites [41, 58, 68, 138], with coordination of the zirconium atoms ranging from 8 to 6. The structure of UiO-66 is however preserved and the brick can easily be hydrated again with a reversible mechanism, giving evidence that the inorganic SBU can undergo dynamic

processes. During these structural rearrangements, the presence of a infrared band related to hydroxy groups was observed by Nishida *et al.* [139] and by Shearer *et al.* [138]. The mechanism of dehydration was first studied by Vandichel *et al.* by means of nudge elastic band calculations [64], showing the presence of loose hydroxyl groups and partially decoordination linkers. These findings point towards an intrinsic mobility of the framework structure, that can accommodate rearrangements without disrupting its stability. However, the static study of this process possesses serious limitations.

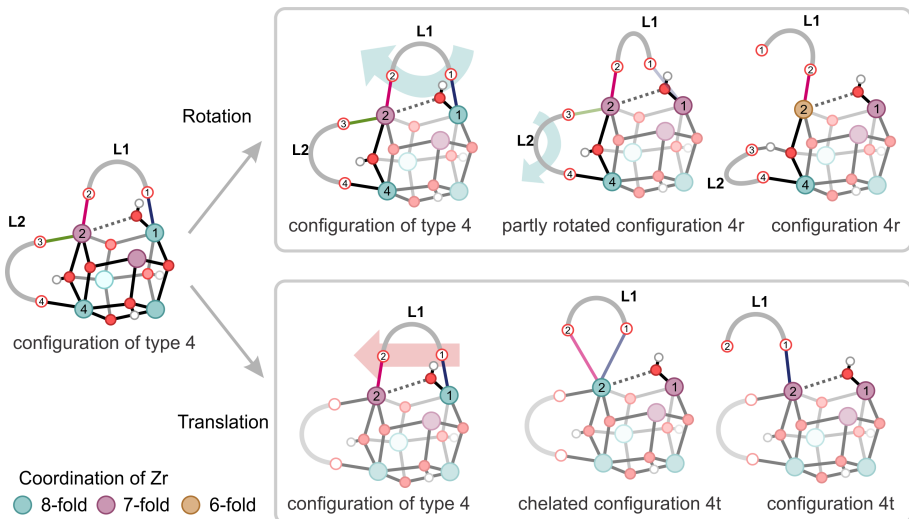


Figure 3.7: Umbrella sampling in two windows of $\text{CV} = 1.45$ and 1.51 , showing two distinct motions of the linkers. On the left column, a translation of the linker L1 generates a chelated structure and a subsequent shift in the carboxylic oxygen connected to Zr2 (configuration 4t). On the right column, a rotation of the linker L1 and a partial decoordination of linker L2 forming a hydrogen bond with an μ_3 -OH hydroxyl group is shown (configuration 4r). A proton transfer between the carboxylic oxygen O3 and the bridging μ_3 -O is also observed and is an indication of the occurrence of an intrinsic dynamic acidity. Colors indicate the coordination number of zirconium atoms.

Therefore, in **PAPER III**, we follow on the fly the fast dynamic of the UiO-66 material at dehydration temperature of 573 K by means of umbrella sampling simulations. The results show an intrinsic dynamic behavior of the material, with open metal sites being created by continuous changes in the network connectivity due to labile M–L bonds. We identify two types of motions of the linkers, namely translation along the axis connecting the two adjacent zirconium atoms, and rotation along the linker axis connecting the two inorganic SBUs, as shown in Fig. 3.7. At the same time, these motions are accompanied by a high mobility

of hydroxy groups created by decoordination of the μ_3 -OH groups. These results show that linkers are more mobile than originally anticipated. The high connectivity between the two SBUs of UiO-66 allows all these reversible rearrangements with activation barriers that can be easily accessible at experimental conditions.

Thermal activation of MOF-808

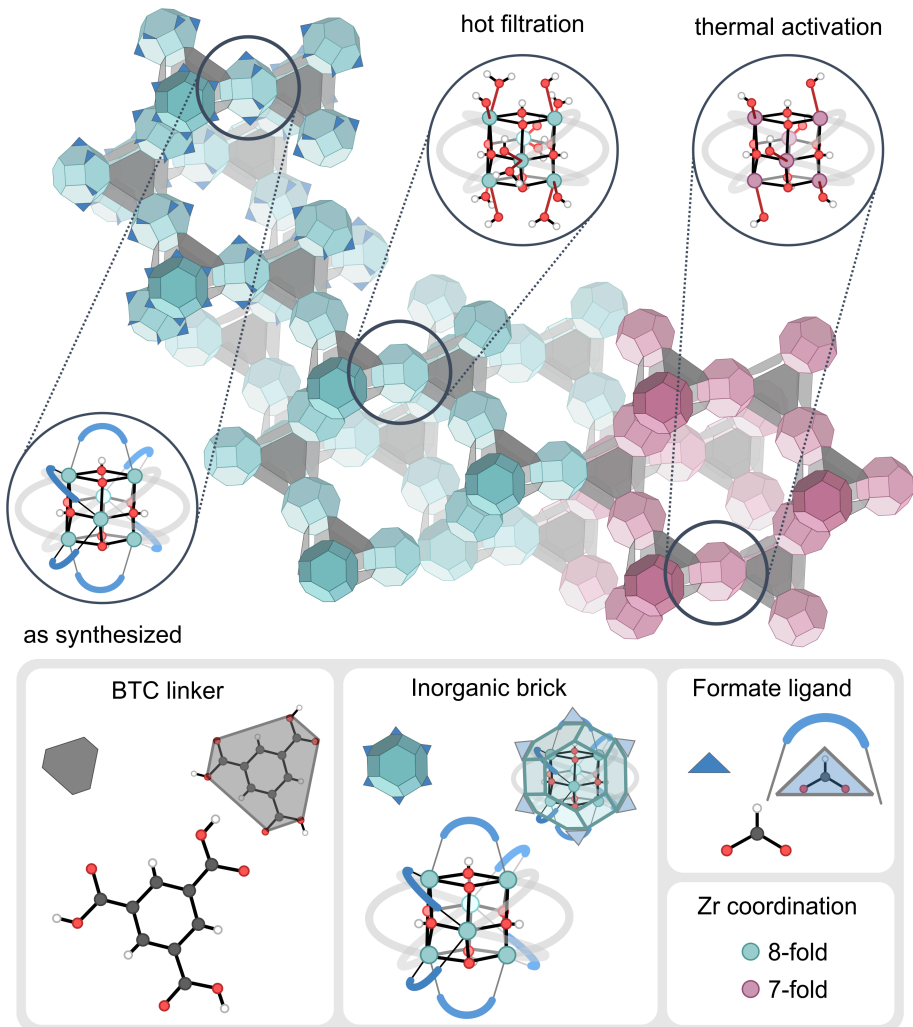


Figure 3.8: Schematic representation of as synthesized and upon activation MOF-808 structures

The active sites and coordination changes upon thermal activation have been studied in MOF-808 in **PAPER VI**. MOF-808 shares the Zr₆O₄OH₄ brick with UiO-66, but the brick is connected to only six tritopic BTC linkers, making it

the least connected MOF in the Zr-MOF family. The material possesses a high catalytic potential due to the intrinsic presence of defective sites of complex nature. In the as synthesized material (Fig. 3.8), the zirconium atoms that are not connected to BTC linkers are capped by formate groups. The material is activated by hot filtration, whereby each formate is replaced by water and hydroxyl group, for a total of six water molecules and six hydroxyl groups per inorganic SBU. Each pair of adjacent zirconium atoms has a similar configuration as the stable configuration 2 of Fig. 3.2, but the presence of multiple Brønsted sites in close proximity gives rise to a more complex nature of the active sites. By thermal activation, similarly to UiO-66, water can be removed from the active sites to open Lewis acid sites for catalysis. In a second stage, up to four of the hydroxyl groups could be also decoordinated by extracting a μ_3 -OH proton from the brick to form water, giving rise to mixed-coordination bricks with 6 and 7-fold coordinated zirconium atoms.

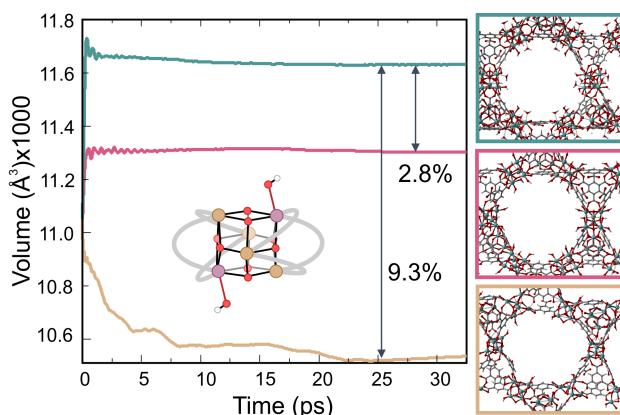


Figure 3.9: Change of volume in time of the three investigated structures with different Zr coordination

In **PAPER VI**, the behavior and stability of the material upon activation processes was investigated by means of a series of independent MD simulations at 300 K at variable unit cell parameters. We show that the dehydration of the inorganic brick substantially affects the stability of the structure. In the hydrated form, the material possesses a high number of Brønsted sites that show dynamic acidity in the form of proton transfer between water and hydroxyl groups that are located in close proximity. This may be important for proton conductivity. The physisorbed water is removed upon thermal treatment leading to a homogeneous distribution of 7-fold coordinated zirconium atoms in the brick (Fig. 3.1). Upon this dehydration, only a slight decrease in the unit cell volume is observed (Fig. 3.9), and the structure remains stable, even though it possesses a high amount of undercoordinated sites. Moreover, these Lewis sites are located in proximity to Brønsted sites arising from hydroxyl groups, making dehydrated MOF-808 a dual heterogeneous catalyst. Further removal of the hydroxyl groups together with the

μ_3 -OH protons causes a collapse of the structure. Due to the overall low structure connectivity the adsorbed hydroxyl groups have to be considered as inherent part of the framework composition and their separation results in the collapse of the material. In contrast to UiO-66, that can undergo reversible dehydration processes where the coordination of the zirconium atoms can be lowered to 6 without disrupting the structure, MOF-808 cannot sustain such decrease in coordination. The physical and chemical properties of UiO-66 cannot be easily extended to MOF-808, even though they share the same inorganic SBU.

Linker functionalization on UiO-66

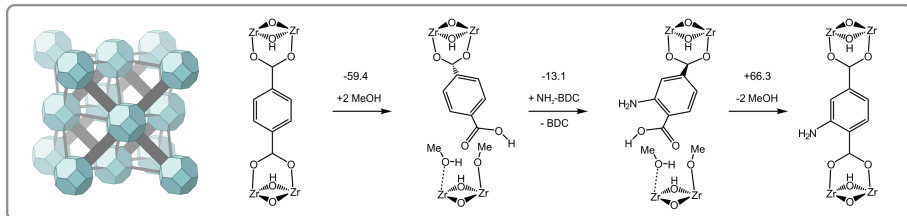
The following results concern the linker functionalization on UiO-66 and its effects on the catalytic activity of the material. The ease of functionalization of UiO-66 can be exploited to tune its catalytic properties.

Post synthetic linker exchange

As reported in Chapter 1, functionalization in UiO-66 can be induced by PSLE, exploiting the robustness of the framework, which can easily undergo coordination changes. In **PAPER IV**, the mechanism was investigated in a dual experimental–computational study performed in collaboration with the group of Prof. Rob Ameloot. The PSLE in UiO-66 that leads to functionalization of the BDC linkers with amino groups was performed in methanol at mild conditions (313 K). Results show that the initial amount of missing linkers did not have an effect on the final composition of the material, pointing towards low energy barriers for the exchange. Moreover, the process was accompanied by an initial lowering of the BET surface area.

In light of these experimental observations and the computational findings reported in Fig. 3.6, a hypothetical exchange mechanism was modeled starting from both pristine and defective material (Fig. 3.10). In the proposed mechanism, linker exchange is initiated by coordination of methanol on the zirconium sites, causing a partial hydrolysis of one of the BDC linkers. This metastable state is characterized by a dangling linker which is stabilized by hydrogen bonds with other carboxylic oxygen atoms and the μ_3 -OH hydrogen from the brick, in a similar fashion as what observed in **PAPER III**. This structure causes a hindrance of the pore in agreement with the reduction in BET surface area. From this configuration, exchange of mono-coordinated BDC linkers with NH₂-BDC quickly ensues, with partial coordination of the new linker. In a following step, methanol is desorbed from the active site and the linker can connect to the zirconium atoms, reestablishing the binding between the two bricks. This preferential adsorption of BDC-NH₂ is explained by the lowering of the enthalpy of about 7 kJ/mol per linker. When starting from a defective material, a similar mechanism can be proposed. In this second scenario, the synthesized material contains formate on

Non-defective material:



Defective material:

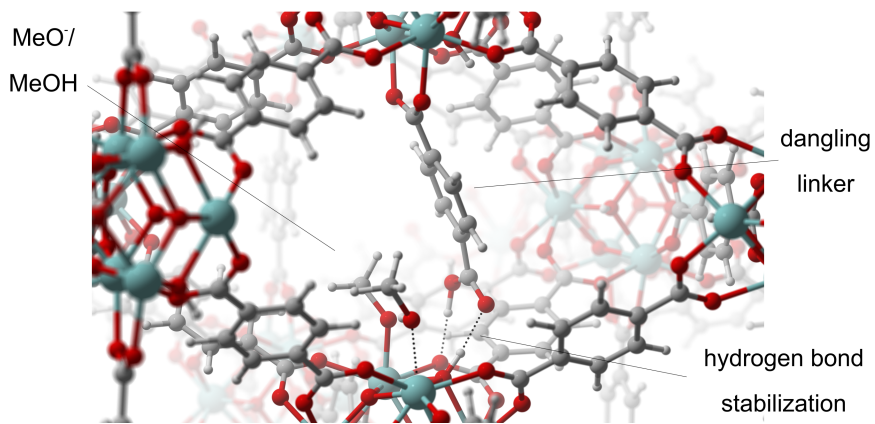
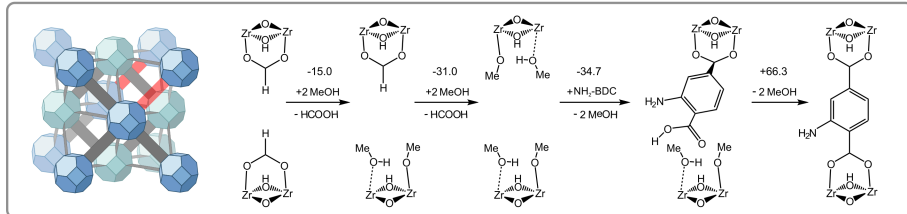


Figure 3.10: Proposed PSE mechanism in non-defective and defective $\text{UiO}-66$. MeOH facilitates ligand exchange through the creation and stabilization of defects. Enthalpy differences are given in kJ/mol at 313 K (PSE temperature)

both defective sides. Formate will be substituted by methanol present in solution, and the defect healing can proceed in a similar way as in the previous case. All these rearrangements are supposedly characterized by low activation barriers, as the final composition of the material does not depend on the initial percentage of functionalized or missing linkers. During the process, the zirconium atoms rapidly change their coordination number, however, giving preference to 8-fold coordinated active sites that enhance the stability of the structure.

Effect of linker functionalization on Fischer esterification in UiO–66

In order to understand the effect of the functionalization of the BDC linkers on the catalytic activity of defective UiO–66, the esterification reaction (Fig. 3.4) was investigated also on the amino functionalized UiO–66-NH₂. Amino functionalization on UiO–66 brings an electrodonating group that would in principle lower the strength of the Lewis acid site. However, experimental insights into the Fischer esterification reaction showed that the amino functionalized UiO–66 was more catalytically active than its non-functionalized counterpart. For this reason, it was speculated that amino groups located in proximity to the defect sites would play an active role during the reaction. Our computational results show no possible reaction pathway that involves proton transfers with the amino groups. We therefore studied the reaction following the same pathway that we propose for the hydrated brick (Fig. 3.4) in the non-functionalized material.

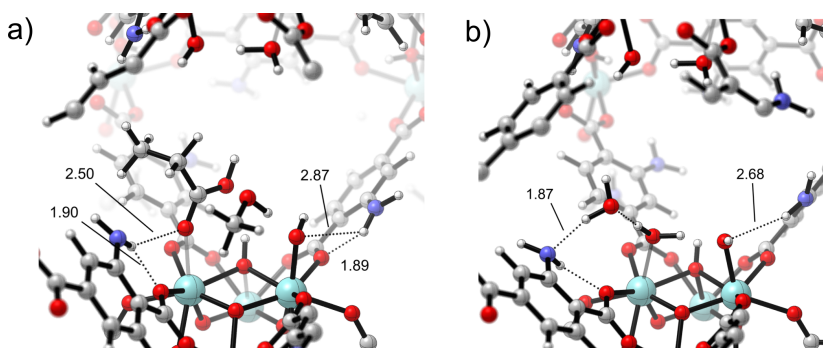


Figure 3.11: Network of hydrogen bonds between acid, methanol, hydroxyl group and amino groups. a) reactive complex 8, b) an additional water molecule present in solution.

The decrease in Lewis acidity upon amino functionalization is indeed confirmed by the increase of the Zr–O distances of the adsorbates [60]. However, for UiO–66-NH₂, stronger stabilization of the adsorbates is observed, as well as a slight decrease in the overall energy barrier of about 11 kJ/mol, which confirms the experimental findings [74, 75]. The amino groups, although not playing an active role in the reaction mechanism, indirectly modulate the properties of the Lewis and

Brønsted sites. A stronger adsorption of the reactants is caused by the formation of a network of hydrogen bonds with the amino groups that cannot be observed in the pristine material. Amino groups provide additional sites where solvent can form hydrogen bonds, as displayed in Fig. 3.11. This indirect positive effect of amino groups on the catalytic properties was observed as well by Hajek et al. for aldol condensation [58]. The effect of other functional groups was further analyzed (see Supplementary Material of **PAPER I**). Electron-withdrawing substituents such as $-\text{NO}_2$ did not decrease the energy barriers, although increasing the Lewis acidity of the metal. Once again, this confirms the dual Lewis/Brønsted character of the UiO-66 catalyst, that can be enhanced by the presence of additional sites within molecular distance.

3.2 Role of solvent: towards operating conditions

So far, a simple model to represent the active sites was used, where only the species immediately coordinated to the zirconium atoms were considered. A more complex model can be constructed by microsolvation, adding a small amount of solvent molecules. However, the findings of the previous section point towards a complex nature of the active sites in the material, where solvent may play an active role in reactive processes and structural modifications. For instance, water was shown to have a beneficial effect on the catalytic performance by providing additional Brønsted sites as well as stabilization of intermediates through hydrogen bonding. For this reason, in **PAPER II** and **PAPER V** we went a step forward in complexity by including an explicit treatment of the solvent in the pores of the UiO-66 material, as indicated in Fig. 3.12. This increase in complexity of the model allows to take into account the processes that can occur at operating conditions, and to represent the full solvent environment within the pores at realistic temperatures and pressures.

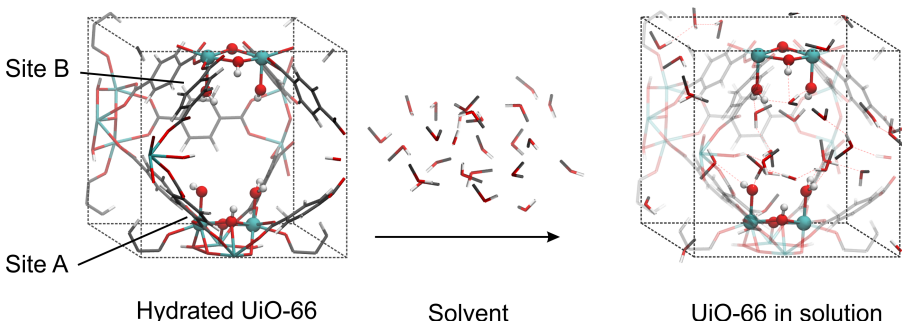


Figure 3.12: Schematic representation of solvent being inserted in the UiO-66 unit cell.

Interaction between UiO–66 and solvent

To understand how a protic solvent such as water and methanol interacts within the material, three independent *ab initio* MD simulations were performed in which a full loading of methanol and two different loadings of water are included in the pores, as well as for the empty material. Molecular simulations allow to investigate how the material is influenced by the presence of the solvent and how the solvent behaves when it is confined in the pores. For the sake of the analysis of these properties, the system can be divided in two components: material and solvent. This way, the properties of the solvated material can be compared to the empty one, and the properties of the confined solvent can be compared to the bulk solvent. Fig. 3.13 displays the vibrational density of states obtained from the power spectrum of the velocity autocorrelation function for the atoms of material and solvent.

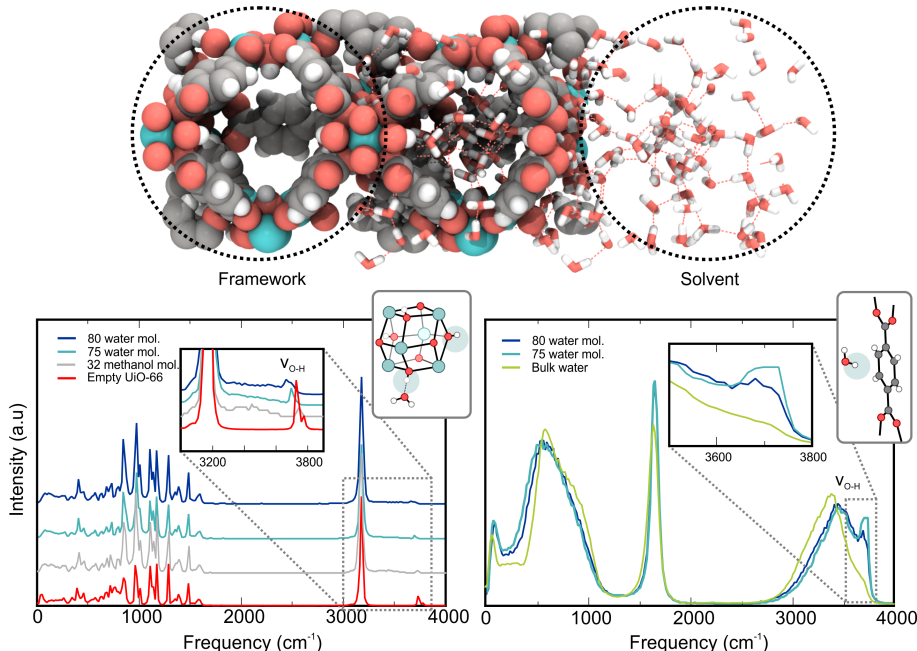


Figure 3.13: Top: schematic representation of the empty pore, pore with the solvent, and confined solvent without the material. Bottom: vibrational density of states obtained from the velocity autocorrelation function power spectra of selected atoms of the simulation. Bottom left: solvated material compared to the empty material. Bottom right: water in the pores compared to bulk water.

The spectrum of the UiO–66 atoms can under 3000 cm^{-1} shows no shifts in the peaks between empty and solvated pores, giving insight on the stability of the

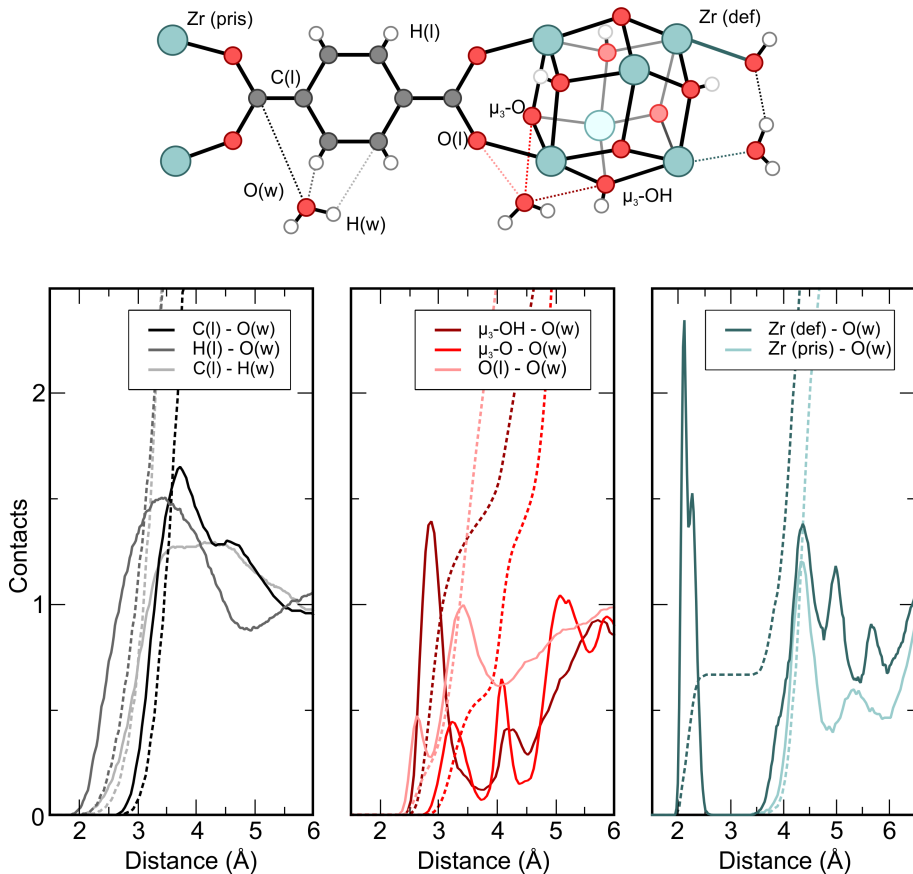


Figure 3.14: Radial distribution functions or pair correlation functions $g(r)$ between oxygen and hydrogen of water ($O(w)$, $H(w)$), and different atoms of the material obtained from the simulation with 80 water molecules in the unit cell. Full lines indicate the $g(r)$, dashed lines indicate its integral. Left panel: RDFs between water and linker carbons and hydrogens ($C(I)$, $H(I)$); middle panel: RDFs between water and oxygen atoms of the linkers and bricks ($O(I)$, $\mu_3\text{-OH}$, $\mu_3\text{-O}$); right panel: RDFs between water and zirconium atoms of defective and pristine bricks ($Zr(\text{def})$, $Zr(\text{pris})$).

framework in protic solvents. For the OH stretching at 3750 cm^{-1} , however, there is a broadening when solvent is included. This is due to the strong interactions between μ_3 -OH hydrogens of the bricks and oxygens of solvent, that form hydrogen bonds. To further investigate this, we analysed the vibrational density of states for the solvent and compared it to the bulk solvent simulated in the same unit cell and at the same conditions. We can notice the appearance of a peak at $\nu > 3700\text{ cm}^{-1}$ in the confined solvent, which is due to O-H bonds that do not form hydrogen bonds. This peak is due to the water molecules whose hydrogen atoms are pointed towards the linkers and do not interact with them, in line with previous reports on hydrophobic confinement [140–142].

These results point towards a dual hydrophobic–hydrophilic interaction between solvent and material, where on the one hand, the solvent experiences a hydrophobic confinement due to the interaction with the linkers, on the other it binds strongly to the μ_3 -OH hydrogens of the bricks. To further gain insight into this behavior, we analyzed the RDFs for specific pairs of atoms of material and solvent. The results in case of water are displayed in Fig. 3.14. The RDF between carbon atoms of the linkers and water clearly shows a hydrophobic confinement behavior, being nearly zero at distances below 3 Å. On the other hand, a strong interaction is observed between water and oxygen atoms belonging to bricks and linkers, showing formation of a network of hydrogen bonds. The coordination between zirconium atoms and water is also analyzed. In the defective brick, the first peak is due to the coordination between water and zirconium on the defect site.

From this data, we can conclude that solvent does not leave the active site during the simulation time, as the interaction is rather strong, in agreement with the previous static calculations and dynamic results on small models. These simulations give indication of the changes in behavior of the solvent upon confinement and the strong interactions around the bricks and in particular on the active site. However, such analysis gives only an insight on the average behavior and not on the dynamic processes that can occur, which will be examined in the next two sections.

Interaction between methanol molecules on the UiO–66 defective site

In **PAPER II**, we used a multilevel modeling approach to analyse the behaviour of methanol solvent around the active site generated by linker removal. We observe a breakage of the symmetry for the two active sites generated by linker removal. The site denoted as Site A shows a trigonal network, similar to what reported in static calculations where three molecules were taken into account. This configuration is not broken during the simulation, giving evidence of its stability. Moreover, proton transfers in a similar fashion to what was reported by Ling and Slater [63] are observed between hydroxyl group and physisorbed water, with the bridging methanol molecule shuttling the proton from one site to the other (Fig. 3.15).

No proton transfers are observed from the μ_3 -OH proton to the hydrogen–bonded methanol molecule, as this configuration is higher activated. Site B, however, shows a more complex evolution, with chains of hydrogen bonds connecting up to 5–6 methanol molecules and forming closed loops. This evolution is reported in Fig. 3.16, where the number of molecules involved in these loops is followed during the simulation time. The system alternates between 4 to 6–membered rings that are anchored on the defect–coordinating water species and the μ_3 -OH group.

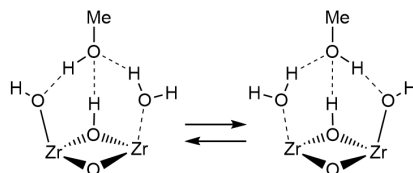


Figure 3.15: Dynamic Brønsted acidity in one of the structures established on the active site in defective UiO-66 and liquid methanol in the pores.

The behaviour is similar to what observed for bulk methanol [143–145], in which a mixture of chain and ring structures formed by six to eight methanol molecules was observed. In this case, the chains are shorter because of confinement, nevertheless, the pore size of defective UiO-66 allows these structures to form. Moreover, open chains of methanol molecules are observed that for part of the simulation connect the two active sites and can in principle provide a way to transfer protons from one site to the other. However, during the simulation time this event is not observed due to the barrier associated to the charge separation.

Proton mobility in the pores of the material was further analyzed. A charge displacement was induced by artificially removing a proton from the active site and inserting it in different positions in the pore of the material (Fig. 3.17) and the system response was followed. In the methanol solvent, the proton can be either stabilized by solvent molecules and maintain its position in the unit cell, or a Grotthuss charge transfer mechanism can occur in which the charge defect travels through a chain of hydrogen bonds, similarly as what observed by Morrone et al. [145]. In one of the simulations, the proton is transported towards the other active site (Fig. 3.17). A configuration is obtained where the original site remains deprotonated and the other is protonated. This configuration is retained for the whole remaining simulation time and is stabilized by the presence of solvent molecules. The zirconium–oxygen distance in the protonated case increases, and the two water molecules physisorbed on the site are more mobile and prone to leave the active site, and a proton transfer could be the initiator to reactant exchanges on the active site. Static periodic calculations were performed to investigate the energy difference related to this charge separation which report a value of 89.4 kJ/mol difference in free energy. Such difference between static and dynamic

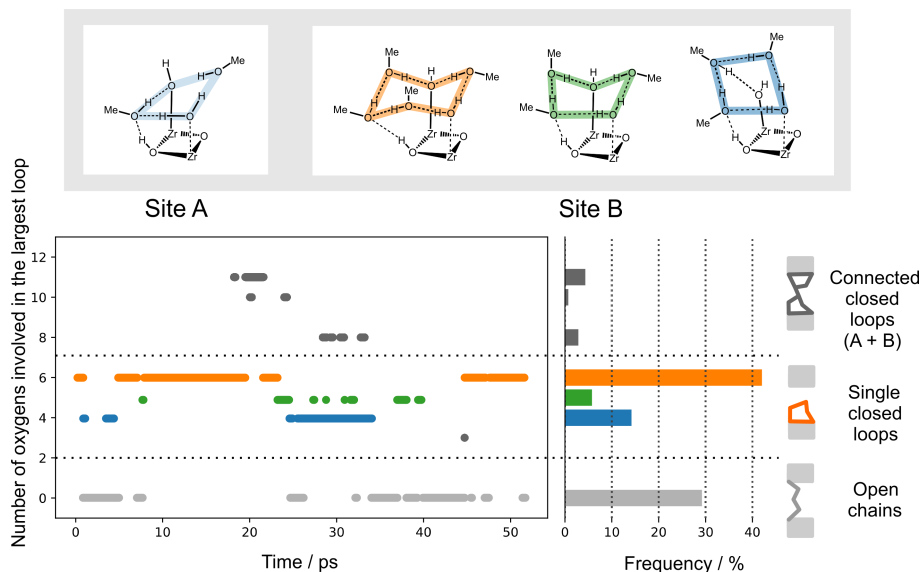


Figure 3.16: Top: Ring configurations observed at site A and site B originating from the interaction between the Zr-bonded hydroxo and water and the solvent molecules. Bottom: Appearance of the various structures during the simulation. The frequency of occurrence of the different structures is also reported. A threshold of 2.2 \AA for the donor-acceptor distance was chosen to determine a hydrogen bond and observations were smoothed over 0.5 ps.

picture gives indication of the positive role of a protic solvent in stabilizing charged configurations that can be reflected in the stabilization of charged intermediates during catalytic processes. These simulations shed light on the role of Brønsted sites in the material. The μ_3 -OH group is heavily involved in the stabilization of supramolecular structures around the active site, but does not deprotonate to the solvent, contrary to water and hydroxyl groups that show dynamic acidic behavior. These findings show the importance of a solvent beyond being a substrate in the reaction, as it can exchange protons, affect reaction mechanisms, and stabilize intermediates through its remarkable interactions with the active sites. In the next section we will see how solvent can be exchanged on the active sites and induce structural rearrangements in the material.

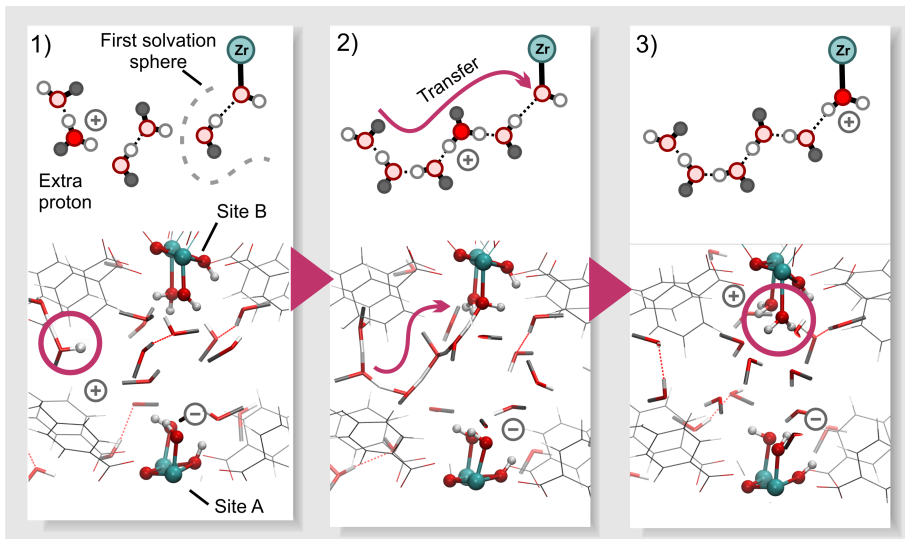


Figure 3.17: Three snapshots of the molecular dynamics simulation which starts from a deprotonated site A and a protonated methanol molecule, with corresponding schematic representation of the process (above). 1) starting structure with protonated solvent 2) a snake-like chain of hydrogen bonds is formed which leads a proton to site B 3) site B is protonated, while site A is missing a proton.

Activated processes related to dynamic changes in the zirconium coordination number

In PAPER V, we focus on the dynamic changes in coordination of the zirconium atoms on the defective sites. Previous regular MD simulations do not show any change in the zirconium coordination, as such processes are rare events characterized by an activation barrier that does not allow their sampling at normal conditions.

However, Zr–O bond breaking is a fundamental event in many processes, such as in the exchange of solvent around the active sites, dehydration, defect formation or PSLE. For this reason, we made use of enhanced sampling by means of a series of independent MTD simulations to investigate the coordination changes around the defective zirconium atoms in water solvent.

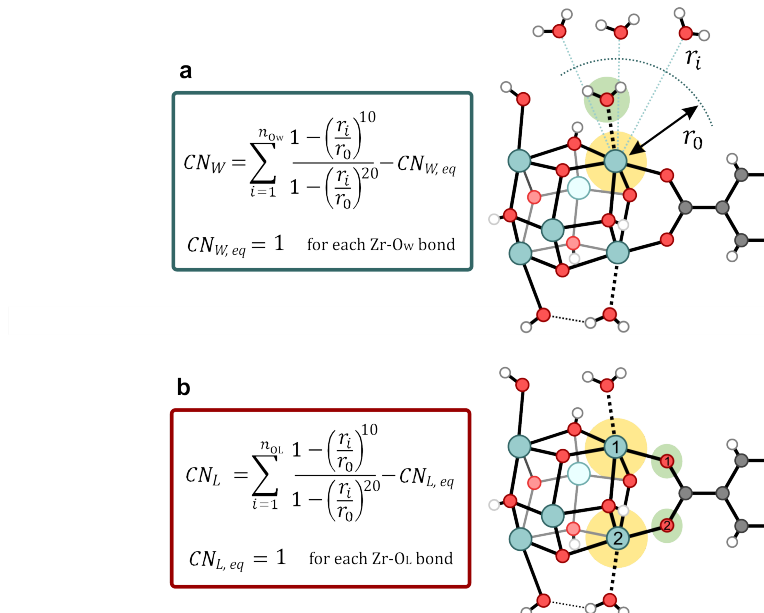


Figure 3.18: Coordination numbers used in the simulation a: coordination number CN_W between zirconium and all water oxygens. Also the linker that shows dynamic movement which induces changes in the zirconium coordination number is visualized. b: coordination number CN_L between each zirconium atom and linker oxygen atoms. n_{Ow} and n_{Ol} are the number of oxygen atoms considered in the two cases, r_i is the zirconium-oxygen distance, r_0 a cutoff distance of 2.9 Å. In yellow, the zirconium atoms considered in the CN. In green, the oxygen atoms that have a weight close to one and substantially different from zero in the summation.

Two CVs were chosen, as displayed in Fig. 3.18: a first one, denoted as CN_W , representing the coordination between zirconium and oxygen atoms of water, and a second one, denoted as CN_L , describing the coordination between zirconium and oxygen atoms of a defect–bridging linker. Both CVs refer to the difference between the coordination state and its equilibrium state. Therefore, starting from an equilibrium value of zero, when a bond is broken, the coordination will decrease by one, or increase by one if an additional bond is formed. Using these two coordination numbers, it is possible to describe many events taking place around the brick, which are schematically reported in Fig. 3.19. In the equilibrated structure,

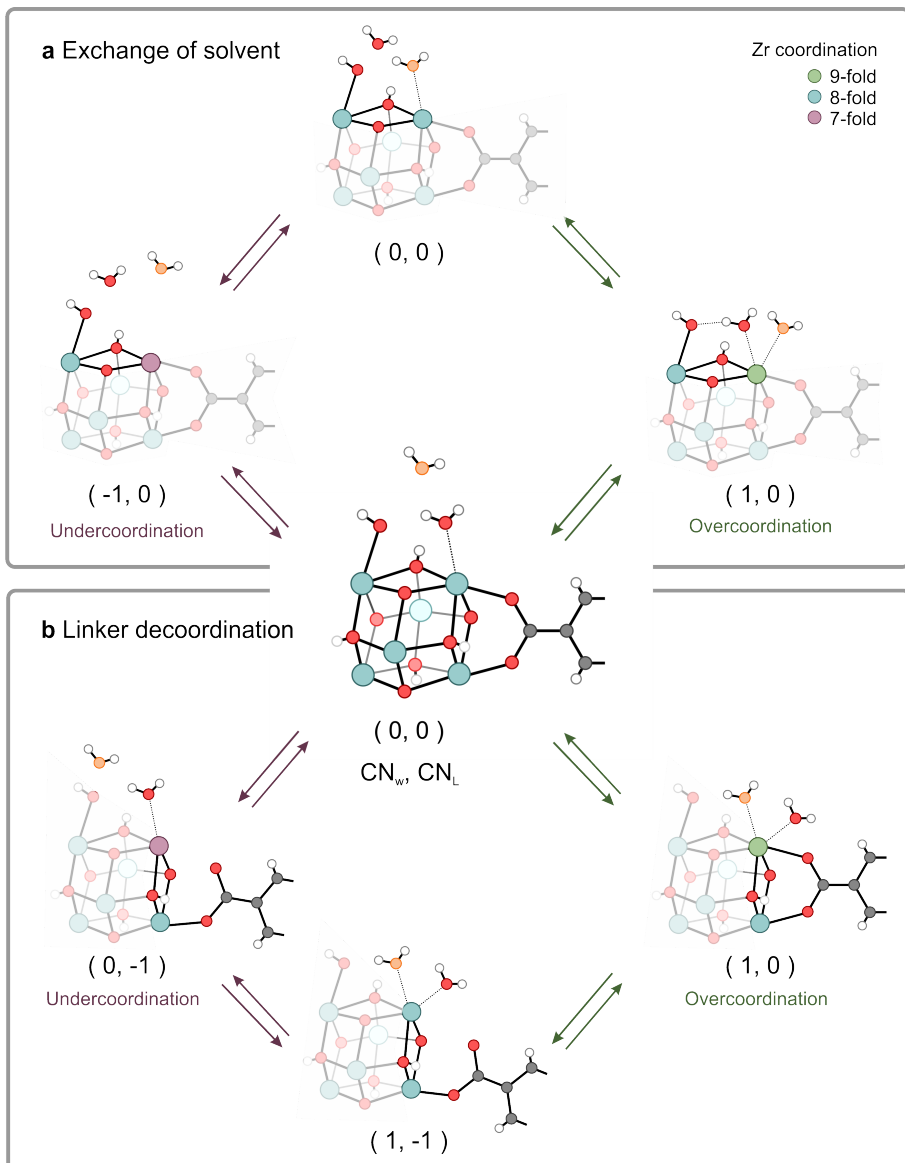


Figure 3.19: Coordination and value of the CV during (a) the exchange of solvent and (b) linker decoordination in the MTD simulations. top paths: stepwise pathway which goes through undercoordinated zirconium; bottom paths: concerted pathways which go through overcoordinated zirconium.

the state defined by the two CNs is (0,0), where the numbers refer to the values of CN_W and CN_L , respectively. Undercoordination and creation of open Lewis acid sites, which can occur by desorption of water or by breakage of Zr–linker bond, can this way be followed. However, on the defective site the system can display also overcoordination, when an additional water molecules coordinates to the zirconium atom increasing its coordination number to a value of 9.

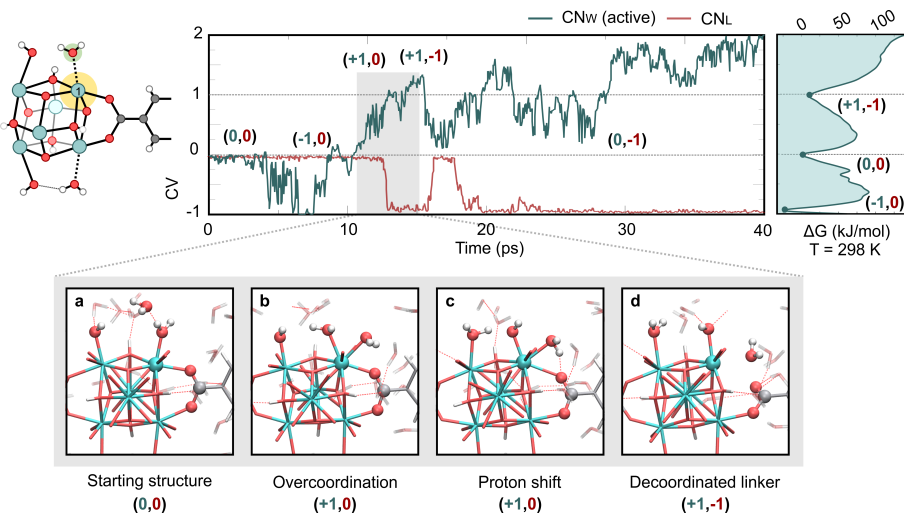


Figure 3.20: Top: evolution of the collective variable CN_W and free energy profile for the first MTD simulation along the CV representing the coordination between the zirconium atom Zr1, highlighted in yellow, and all water molecules (green curve). CN_L between Zr1 and the neighbouring defect-bridging linker oxygen (red curve) is also monitored; bottom: snapshots on the linker decoordination triggered by overcoordination

In a first case study, the coordination CN_W between one of the defective zirconium atom and the water oxygens was biased. At the same time the CN_L between the same zirconium atom and the oxygen belonging to the defect bridging linker is monitored, as displayed in Fig.3.20. In this simulation, fluctuations of the coordination towards negative values are observed, where the open Lewis acid site is created. Via this undercoordinated pathway, solvent molecules can be exchange on the active site in a stepwise fashion. After this process has been sampled, the system evolves towards an overcoordination of the zirconium atom, to which an additional water molecule is coordinated. From this metastable configuration, the system evolves with structural rearrangements which are reported in the bottom of Fig.3.20. After the second water molecule has entered the coordination sphere of zirconium, it transfers a proton to the neighboring hydroxyl group and pushes the parent water molecule closer to the linker. The water molecule forms a hydrogen bond interaction with the linker which is in turn decoordinated from the zirconium

atom, restoring the equilibrium coordination of 8 in the zirconium atom. After these events, the linker recoordinates to the zirconium, to decoordinate again few ps later. In the simulation, we observe a plethora of events such as undercoordination and overcoordination of zirconium, proton transfers, exchange of solvent molecules, and reversible linker decoordination. These fluctuations show how the role of solvent is crucial in inducing such coordination changes and in stabilizing partially decoordinated linkers that can lead to structural rearrangements, while maintaining the stability of the material.

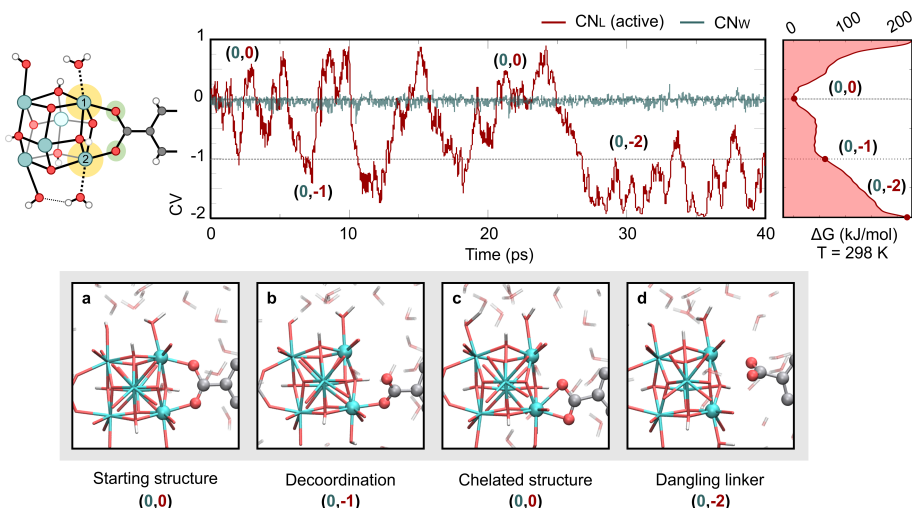


Figure 3.21: Top: free energy profile for the first MTD simulation along the CV representing the coordination between two zirconium atoms and a linker, middle: evolution of the collective variable, bottom: snapshots of the linker decoordination

In a second case study, we biased the coordination CN_L between one linker and two defective zirconium atoms, and at the same time monitored the coordination CN_W between the latter atoms and solvent water. In this case, we are directly biasing the coordination between zirconium and the linker. The evolution of the collective variable is displayed in Fig. 3.21, as well as snapshots that offer mechanistic insights on the different processes. During the simulation, different states are explored, in which the linker is partially decoordinated, can translate to give chelated structures, similarly to what observed in **PAPER III**, or be in a dangling state where both Zr–O bonds are broken, giving an indication of what postulated in **PAPER IV**. In this case, the linker is decoordinated without intermediate role of solvent, and represents an alternate mechanism by which PSLE, defect creation, or even hydrolysis of the material could occur. This dangling linker scenario is stabilized by hydrogen bonding interactions with the solvent. The process would be completed if two water molecules would diffuse to the zirconium

atom and restore the 8-fold coordination, while at the same time one of the two deprotonates to the linker. However this is not observed during the simulation time, as water does not have the time to diffuse, while hindered by the motions of the linker.

By means of this series of simulations, we conclude that both solvent exchange around the active sites and structural rearrangements can either occur via a step-wise mechanism where zirconium atoms are undercoordinated or a concerted one, mediated by an overcoordination. The mobility of the linkers observed in **PAPER III** is herein observed without rearrangements of the bricks that are induced at dehydration conditions. In the presence of a solvent, such processes can undergo at much milder conditions, without disrupting the stability of the material. The role of solvent in allowing these processes is crucial, as it provides hydrogen bonds that can stabilize charged configurations, and can itself strongly interact with the zirconium atoms.

4

Conclusions and Perspectives

In this work of thesis, we shed light on the molecular characterization of the active sites in MOFs by means of different computational techniques. Molecular modeling can offer a rich toolbox to understand the properties of materials and how these properties can be tuned to target specific applications. This is especially true in MOF catalysis, where the active sites are often elusive and arise from disorder in the material that cannot be easily tracked experimentally. We particularly focus on UiO-66, which is an example of an extremely stable MOF that due to its exceptional connectivity can be easily tuned and undergo modifications without losing its crystallinity. In close collaboration with experimental partners, we gained insight into the properties of this promising material, and on the role of complex events that can be observed when modeling processes at operating conditions. Some of the information obtained on UiO-66 can in principle be extended to other zirconium-MOFs such as MOF-808. However, the behavior of UiO-66 cannot be easily generalized, as the exceptionally high connectivity and the local environment can play a major role in the stability and activity of the material.

In **PAPER I**, a Lewis catalyzed reaction was modeled on UiO-66 in close synergy with experimentalists, focusing on the role of the hydration state of the defective site and the functionalization of the material. From theoretical models, in agreement with previous reports, we show that in the most stable configuration, water is coordinated to the defective zirconium atoms. In the proposed reaction mechanism, the chemisorbed water acts as a Brønsted site that actively takes part

in the reaction, along with the zirconium Lewis acid site. An alternative mechanism was investigated on the dehydrated material, where the reaction proceeds without the assistance of water. We show that in this case, the catalytic activity is remarkably decreased due to higher energy barriers, in agreement with the experimental findings. In both proposed mechanisms, UiO–66 acts as dual Lewis/Brønsted catalyst where reactions proceed with a close synergy between the two catalytic centers. The acidic/basic character of protons and oxygens on the brick seems to play a major role, and could be further investigated by pKa calculations.

The role of linker functionalization was also investigated. We show that amino groups play a positive role in the reaction although not actively taking part in the mechanism. Even if the Lewis acidity of the metal centers is decreased, stronger adsorptions and lower energy barriers are observed for the functionalized material. Such counterintuitive result is an indication of the complex nature of the active site on Zr-MOFs. Investigation of the reactants geometries and experimental results points towards an increase on water adsorption around the active site due to a stronger network of hydrogen bonds supported by the amino groups. This stabilization could play a positive role in facilitating certain reactant geometries and supporting intermediate configurations. Theoretical modeling sheds light on the crucial role of water in the reaction and on the complex nature of the active sites and their interaction with protic solvents. Defective UiO–66 and its variants have a high potential as catalysts due to their dual acid/base character and the facile way by which its composition can be tuned. This material can be considered as a prototype MOF that can be designed to possess all the ingredients needed for a dual Lewis/Brønsted catalyst. For this reason, understanding of the role of solvent close to the active site as substrate for proton transfers cannot be neglected. Solvent molecules could play an active role in other UiO–66 catalyzed reactions, as well as in other Zr-MOF, such as NU–1000 or MOF–808, which possess the same inorganic SBU.

In **PAPER VI** we further investigated how MOF–808 responds to similar activation processes such as the UiO–66 dehydration of **PAPER I**. We show that the material possesses an exceptional amount of Brønsted sites that can be created upon hot filtration. By thermal activation, Lewis sites can be created in proximity of the Brønsted sites without disrupting the stability of the structure, offering great potential for future catalytic applications. However, we also observe that further dehydration generates a collapse of the framework and loss of crystallinity.

Much of the insight gained on reactive processes in MOFs stems from the more established computational research done in zeolites. Unlike processes in zeolites, however, reactions in MOFs are often performed at milder conditions in presence of a liquid solvent, that adds further complexity to the model. Moreover, the M–L bonds in MOFs are more labile than the covalent bonds in zeolites and this makes these materials more prone to structural rearrangements and modifications. It is a

challenge to understand in how far the description of the active site corresponds to reality, and for this reason, it is imperative to understand the behavior of the solvent in the pores of the material. Solvent can have an impact on the creation of active sites, be a substrate, determine the formation of particular isomers, influence the rate and selectivity, affect the reaction mechanism, or even activate or deactivate a specific reaction.

The role of solvent was further investigated in **PAPER II**, in which a multilevel modeling approach was employed to study the behavior of defective UiO–66 in presence of solvent methanol. Starting from the insight gained in **PAPER I**, we further investigated the possible adsorption geometries for water and methanol. We then filled the pores of the material with methanol solvent, to replicate the temperature and pressure conditions during a reactive process. We observed a remarkable behavior of the solvent. Supramolecular structures formed by hydrogen bonds are formed around the active sites and evolve dynamically during the simulations. Within these active sites, a dynamic behavior of the protons is observed, as anticipated in **PAPER I**. Such proton transfers may play a substantial role in catalytic processes, such as Fisher esterification, or in structural rearrangements like during PSLE. Moreover, solvent can transfer protons on longer distances within the pores and charged configurations in proximity of the active site can be stabilized, pointing towards a positive role in reactions involving charged intermediates, that goes beyond simple solvation. These simulations shed light on how the active sites may be modulated via these dynamic interactions.

In **PAPER IV**, we studied the PSLE mechanism and showed the active role of methanol during the process. From the computational and experimental insight, we postulate the presence of dangling linkers as intermediate states during the exchange, that are induced and stabilized by interaction with the methanol solvent. These structural rearrangements in the material lead to the replacement of BDC with BDC–NH₂ and a resulting structure characterized by a specific concentration of defects that does not depend on the initial defectivity. This gives insight on the low energy barriers that characterize the process.

PAPER III unraveled the exceptional intrinsic dynamic nature of the UiO–66 material. At dehydration conditions, the material showed reversible mobility of the linkers induced by the brick dehydration. We show that linkers can decoordinate and recoordinate to the brick without disrupting the stability of the material. In **PAPER V**, we further examine the interaction between a protic solvent and material during the structural rearrangements of the PSLE process. By means of a series of MD simulations, we identified a hydrophobic and a hydrophilic region in the material. We show that on the one hand, the linkers provide hydrophobic confinement, on the other, solvent strongly interacts with the inorganic SBUs and in particular with the zirconium atoms on the defective sites. To understand the dynamic interaction between solvent and material on these sites and explore the events that

can take place, we performed a series of independent MTD simulations, where a change in the coordination of the zirconium atoms is induced. These simulations show that Lewis acid sites can be created by decoordination of water, but we also report overcoordination of the zirconium atoms by adsorption of an additional water molecule. Via these two changes in coordination, exchange of solvent molecules on the active site has been observed. Moreover, structural rearrangements in the material have been induced. The strong interaction between solvent molecules and defective sites can lead to a dynamic behavior of the linker, similarly as what observed in **PAPER III**, but this time at milder conditions, by solvent mediation and without alteration of the brick. These findings shed light on the dynamic interplay between a protic solvent and the UiO–66 material at operating conditions during PSLE. Moreover, one can postulate that these active sites may be dynamically opened for catalysis by temporary linker decoordination, giving a variable Lewis acidity to the metals and more opportunities for Lewis catalyzed reactions. The highly connected UiO–66 structure allows all these structural rearrangements where a plethora of active sites that can work in synergy can be generated without losing its crystallinity.

The findings reported in this work of thesis gave valuable insight into the complexity of the Zr–MOF catalysts, with UiO–66 as main case study. We investigated how the presence of disorder and the interactions with solvent lead to the creation of a plethora of active sites that can work in close synergy to bring a beneficial effect in Lewis catalyzed reactions. The exceptional chemical versatility of MOFs can be exploited only if we gain enough understanding at the molecular level of their properties and how these properties can be affected and tuned. Knowing the sources of error is imperative, and for this reason, theory and experiments have to go hand in hand. For this purpose, the use of well-studied model systems such as UiO–66 is crucial. In the past years, computational research in MOFs has evolved from providing simple representations of model systems to more complex models that can represent the events that can occur at operating conditions. The growth in computational power will allow to access larger time and length scales, and to make models that can more and more represent processes at realistic conditions, especially in complex fields such as heterogeneous catalysis. The further step is the understanding of how computational modeling can help to design active sites and how databases of possible structures can be screened to target a specific property. The multiple theoretical and experimental tools that have been developed represent each a different point of view from which a certain phenomenon can be investigated. For this reason, the creation of databases in which different computational and experimental results can be stored and accessed will be more and more important in the future of MOF research.

Part II

Published papers

A

Publication List

Updated May 2019

Publications in international peer-reviewed journals

1. M. Filez, C. Caratelli, M. Rivera-Torrente, F. Muniz-Miranda, M. Hoek, M. F.M. Altelaar, A. J.R. Heck, A.K Dutta Chowdhury, V. Van Speybroeck, B. M. Weckhuysen, *Molecular Nucleation Mechanism of Zeolitic Imidazolate Frameworks*, in preparation
2. J. Hajek, C. Caratelli, ... M. Waroquier, V. Van Speybroeck, *Investigating zirconium coordination changes in MOF-808 upon activation processes*, in preparation
3. C. Caratelli, J. Hajek, E.J. Meijer, B. Ensing, M. Waroquier, V. Van Speybroeck, *Dynamic interplay between defective UiO-66 and protic solvents in activated processes*, in preparation
4. J. Marreiros, C. Caratelli, J. Hajek, A. Krajnc, G. Fleury, B. Bueken, D. De Vos, G. Mali, M. Roeffaers, V. Van Speybroeck, R. Ameloot, *Active*

Role of Methanol in Post-Synthetic Linker Exchange in the Metal-Organic Framework UiO-66, Chemistry of Materials, **31** (4), 1359–1369 (2019)
IF: 9.890

5. J. Hajek, C. Caratelli, R. Demuynck, K. De Wispelaere, L. Vanduyfhuys, M. Waroquier, V. Van Speybroeck, *On the intrinsic dynamic nature of the rigid UiO-66 metal-organic framework*, Chemical Science, **8**, 2723–2732 (2018)
IF: 8.688
6. C. Caratelli, J. Hajek, S.M.J. Rogge, S. Vandenbrande, E.J. Meijer, M. Waroquier, V. Van Speybroeck, *Influence of a confined methanol solvent on the reactivity of active sites in UiO-66*, ChemPhysChem, **19**, 420–4290 (2018)
IF: 3.075
7. C. Caratelli, J. Hajek, F. G. Cirujano, M. Waroquier, F. X. Llabrés i Xamena, V. Van Speybroeck, *Nature of active sites on UiO-66 and beneficial influence of water in the catalysis of Fischer esterification*, Journal of Catalysis, **352**, 401–414 (2017)
IF: 6.844

Conference contributions

Oral presentations

1. Dynamic interplay between defective UiO-66 and confined solvent: insights into a reaction environment at operating conditions
C. Caratelli, J. Hajek, S. M.J. Rogge, A. Lamaire, M. Waroquier, V. Van Speybroeck
XXth Netherlands' Catalysis and Chemistry Conference (NCCC XX), Noordwijkerhout, The Netherlands, Mar 4–6 2019
2. Modeling nanoporous materials at the nanoscale: the role of high performance computing in materials science
C. Caratelli
HPC-UGent User Meeting, Ghent, Belgium, Jan 28 2019
3. Post synthetic linker exchange of UiO-66: understanding the role of solvent and defects by time resolved characterization
J. Marreiros, C. Caratelli, J. Hajek, A. Krajnc, G. Fleury, B. Bueken, D. De Vos, V. Van Speybroeck, G. Mali, M. Roeffaers, R. Ameloot
IVth International Conference on Metal-Organic Frameworks and Open Framework Compounds (MOF 2018), Auckland, New Zealand, 9–13 December 2018

4. Investigating solvent effect in the acidity of UiO-66 metal organic framework for catalysis
C. Caratelli, J. Hajek, A. Tiwari, S. M.J. Rogge, B. Ensing, M. Waroquier, E.J. Meijer, V. Van Speybroeck
IVth International Conference on Metal-Organic Frameworks and Open Framework Compounds (MOF 2018), Auckland, New Zealand, 9–13 December 2018
5. Towards a molecular level understanding of chemical and physical phenomena in metal-organic frameworks
J. Wieme, C. Caratelli, R. Demuynck, A. De Vos, J. Hajek, A. E. J. Hoffman, A. Lamaire, K. Lejaeghere, S. M.J. Rogge, S. Vandenbrande, L. Vanduyfhuys, M. Waroquier, V. Van Speybroeck
Congrès français des MOFs, Paris, France, 16–18 May 2018
6. Influence of structural topology on the catalytic properties of Zr based MOFs: the case of UiO-66 and MOF-808
J. Hajek, C. Caratelli, M. Waroquier, V. Van Speybroeck
XIXth Netherlands' Catalysis and Chemistry Conference (NCCC XIX), Noordwijkerhout, The Netherlands, 5–7 March 2018
7. Influence of a confined methanol solvent on the reactivity of active sites on UiO-66
C. Caratelli, J. Hajek, M. Waroquier, E.J. Meijer, V. Van Speybroeck
2nd DEFNET School, Bochum, Germany, 18–21 September 2017
8. First principle study of active sites on UiO-66 for Fischer esterification
C. Caratelli, J. Hajek, F. G. Cirujano, M. Waroquier, F.X. Llabrés i Xamena, V. Van Speybroeck
Europacat 2017, Florence, Italy, 27–31 August 2017
9. First principle characterization of active sites on UiO-66 and their role in the catalysis of Fischer esterification
C. Caratelli, J. Hajek, F. G. Cirujano, M. Waroquier, F. X. Llabrés i Xamena, V. Van Speybroeck
XVIIIth Netherlands' Catalysis and Chemistry Conference (NCCC XVIII), Noordwijkerhout, The Netherlands, 6–8 March 2017
10. Nature of active sites on UiO-66 and UiO-66-NH₂ in the catalysis of Fischer esterification
C. Caratelli, J. Hajek, G. Cirujano, A. Corma, M. Waroquier, F.X. Llabrés i Xamena, V. Van Speybroeck
Chemical Research in Flanders Symposium (CRF-1), Blankenberge, Belgium, 24–26 October 2016
11. Mechanistic study of Fischer esterification on UiO-66 and UiO-66-NH₂
C. Caratelli, J. Hajek, F.G. Cirujano, A. Corma, M. Waroquier, F.X. Llabrés

i Xamena, V. Van Speybroeck
1st DEFNET School, Valencia, Spain, 21–24 June 2016

Poster presentations

1. How the connectivity of stable Zr-based MOFs affects the metal coordination and the nature of the active sites
J. Hajek, C. Caratelli, M. Waroquier, V. Van Speybroeck
MOFSIM 2019, Ghent, Belgium, Apr 10–12 2019
2. Dynamic creation of active sites on UiO-66 by interaction with protic solvents
C. Caratelli, J. Hajek, S. M.J. Rogge, M. Waroquier, B. Ensing, E.J. Meijer, V. Van Speybroeck
MOFSIM 2019, Ghent, Belgium, Apr 10–12 2019
3. Dynamic creation of active sites on UiO-66 by interaction with protic solvents
C. Caratelli, J. Hajek, S. M.J. Rogge, M. Waroquier, B. Ensing, E.J. Meijer, V. Van Speybroeck
1st KNCV-CTC symposium, Amsterdam, The Netherlands, Mar 26 2019
4. How the connectivity of stable Zr-based MOFs affects the metal coordination and the nature of the active sites
J. Hajek, C. Caratelli, M. Waroquier, V. Van Speybroeck
XXth Netherlands' Catalysis and Chemistry Conference (NCCC XX), Noordwijkerhout, The Netherlands, Mar 4–6 2019
5. Exploring the intrinsic dynamics of rigid Zr-based MOFs
J. Hajek, C. Caratelli, R. Demuynck, K. De Wispelaere, L. Vanduyfhuys, M. Waroquier, V. Van Speybroeck
IVth International Conference on Metal-Organic Frameworks and Open Framework Compounds (MOF 2018), Auckland, New Zealand, 9–13 December 2018
6. Modeling reactive processes in nanoporous materials: a look into the complexity
C. Caratelli, K. De Wispelaere, J. Hajek, P. Cnudde, S. M.J. Rogge, S. Vandenbrande, R. Demuynck, L. Vanduyfhuys, M. Waroquier, V. Van Speybroeck
Ghent, Belgium, Jun 1 2018
7. Investigating the outstanding dynamic behavior of protons on UiO-66 defective sites
C. Caratelli, J. Hajek, A. Tiwari, M. Waroquier, B. Ensing, E. Jan Meijer, V. Van Speybroeck
EuroMOF 2017, Delft, The Netherlands, Oct 29 -- Nov 1 2017

8. Post synthetic linker exchange of UiO-66: understanding the role of solvent and defects by time resolved characterization
J. Marreiros, C. Caratelli, J. Hajek, A. Krajnc, G. Fleury, V. Van Speybroeck, G. Mali, M. Roeffaers, R. Ameloot
EuroMOF 2017, Delft, The Netherlands, Oct 29 -- Nov 1 2017
9. Influence of a confined methanol solvent on the reactivity of active sites in UiO-66
C. Caratelli, J. Hajek, S. M.J. Rogge, S. Vandenbrande, E.J. Meijer, M. Waroquier, V. Van Speybroeck
XIXth Netherlands' Catalysis and Chemistry Conference (NCCC XIX), Noordwijkerhout, The Netherlands, Mar 5–7 2018
10. Catalytic sites on UiO-66 for Fischer esterification
C. Caratelli, J. Hajek, G. Cirujano, A. Corma, M. Waroquier, F.X. Llabrés i Xamena, V. Van Speybroeck
MOLSIM 2017: Understanding Molecular Simulations, Amsterdam, The Netherlands, Jan 9–20 2017
11. Catalytic sites on UiO-66 for Fischer esterification
C. Caratelli, J. Hajek, G. Cirujano, A. Corma, M. Waroquier, F.X. Llabrés i Xamena, V. Van Speybroeck
Annual IAP Meeting IAP-PAI P7/05, Liège, Belgium, 12 October 2016
12. Catalytic role of UiO-66 and UiO-66-NH₂ in Fischer esterification: a mechanistic study
C. Caratelli, J. Hajek, G. Cirujano, A. Corma, M. Waroquier, F.X. Llabrés i Xamena, V. Van Speybroeck
3rd DEFNET workshop, Ghent, Belgium, 22–24 March 2016
13. Catalytic role of UiO-66 and UiO-66-NH₂ in Fischer esterification: a mechanistic study
C. Caratelli, J. Hajek, G. Cirujano, A. Corma, M. Waroquier, F.X. Llabrés i Xamena, V. Van Speybroeck
XVIIth Netherlands' Catalysis and Chemistry Conference (NCCC XVII), Noordwijkerhout, The Netherlands, 7–9 March 2016

Bibliography

- [1] I. Atadashi, M. Aroua, and A. A. Aziz, "Biodiesel separation and purification: a review," *Renewable Energy*, vol. 36, no. 2, pp. 437–443, 2011.
- [2] A. S. Chouhan and A. Sarma, "Modern heterogeneous catalysts for biodiesel production: A comprehensive review," *Renewable and Sustainable Energy Reviews*, vol. 15, no. 9, pp. 4378–4399, 2011.
- [3] A. D. McNaught and A. D. McNaught, *Compendium of chemical terminology*, vol. 1669. Blackwell Science Oxford, 1997.
- [4] O. K. Farha, I. Eryazici, N. C. Jeong, B. G. Hauser, C. E. Wilmer, A. A. Sarjeant, R. Q. Snurr, S. T. Nguyen, A. z. Yazaydin, and J. T. Hupp, "Metal–organic framework materials with ultrahigh surface areas: Is the sky the limit?," *Journal of the American Chemical Society*, vol. 134, no. 36, pp. 15016–15021, 2012. PMID: 22906112.
- [5] I. M. Hönicke, I. Senkovska, V. Bon, I. A. Baburin, N. Bönisch, S. Raschke, J. D. Evans, and S. Kaskel, "Balancing mechanical stability and ultrahigh porosity in crystalline framework materials," *Angewandte Chemie International Edition*, vol. 57, no. 42, pp. 13780–13783, 2018.
- [6] J. Liang, Z. Liang, R. Zou, and Y. Zhao, "Heterogeneous catalysis in zeolites, mesoporous silica, and metal–organic frameworks," *Advanced Materials*, vol. 29, no. 30, p. 1701139, 2017.
- [7] V. Van Speybroeck, K. Hemelsoet, L. Joos, M. Waroquier, R. G. Bell, and C. R. A. Catlow, "Advances in theory and their application within the field of zeolite chemistry," *Chemical Society Reviews*, vol. 44, no. 20, pp. 7044–7111, 2015.
- [8] S. R. Batten, B. F. Hoskins, and R. Robson, "Two interpenetrating 3d networks which generate spacious sealed-off compartments enclosing of the order of 20 solvent molecules in the structures of $\text{zn}(\text{cn})(\text{no}_3)(\text{tpt})\frac{2}{3}\cdot\text{cntdot}\cdot\text{solv}$ ($\text{tpt}=2, 4, 6$ -tri (4-pyridyl)-1, 3, 5-triazine, $\text{solv}=\text{apprx. } \frac{3}{4}\text{c}_2\text{h}_2\text{cl}_4$. $\text{cntdot. } \frac{3}{4}\text{ch}_3\text{oh}$ or. $\text{apprx. } \frac{3}{2}\text{chcl}_3$. $\text{cntdot. } \frac{1}{3}\text{ch}_3\text{oh}$)", *Journal of the American Chemical Society*, vol. 117, no. 19, pp. 5385–5386, 1995.

- [9] B. Hoskins and R. Robson, "Design and construction of a new class of scaffolding-like materials comprising infinite polymeric frameworks of 3d-linked molecular rods. a reappraisal of the zinc cyanide and cadmium cyanide structures and the synthesis and structure of the diamond-related frameworks [n (ch3) 4][cuiznii (cn) 4] and cui [4, 4', 4'', 4'''-tetracyanotetraphenylmethane] bf4. xc6h5no2," *Journal of the American Chemical Society*, vol. 112, no. 4, pp. 1546–1554, 1990.
- [10] S. Kitagawa, S. Matsuyama, M. Munakata, and T. Emori, "Synthesis and crystal structures of novel one-dimensional polymers,[{M (bpen) X} ∞][[m= cu i, x= pf 6–; m= ag i, x= clo 4–; bpen= trans-1, 2-bis (2-pyridyl) ethylene] and [{Cu (bpen)(CO)(CH 3 CN)(PF 6)} ∞]," *Journal of the Chemical Society, Dalton Transactions*, no. 11, pp. 2869–2874, 1991.
- [11] S. Kitagawa, S. Kawata, Y. Nozaka, and M. Munakata, "Synthesis and crystal structures of novel copper (i) co-ordination polymers and a hexacopper (i) cluster of quinoline-2-thione," *Journal of the Chemical Society, Dalton Transactions*, no. 9, pp. 1399–1404, 1993.
- [12] O. Yaghi and H. Li, "Hydrothermal synthesis of a metal-organic framework containing large rectangular channels," *Journal of the American Chemical Society*, vol. 117, no. 41, pp. 10401–10402, 1995.
- [13] D. Riou and G. Férey, "Hybrid open frameworks (mil-n). part 3 crystal structures of the ht and lt forms of mil-7: a new vanadium propylenediphosphonate with an open-framework. influence of the synthesis temperature on the oxidation state of vanadium within the same structural type," *Journal of Materials Chemistry*, vol. 8, no. 12, pp. 2733–2735, 1998.
- [14] H. Furukawa, K. E. Cordova, M. O'Keeffe, and O. M. Yaghi, "The chemistry and applications of metal-organic frameworks," *Science*, vol. 341, no. 6149, p. 1230444, 2013.
- [15] N. Stock and S. Biswas, "Synthesis of metal-organic frameworks (mofs): routes to various mof topologies, morphologies, and composites," *Chemical reviews*, vol. 112, no. 2, pp. 933–969, 2011.
- [16] H.-C. Zhou and S. Kitagawa, "Metal-organic frameworks (mofs).," 2014.
- [17] H.-C. Zhou, J. R. Long, and O. M. Yaghi, "Introduction to metal-organic frameworks," 2012.
- [18] M. Eddaoudi, J. Kim, N. Rosi, D. Vodak, J. Wachter, M. O'keeffe, and O. M. Yaghi, "Systematic design of pore size and functionality in isoreticular mofs and their application in methane storage," *Science*, vol. 295, no. 5554, pp. 469–472, 2002.

- [19] D. S. Sholl and R. P. Lively, "Defects in metal–organic frameworks: Challenge or opportunity?," *The Journal of Physical Chemistry Letters*, vol. 6, no. 17, pp. 3437–3444, 2015. PMID: 26268796.
- [20] Z. Fang, B. Bueken, D. E. De Vos, and R. A. Fischer, "Defect-engineered metal–organic frameworks," *Angewandte Chemie International Edition*, vol. 54, no. 25, pp. 7234–7254, 2015.
- [21] M. J. Cliffe, W. Wan, X. Zou, P. A. Chater, A. K. Kleppe, M. G. Tucker, H. Wilhelm, N. P. Funnell, F.-X. Coudert, and A. L. Goodwin, "Correlated defect nanoregions in a metal–organic framework," *Nature communications*, vol. 5, p. 4176, 2014.
- [22] M. Fujita, Y. J. Kwon, S. Washizu, and K. Ogura, "Preparation, clathration ability, and catalysis of a two-dimensional square network material composed of cadmium(ii) and 4,4'-bipyridine," *Journal of the American Chemical Society*, vol. 116, no. 3, pp. 1151–1152, 1994.
- [23] D. Yang and B. C. Gates, "Catalysis by metal organic frameworks: Perspective and suggestions for future research," *ACS Catalysis*, vol. 9, no. 3, pp. 1779–1798, 2019.
- [24] Z. Wang and S. M. Cohen, "Postsynthetic modification of metal–organic frameworks," *Chem. Soc. Rev.*, vol. 38, pp. 1315–1329, 2009.
- [25] Y. Z. Baiyan Li, Matthew Chrzanowski and S. Ma, "Applications of metal–organic frameworks featuring multi-functional sites," *Coordination Chemistry Reviews*, vol. 307, pp. 106 – 129, 2016. Chemistry and Applications of Metal Organic Frameworks.
- [26] K. W. Chapman, G. J. Halder, and P. J. Chupas, "Pressure-induced amorphization and porosity modification in a metal- organic framework," *Journal of the American Chemical Society*, vol. 131, no. 48, pp. 17546–17547, 2009.
- [27] P. Horcajada, T. Chalati, C. Serre, B. Gillet, C. Sebrie, T. Baati, J. F. Eubank, D. Heurtaux, P. Clayette, C. Kreuz, *et al.*, "Porous metal–organic-framework nanoscale carriers as a potential platform for drug delivery and imaging," *Nature materials*, vol. 9, no. 2, p. 172, 2010.
- [28] S. Keskin, T. M. van Heest, and D. S. Sholl, "Can metal–organic framework materials play a useful role in large-scale carbon dioxide separations?," *ChemSusChem*, vol. 3, no. 8, pp. 879–891, 2010.
- [29] J. Canivet, A. Fateeva, Y. Guo, B. Coasne, and D. Farrusseng, "Water adsorption in mofs: fundamentals and applications," *Chemical Society Reviews*, vol. 43, no. 16, pp. 5594–5617, 2014.

- [30] A. C. Kizzie, A. G. Wong-Foy, and A. J. Matzger, "Effect of humidity on the performance of microporous coordination polymers as adsorbents for co₂ capture," *Langmuir*, vol. 27, no. 10, pp. 6368–6373, 2011.
- [31] J. A. Greathouse and M. D. Allendorf, "The interaction of water with mof-5 simulated by molecular dynamics," *Journal of the American Chemical Society*, vol. 128, no. 33, pp. 10678–10679, 2006.
- [32] J. J. Low, A. I. Benin, P. Jakubczak, J. F. Abrahamian, S. A. Faheem, and R. R. Willis, "Virtual high throughput screening confirmed experimentally: porous coordination polymer hydration," *Journal of the American Chemical Society*, vol. 131, no. 43, pp. 15834–15842, 2009.
- [33] S. S. Kaye, A. Dailly, O. M. Yaghi, and J. R. Long, "Impact of preparation and handling on the hydrogen storage properties of zn4o (1, 4-benzenedicarboxylate) 3 (mof-5)," *Journal of the American Chemical Society*, vol. 129, no. 46, pp. 14176–14177, 2007.
- [34] J. B. DeCoste, G. W. Peterson, B. J. Schindler, K. L. Killops, M. A. Browe, and J. J. Mahle, "The effect of water adsorption on the structure of the carboxylate containing metal–organic frameworks cu-btc, mg-mof-74, and uio-66," *Journal of Materials Chemistry A*, vol. 1, no. 38, pp. 11922–11932, 2013.
- [35] S. Kitagawa and M. Kondo, "Functional micropore chemistry of crystalline metal complex-assembled compounds," *Bulletin of the Chemical Society of Japan*, vol. 71, no. 8, pp. 1739–1753, 1998.
- [36] R. Matsuda, R. Kitaura, S. Kitagawa, Y. Kubota, T. C. Kobayashi, S. Horike, and M. Takata, "Guest shape-responsive fitting of porous coordination polymer with shrinkable framework," *Journal of the American Chemical Society*, vol. 126, no. 43, pp. 14063–14070, 2004.
- [37] F.-X. Coudert, "Responsive metal–organic frameworks and framework materials: under pressure, taking the heat, in the spotlight, with friends," *Chemistry of Materials*, vol. 27, no. 6, pp. 1905–1916, 2015.
- [38] H. Furukawa, F. Gándara, Y.-B. Zhang, J. Jiang, W. L. Queen, M. R. Hudson, and O. M. Yaghi, "Water adsorption in porous metal–organic frameworks and related materials," *Journal of the American Chemical Society*, vol. 136, no. 11, pp. 4369–4381, 2014.
- [39] Y. Bai, Y. Dou, L.-H. Xie, W. Rutledge, J.-R. Li, and H.-C. Zhou, "Zr-based metal–organic frameworks: design, synthesis, structure, and applications," *Chemical Society Reviews*, vol. 45, no. 8, pp. 2327–2367, 2016.
- [40] J. H. Cavka, S. Jakobsen, U. Olsbye, N. Guillou, C. Lamberti, S. Bordiga, and K. P. Lillerud, "A new zirconium inorganic building brick forming metal

- organic frameworks with exceptional stability," *Journal of the American Chemical Society*, vol. 130, no. 42, pp. 13850–13851, 2008.
- [41] L. Valenzano, B. Civalleri, S. Chavan, S. Bordiga, M. H. Nilsen, S. Jakobsen, K. P. Lillerud, and C. Lamberti, "Disclosing the complex structure of uio-66 metal organic framework: a synergic combination of experiment and theory," *Chemistry of Materials*, vol. 23, no. 7, pp. 1700–1718, 2011.
- [42] G. Wißmann, A. Schaate, S. Lilienthal, I. Bremer, A. M. Schneider, and P. Behrens, "Modulated synthesis of zr-fumarate mof," *Microporous and Mesoporous Materials*, vol. 152, pp. 64–70, 2012.
- [43] A. Schaate, P. Roy, A. Godt, J. Lippke, F. Waltz, M. Wiebcke, and P. Behrens, "Modulated synthesis of zr-based metal–organic frameworks: from nano to single crystals," *Chemistry—A European Journal*, vol. 17, no. 24, pp. 6643–6651, 2011.
- [44] A. Schaate, P. Roy, T. Preuße, S. J. Lohmeier, A. Godt, and P. Behrens, "Porous interpenetrated zirconium–organic frameworks (pizofs): A chemically versatile family of metal–organic frameworks," *Chemistry—A European Journal*, vol. 17, no. 34, pp. 9320–9325, 2011.
- [45] S. J. Garibay and S. M. Cohen, "Isoreticular synthesis and modification of frameworks with the uio-66 topology," *Chemical communications*, vol. 46, no. 41, pp. 7700–7702, 2010.
- [46] M. Kim, J. F. Cahill, H. Fei, K. A. Prather, and S. M. Cohen, "Postsynthetic ligand and cation exchange in robust metal–organic frameworks," *Journal of the American Chemical Society*, vol. 134, no. 43, pp. 18082–18088, 2012.
- [47] G. C. Shearer, S. Chavan, J. Ethiraj, J. G. Vitillo, S. Svelle, U. Olsbye, C. Lamberti, S. Bordiga, and K. P. Lillerud, "Tuned to perfection: Ironing out the defects in metal–organic framework uio-66," *Chemistry of Materials*, vol. 26, no. 14, pp. 4068–4071, 2014.
- [48] H. Wu, Y. S. Chua, V. Krungleviciute, M. Tyagi, P. Chen, T. Yildirim, and W. Zhou, "Unusual and highly tunable missing-linker defects in zirconium metal–organic framework uio-66 and their important effects on gas adsorption," *Journal of the American Chemical Society*, vol. 135, no. 28, pp. 10525–10532, 2013.
- [49] G. C. Shearer, S. Chavan, S. Bordiga, S. Svelle, U. Olsbye, and K. P. Lillerud, "Defect engineering: tuning the porosity and composition of the metal–organic framework uio-66 via modulated synthesis," *Chemistry of Materials*, vol. 28, no. 11, pp. 3749–3761, 2016.
- [50] J. Ren, H. W. Langmi, B. C. North, M. Mathe, and D. Bessarabov, "Modulated synthesis of zirconium–metal organic framework (zr-mof) for

- hydrogen storage applications," *international journal of hydrogen energy*, vol. 39, no. 2, pp. 890–895, 2014.
- [51] I. Stassen, B. Bueken, H. Reinsch, J. Oudenhoven, D. Wouters, J. Hajek, V. Van Speybroeck, N. Stock, P. Vereecken, R. Van Schaijk, *et al.*, "Towards metal–organic framework based field effect chemical sensors: Uio-66-nh 2 for nerve agent detection," *Chemical science*, vol. 7, no. 9, pp. 5827–5832, 2016.
- [52] D. Cunha, M. Ben Yahia, S. Hall, S. R. Miller, H. Chevreau, E. Elkaïm, G. Maurin, P. Horcajada, and C. Serre, "Rationale of drug encapsulation and release from biocompatible porous metal–organic frameworks," *Chemistry of Materials*, vol. 25, no. 14, pp. 2767–2776, 2013.
- [53] F. Vermoortele, B. Bueken, G. Le Bars, B. Van de Voorde, M. Vandichel, K. Houthoofd, A. Vimont, M. Daturi, M. Waroquier, V. Van Speybroeck, *et al.*, "Synthesis modulation as a tool to increase the catalytic activity of metal–organic frameworks: the unique case of uio-66 (zr)," *Journal of the American Chemical Society*, vol. 135, no. 31, pp. 11465–11468, 2013.
- [54] S. M. Rogge, A. Bavykina, J. Hajek, H. Garcia, A. I. Olivos-Suarez, A. Sepúlveda-Escribano, A. Vimont, G. Clet, P. Bazin, F. Kapteijn, *et al.*, "Metal–organic and covalent organic frameworks as single-site catalysts," *Chemical Society Reviews*, vol. 46, no. 11, pp. 3134–3184, 2017.
- [55] S. M. J. Rogge, J. Wieme, L. Vanduyfhuys, S. Vandenbrande, G. Maurin, T. Verstraelen, M. Waroquier, and V. Van Speybroeck, "Thermodynamic insight in the high-pressure behavior of uio-66: Effect of linker defects and linker expansion," *Chemistry of Materials*, vol. 28, no. 16, pp. 5721–5732, 2016. PMID: 27594765.
- [56] A. De Vos, K. Hendrickx, P. Van Der Voort, V. Van Speybroeck, and K. Lejaeghere, "Missing linkers: an alternative pathway to uio-66 electronic structure engineering," *Chemistry of Materials*, vol. 29, no. 7, pp. 3006–3019, 2017.
- [57] D. D. Borges, S. Devautour-Vinot, H. Jobic, J. Ollivier, F. Nouar, R. Semino, T. Devic, C. Serre, F. Paesani, and G. Maurin, "Proton transport in a highly conductive porous zirconium-based metal–organic framework: Molecular insight," *Angewandte Chemie International Edition*, vol. 55, no. 12, pp. 3919–3924, 2016.
- [58] M. Vandichel, J. Hajek, F. Vermoortele, M. Waroquier, D. E. De Vos, and V. Van Speybroeck, "Active site engineering in uio-66 type metal–organic frameworks by intentional creation of defects: a theoretical rationalization," *CrystEngComm*, vol. 17, no. 2, pp. 395–406, 2015.
- [59] Y. Liu, R. C. Klet, J. T. Hupp, and O. Farha, "Probing the correlations between the defects in metal–organic frameworks and their catalytic activity

- by an epoxide ring-opening reaction," *Chemical Communications*, vol. 52, no. 50, pp. 7806–7809, 2016.
- [60] F. Vermoortele, M. Vandichel, B. Van de Voorde, R. Ameloot, M. Waroquier, V. Van Speybroeck, and D. E. De Vos, "Electronic effects of linker substitution on lewis acid catalysis with metal–organic frameworks," *Angewandte Chemie International Edition*, vol. 51, no. 20, pp. 4887–4890, 2012.
- [61] S. Øien, D. Wragg, H. Reinsch, S. Svelle, S. Bordiga, C. Lamberti, and K. P. Lillerud, "Detailed structure analysis of atomic positions and defects in zirconium metal–organic frameworks," *Crystal Growth & Design*, vol. 14, no. 11, pp. 5370–5372, 2014.
- [62] C. A. Trickett, K. J. Gagnon, S. Lee, F. Gándara, H.-B. Bürgi, and O. M. Yaghi, "Definitive molecular level characterization of defects in uiö-66 crystals," *Angewandte Chemie International Edition*, vol. 54, no. 38, pp. 11162–11167, 2015.
- [63] S. Ling and B. Slater, "Dynamic acidity in defective uiö-66," *Chemical science*, vol. 7, no. 7, pp. 4706–4712, 2016.
- [64] M. Vandichel, J. Hajek, A. Ghysels, A. De Vos, M. Waroquier, and V. Van Speybroeck, "Water coordination and dehydration processes in defective uiö-66 type metal organic frameworks," *CrystEngComm*, vol. 18, no. 37, pp. 7056–7069, 2016.
- [65] J. M. Taylor, S. Dekura, R. Ikeda, and H. Kitagawa, "Defect control to enhance proton conductivity in a metal–organic framework," *Chemistry of Materials*, vol. 27, no. 7, pp. 2286–2289, 2015.
- [66] R. C. Klet, Y. Liu, T. C. Wang, J. T. Hupp, and O. K. Farha, "Evaluation of brønsted acidity and proton topology in zr-and hf-based metal–organic frameworks using potentiometric acid–base titration," *Journal of Materials Chemistry A*, vol. 4, no. 4, pp. 1479–1485, 2016.
- [67] D. Yang, V. Bernales, T. Islamoglu, O. K. Farha, J. T. Hupp, C. J. Cramer, L. Gagliardi, and B. C. Gates, "Tuning the surface chemistry of metal organic framework nodes: proton topology of the metal-oxide-like zr₆ nodes of uiö-66 and nu-1000," *Journal of the American Chemical Society*, vol. 138, no. 46, pp. 15189–15196, 2016.
- [68] J. B. DeCoste, G. W. Peterson, H. Jasuja, T. G. Glover, Y.-g. Huang, and K. S. Walton, "Stability and degradation mechanisms of metal–organic frameworks containing the zr 6 o 4 (oh) 4 secondary building unit," *Journal of Materials Chemistry A*, vol. 1, no. 18, pp. 5642–5650, 2013.
- [69] M. Kandiah, M. H. Nilsen, S. Usseglio, S. Jakobsen, U. Olsbye, M. Tilset, C. Larabi, E. A. Quadrelli, F. Bonino, and K. P. Lillerud, "Synthesis and

- stability of tagged uio-66 zr-mofs," *Chemistry of Materials*, vol. 22, no. 24, pp. 6632–6640, 2010.
- [70] M. Kandiah, S. Usseglio, S. Svelle, U. Olsbye, K. P. Lillerud, and M. Tilset, "Post-synthetic modification of the metal–organic framework compound uio-66," *Journal of Materials Chemistry*, vol. 20, no. 44, pp. 9848–9851, 2010.
- [71] M. Kim and S. M. Cohen, "Discovery, development, and functionalization of zr (iv)-based metal–organic frameworks," *CrystEngComm*, vol. 14, no. 12, pp. 4096–4104, 2012.
- [72] F. Vermoortele, R. Ameloot, A. Vimont, C. Serre, and D. De Vos, "An amino-modified zr-terephthalate metal–organic framework as an acid–base catalyst for cross-alcohol condensation," *Chemical communications*, vol. 47, no. 5, pp. 1521–1523, 2011.
- [73] M. N. Timofeeva, V. N. Panchenko, J. W. Jun, Z. Hasan, M. M. Matrosova, and S. H. Jhung, "Effects of linker substitution on catalytic properties of porous zirconium terephthalate uio-66 in acetalization of benzaldehyde with methanol," *Applied Catalysis A: General*, vol. 471, pp. 91–97, 2014.
- [74] F. Cirujano, A. Corma, and F. L. i Xamena, "Zirconium-containing metal organic frameworks as solid acid catalysts for the esterification of free fatty acids: Synthesis of biodiesel and other compounds of interest," *Catalysis Today*, vol. 257, pp. 213–220, 2015.
- [75] F. Cirujano, A. Corma, and F. L. i Xamena, "Conversion of levulinic acid into chemicals: Synthesis of biomass derived levulinate esters over zr-containing mofs," *Chemical Engineering Science*, vol. 124, pp. 52–60, 2015.
- [76] J. Hajek, M. Vandichel, B. Van de Voorde, B. Bueken, D. De Vos, M. Waroquier, and V. Van Speybroeck, "Mechanistic studies of aldol condensations in uio-66 and uio-66-nh₂ metal organic frameworks," *Journal of catalysis*, vol. 331, pp. 1–12, 2015.
- [77] E. Plessers, G. Fu, C. Tan, D. De Vos, and M. Roeffaers, "Zr-based mof-808 as meerwein–ponndorf–verley reduction catalyst for challenging carbonyl compounds," *Catalysts*, vol. 6, no. 7, p. 104, 2016.
- [78] H.-H. Mautschke, F. Drache, I. Senkovska, S. Kaskel, and F. L. i Xamena, "Catalytic properties of pristine and defect-engineered zr-mof-808 metal organic frameworks," *Catalysis Science & Technology*, vol. 8, no. 14, pp. 3610–3616, 2018.
- [79] J. Jiang, F. Gándara, Y.-B. Zhang, K. Na, O. M. Yaghi, and W. G. Klemperer, "Superacidity in sulfated metal–organic framework-808," *Journal of the American Chemical Society*, vol. 136, no. 37, pp. 12844–12847, 2014.

- [80] K. D. Wispelaere, L. Vanduyfhuys, and V. V. Speybroeck, "Chapter 6 - entropy contributions to transition state modeling," in *Modelling and Simulation in the Science of Micro- and Meso-Porous Materials* (C. R. A. Catlow, V. V. Speybroeck, and R. A. van Santen, eds.), pp. 189 – 228, Elsevier, 2018.
- [81] P. P. Ewald, "Die berechnung optischer und elektrostatischer gitterpotentiale," *Annalen der Physik*, vol. 369, no. 3, pp. 253–287, 1921.
- [82] M. Born and R. Oppenheimer, "Zur quantentheorie der molekeln," *Annalen der Physik*, vol. 389, no. 20, pp. 457–484, 1927.
- [83] M. Ceriotti, W. Fang, P. G. Kusalik, R. H. McKenzie, A. Michaelides, M. A. Morales, and T. E. Markland, "Nuclear quantum effects in water and aqueous systems: Experiment, theory, and current challenges," *Chemical Reviews*, vol. 116, no. 13, pp. 7529–7550, 2016. PMID: 27049513.
- [84] A. C. T. van Duin, S. Dasgupta, F. Lorant, and W. A. Goddard, "Reaxff: A reactive force field for hydrocarbons," *The Journal of Physical Chemistry A*, vol. 105, no. 41, pp. 9396–9409, 2001.
- [85] L. H. Thomas, "The calculation of atomic fields," *Mathematical Proceedings of the Cambridge Philosophical Society*, vol. 23, no. 5, p. 542–548, 1927.
- [86] E. Fermi, "Eine statistische methode zur bestimmung einiger eigenschaften des atoms und ihre anwendung auf die theorie des periodischen systems der elemente," *Zeitschrift für Physik*, vol. 48, pp. 73–79, Jan 1928.
- [87] P. Hohenberg and W. Kohn, "Inhomogeneous electron gas," *Phys. Rev.*, vol. 136, pp. B864–B871, Nov 1964.
- [88] W. Kohn and L. J. Sham, "Self-consistent equations including exchange and correlation effects," *Phys. Rev.*, vol. 140, pp. A1133–A1138, Nov 1965.
- [89] S. H. Vosko, L. Wilk, and M. Nusair, "Accurate spin-dependent electron liquid correlation energies for local spin density calculations: a critical analysis," *Canadian Journal of Physics*, vol. 58, no. 8, pp. 1200–1211, 1980.
- [90] A. D. Becke, "Density-functional exchange-energy approximation with correct asymptotic behavior," *Phys. Rev. A*, vol. 38, pp. 3098–3100, Sep 1988.
- [91] C. Lee, W. Yang, and R. G. Parr, "Development of the colle-salvetti correlation-energy formula into a functional of the electron density," *Phys. Rev. B*, vol. 37, pp. 785–789, Jan 1988.
- [92] J. P. Perdew, K. Burke, and M. Ernzerhof, "Generalized gradient approximation made simple," *Phys. Rev. Lett.*, vol. 77, pp. 3865–3868, Oct 1996.

- [93] J. P. Perdew, K. Burke, and M. Ernzerhof, "Generalized gradient approximation made simple [phys. rev. lett. 77, 3865 (1996)]," *Phys. Rev. Lett.*, vol. 78, pp. 1396–1396, Feb 1997.
- [94] A. D. Becke, "Density-functional thermochemistry. iii. the role of exact exchange," *The Journal of Chemical Physics*, vol. 98, no. 7, pp. 5648–5652, 1993.
- [95] C. Adamo and V. Barone, "Toward reliable density functional methods without adjustable parameters: The pbe0 model," *The Journal of Chemical Physics*, vol. 110, no. 13, pp. 6158–6170, 1999.
- [96] S. Grimme, J. Antony, S. Ehrlich, and H. Krieg, "A consistent and accurate ab initio parametrization of density functional dispersion correction (dft-d) for the 94 elements h-pu," *The Journal of Chemical Physics*, vol. 132, no. 15, p. 154104, 2010.
- [97] T. Bučko, S. Lebègue, T. Gould, and J. G. Ángyán, "Many-body dispersion corrections for periodic systems: an efficient reciprocal space implementation," *Journal of Physics: Condensed Matter*, vol. 28, p. 045201, jan 2016.
- [98] A. Ambrosetti, A. M. Reilly, R. A. DiStasio, and A. Tkatchenko, "Long-range correlation energy calculated from coupled atomic response functions," *The Journal of Chemical Physics*, vol. 140, no. 18, p. 18A508, 2014.
- [99] J. Wieme, K. Lejaeghere, G. Kresse, and V. Van Speybroeck, "Tuning the balance between dispersion and entropy to design temperature-responsive flexible metal-organic frameworks," *Nature communications*, vol. 9, no. 1, p. 4899, 2018.
- [100] T. Verstraelen, V. Van Speybroeck, and M. Waroquier, "Zeobuilder: A gui toolkit for the construction of complex molecular structures on the nanoscale with building blocks," *Journal of Chemical Information and Modeling*, vol. 48, no. 7, pp. 1530–1541, 2008. PMID: 18543904.
- [101] A. Heyden, A. T. Bell, and F. J. Keil, "Efficient methods for finding transition states in chemical reactions: Comparison of improved dimer method and partitioned rational function optimization method," *The Journal of Chemical Physics*, vol. 123, no. 22, p. 224101, 2005.
- [102] W. H. Press, W. H. Press, B. P. Flannery, B. P. Flannery, S. A. Teukolsky, W. T. Vetterling, and W. T. Vetterling, *Numerical recipes in Pascal: the art of scientific computing*, vol. 1. Cambridge University Press, 1989.
- [103] D. E. Vanpoucke, K. Lejaeghere, V. Van Speybroeck, M. Waroquier, and A. Ghysels, "Mechanical properties from periodic plane wave quantum mechanical codes: The challenge of the flexible nanoporous mil-47 (v) framework," *The Journal of Physical Chemistry C*, vol. 119, no. 41, pp. 23752–23766, 2015.

- [104] F. Birch, "Finite elastic strain of cubic crystals," *Physical review*, vol. 71, no. 11, p. 809, 1947.
- [105] F. Murnaghan, "The compressibility of media under extreme pressures," *Proceedings of the national academy of sciences of the United States of America*, vol. 30, no. 9, p. 244, 1944.
- [106] A. Ghysels, T. Verstraelen, K. Hemelsoet, M. Waroquier, and V. Van Speybroeck, "Tamkin: a versatile package for vibrational analysis and chemical kinetics," 2010.
- [107] A. Ghysels, D. Van Neck, and M. Waroquier, "Cartesian formulation of the mobile block hessian approach to vibrational analysis in partially optimized systems," *The Journal of chemical physics*, vol. 127, no. 16, p. 164108, 2007.
- [108] R. Car and M. Parrinello, "Unified approach for molecular dynamics and density-functional theory," *Physical review letters*, vol. 55, no. 22, p. 2471, 1985.
- [109] P. Ehrenfest, "Bemerkung über die angenäherte gültigkeit der klassischen mechanik innerhalb der quantenmechanik," *Zeitschrift für Physik A Hadrons and Nuclei*, vol. 45, no. 7, pp. 455–457, 1927.
- [110] D. Marx and J. Hutter, *Ab initio molecular dynamics: basic theory and advanced methods*. Cambridge University Press, 2009.
- [111] G. J. Martyna, D. J. Tobias, and M. L. Klein, "Constant pressure molecular dynamics algorithms," *The Journal of Chemical Physics*, vol. 101, no. 5, pp. 4177–4189, 1994.
- [112] R. Kubo, "Statistical-mechanical theory of irreversible processes. i. general theory and simple applications to magnetic and conduction problems," *Journal of the Physical Society of Japan*, vol. 12, no. 6, pp. 570–586, 1957.
- [113] E. Cances, B. Mennucci, and J. Tomasi, "A new integral equation formalism for the polarizable continuum model: Theoretical background and applications to isotropic and anisotropic dielectrics," *The Journal of chemical physics*, vol. 107, no. 8, pp. 3032–3041, 1997.
- [114] O. Valsson, P. Tiwary, and M. Parrinello, "Enhancing important fluctuations: Rare events and metadynamics from a conceptual viewpoint," *Annual review of physical chemistry*, vol. 67, pp. 159–184, 2016.
- [115] A. Laio and M. Parrinello, "Escaping free-energy minima," *Proceedings of the National Academy of Sciences*, vol. 99, no. 20, pp. 12562–12566, 2002.
- [116] L. Sutto, S. Marsili, and F. L. Gervasio, "New advances in metadynamics," *Wiley Interdisciplinary Reviews: Computational Molecular Science*, vol. 2, no. 5, pp. 771–779, 2012.

- [117] E. Carter, G. Ciccotti, J. T. Hynes, and R. Kapral, "Constrained reaction coordinate dynamics for the simulation of rare events," *Chemical Physics Letters*, vol. 156, no. 5, pp. 472–477, 1989.
- [118] E. Darve and A. Pohorille, "Calculating free energies using average force," *The Journal of Chemical Physics*, vol. 115, no. 20, pp. 9169–9183, 2001.
- [119] C. Jarzynski, "Nonequilibrium equality for free energy differences," *Physical Review Letters*, vol. 78, no. 14, p. 2690, 1997.
- [120] L. Rosso, P. Mináry, Z. Zhu, and M. E. Tuckerman, "On the use of the adiabatic molecular dynamics technique in the calculation of free energy profiles," *The Journal of chemical physics*, vol. 116, no. 11, pp. 4389–4402, 2002.
- [121] J. R. Gullingsrud, R. Braun, and K. Schulten, "Reconstructing potentials of mean force through time series analysis of steered molecular dynamics simulations," *Journal of Computational Physics*, vol. 151, no. 1, pp. 190–211, 1999.
- [122] K. De Wispelaere, C. S. Wondergem, B. Ensing, K. Hemelsoet, E. J. Meijer, B. M. Weckhuysen, V. Van Speybroeck, and J. Ruiz-Martínez, "Insight into the effect of water on the methanol-to-olefins conversion in h-sapo-34 from molecular simulations and in situ microspectroscopy," *ACS Catalysis*, vol. 6, no. 3, pp. 1991–2002, 2016.
- [123] K. De Wispelaere, B. Ensing, A. Ghysels, E. J. Meijer, and V. Van Speybroeck, "Complex reaction environments and competing reaction mechanisms in zeolite catalysis: insights from advanced molecular dynamics," *Chemistry—A European Journal*, vol. 21, no. 26, pp. 9385–9396, 2015.
- [124] V. Van Speybroeck, K. De Wispelaere, J. Van der Mynsbrugge, M. Vandichel, K. Hemelsoet, and M. Waroquier, "First principle chemical kinetics in zeolites: the methanol-to-olefin process as a case study," *Chemical Society Reviews*, vol. 43, no. 21, pp. 7326–7357, 2014.
- [125] P. Cnudde, K. De Wispelaere, J. Van der Mynsbrugge, M. Waroquier, and V. Van Speybroeck, "Effect of temperature and branching on the nature and stability of alkene cracking intermediates in h-zsm-5," *Journal of catalysis*, vol. 345, pp. 53–69, 2017.
- [126] V. Haigis, F.-X. Coudert, R. Vuilleumier, A. Boutin, and A. H. Fuchs, "Hydrothermal breakdown of flexible metal–organic frameworks: a study by first-principles molecular dynamics," *The journal of physical chemistry letters*, vol. 6, no. 21, pp. 4365–4370, 2015.
- [127] T. Bučko, L. Bencó, J. Hafner, and J. G. Ángyán, "Monomolecular cracking of propane over acidic chabazite: An ab initio molecular dynamics and

- transition path sampling study," *Journal of catalysis*, vol. 279, no. 1, pp. 220–228, 2011.
- [128] G. Fraux and F.-X. Coudert, "Recent advances in the computational chemistry of soft porous crystals," *Chemical Communications*, vol. 53, no. 53, pp. 7211–7221, 2017.
- [129] C. Dellago, P. G. Bolhuis, and P. L. Geissler, "Transition path sampling," *Advances in chemical physics*, vol. 123, pp. 1–78, 2002.
- [130] Y. Sugita and Y. Okamoto, "Replica-exchange molecular dynamics method for protein folding," *Chemical physics letters*, vol. 314, no. 1-2, pp. 141–151, 1999.
- [131] G. M. Torrie and J. P. Valleau, "Nonphysical sampling distributions in monte carlo free-energy estimation: Umbrella sampling," *Journal of Computational Physics*, vol. 23, no. 2, pp. 187–199, 1977.
- [132] G. Patey and J. Valleau, "A monte carlo method for obtaining the interionic potential of mean force in ionic solution," *The Journal of Chemical Physics*, vol. 63, no. 6, pp. 2334–2339, 1975.
- [133] M. A. Rohrdanz, W. Zheng, and C. Clementi, "Discovering mountain passes via torchlight: Methods for the definition of reaction coordinates and pathways in complex macromolecular reactions," *Annual review of physical chemistry*, vol. 64, pp. 295–316, 2013.
- [134] A. Barducci, M. Bonomi, and M. Parrinello, "Metadynamics," *Wiley Interdisciplinary Reviews: Computational Molecular Science*, vol. 1, no. 5, pp. 826–843, 2011.
- [135] S. Kumar, J. M. Rosenberg, D. Bouzida, R. H. Swendsen, and P. A. Kollman, "The weighted histogram analysis method for free-energy calculations on biomolecules. i. the method," *Journal of computational chemistry*, vol. 13, no. 8, pp. 1011–1021, 1992.
- [136] J. Canivet, M. Vandichel, and D. Farrusseng, "Origin of highly active metal–organic framework catalysts: defects? defects!," *Dalton Transactions*, vol. 45, no. 10, pp. 4090–4099, 2016.
- [137] P. Ghosh, Y. J. Colón, and R. Q. Snurr, "Water adsorption in uiO-66: the importance of defects," *Chemical Communications*, vol. 50, no. 77, pp. 11329–11331, 2014.
- [138] G. C. Shearer, S. Forslev, S. Chavan, S. Bordiga, K. Mathisen, M. Bjørgen, S. Svelle, and K. P. Lillerud, "In situ infrared spectroscopic and gravimetric characterisation of the solvent removal and dehydroxylation of the metal organic frameworks uiO-66 and uiO-67," *Topics in Catalysis*, vol. 56, no. 9–10, pp. 770–782, 2013.

- [139] J. Nishida, A. Tamimi, H. Fei, S. Pullen, S. Ott, S. M. Cohen, and M. D. Fayer, "Structural dynamics inside a functionalized metal–organic framework probed by ultrafast 2d ir spectroscopy," *Proceedings of the National Academy of Sciences*, vol. 111, no. 52, pp. 18442–18447, 2014.
- [140] F.-X. Coudert, R. Vuilleumier, and A. Boutin, "Dipole moment, hydrogen bonding and ir spectrum of confined water," *ChemPhysChem*, vol. 7, no. 12, pp. 2464–2467, 2006.
- [141] S. Dalla Bernardina, E. Paineau, J.-B. Brubach, P. Judeinstein, S. Rouziére, P. Launois, and P. Roy, "Water in carbon nanotubes: the peculiar hydrogen bond network revealed by infrared spectroscopy," *Journal of the American Chemical Society*, vol. 138, no. 33, pp. 10437–10443, 2016.
- [142] G. Cicero, J. C. Grossman, E. Schwegler, F. Gygi, and G. Galli, "Water confined in nanotubes and between graphene sheets: A first principle study," *Journal of the American Chemical Society*, vol. 130, no. 6, pp. 1871–1878, 2008.
- [143] S. Kashtanov, A. Augustson, J.-E. Rubensson, J. Nordgren, H. Ågren, J.-H. Guo, and Y. Luo, "Chemical and electronic structures of liquid methanol from x-ray emission spectroscopy and density functional theory," *Physical Review B*, vol. 71, no. 10, p. 104205, 2005.
- [144] M. Pagliai, G. Cardini, R. Righini, and V. Schettino, "Hydrogen bond dynamics in liquid methanol," *The Journal of chemical physics*, vol. 119, no. 13, pp. 6655–6662, 2003.
- [145] J. A. Morrone and M. E. Tuckerman, "Ab initio molecular dynamics study of proton mobility in liquid methanol," *The Journal of chemical physics*, vol. 117, no. 9, pp. 4403–4413, 2002.